

**A STUDY OF NEGATIVE FEEDBACK DAMPING PROPERTY OF ROLL-
COUPLED HYDRO-PNEUMATIC SUSPENSIONS**

Navaneethan Sundaresan

A Thesis
in
The Department
of
Mechanical, Industrial and Aerospace Engineering

**Presented in Partial Fulfillment of the Requirements
for the Degree of Masters of Applied Science at**

Concordia University

Montreal, Quebec, Canada

June 2018

© Navaneethan Sundaresan, 2018

CONCORDIA UNIVERSITY

School of Graduate Studies

This is to certify that the thesis prepared

By: **Navaneethan Sundaresan**

Entitled: **“A study of Negative Feedback Damping Property of Roll-coupled Hydro-pneumatic suspensions”**

and submitted in partial fulfillment of the requirements for the degree of

Master of Applied Science (Mechanical Engineering)

Complies with the regulations of the university and meets the accepted standards with respect to originality and quality.

Signed by the final examining committee:

_____ Chair
Dr. Javed Dargahi

_____ MIE Examiner
Dr. Chun- Yi Su

_____ External Examiner
Dr. Saifur Rahaman

_____ Supervisor
Dr. Subhash Rakheja

_____ Supervisor
Dr. A.K.W. Ahmed

Approved by _____
Dr. S. Narayanswamy, Graduate Program director

Dr. Amir Asif, Dean
Faculty of Engineering & Computer Science

Date _____

ABSTRACT

A STUDY OF NEGATIVE FEEDBACK DAMPING PROPERTY OF ROLL-COUPLED HYDRO-PNEUMATIC SUSPENSIONS

NAVANEETHAN SUNDARESAN

The design of a vehicle suspension involves complex compromises due to conflicting ride comfort and handling requirements. High load capacity and high mass center commercial vehicles, especially, impose greater design challenges due to their relatively low rollover immunity. Road vehicles, invariably, employ auxiliary roll stiffeners such as antiroll bars to realize a better compromise among the roll dynamic and ride comfort performance. The anti-roll bars, however, add considerable weight, exhibit negligible damping and cause stronger coupling between the roll and vertical modes. Alternatively, roll-connected hydro-pneumatic suspensions offer superior anti-roll performance, while preserving the soft vertical ride characteristics. Reported studies have shown that such suspensions can provide anti-roll characteristics similar to an antiroll bar but with considerable roll damping and less weight. The feedback effects of the hydraulic couplings in such suspensions yield negative damping force in the vertical mode, which have not yet been explored.

This thesis research presents a systematic study of negative damping features of the roll-coupled hydro-pneumatic suspensions and its significance for realizing variable damping properties. Three different configurations of hydro-pneumatic struts were conceived for realizing hydraulic couplings in the roll plane. Analytical models of the roll-coupled suspensions were formulated considering ideal gas law, turbulent flows through orifices and damping valves, laminar flows through interconnections, floating piston dynamics and fluid compressibility. The analytical formulations were used to describe the negative damping feature attributed to the flow feedbacks. The vertical and roll mode damping and stiffness properties of the proposed configurations were derived via analytical relations, which showed that hydraulic couplings yield high roll stiffness and damping with only minimal effect on the vertical mode properties. The simulation results demonstrated two negative damping force components of a strut attributed to flows through the interconnecting pipes and flows through orifices in the connected strut. These negative damping force components, however, contributed to only positive roll damping moment. A methodology to enhance negative damping force of the connected struts was proposed for realizing variable damping properties similar to those of the conventional damping valves. Deployments of small size multiple interconnections or the flow-control valves across the struts resulted in comprehensive magnitudes of negative damping force components. Simulation results

were obtained under lateral acceleration excitation idealizing the centrifugal force encountered during a steady-turn maneuver, a road bump, and in-phase and out-of-phase harmonic road excitations. The results were obtained for unconnected and connected struts with and without the damping valves and interconnection flow valves. Comparisons of the results revealed that interconnection valves can provide variable damping properties similar to the damping valves. The interconnection valves, however, offer greater design/tuning flexibility since these are mounted externally. The results suggested that further efforts in parameterization of the coupling flows will be worthy for realizing optimal damping properties of the roll-coupled hydro-pneumatic suspensions.

ACKNOWLEDGEMENTS

I would like to express my sincere appreciation to my supervisors, Dr. Subhash Rakheja and, Dr. A.K.W. Ahmed for their persistent guidance throughout the realization of this investigation.

The author also thanks the colleagues, faculty and staff at the Department of Mechanical, Industrial and Aerospace Engineering for their contributions to this thesis work.

Finally, the author would like to express his special thanks to his parents and family members for their encouragements and supports. The author would like to dedicate this thesis to his father, Sundaresan Chelliah.

TABLE OF CONTENTS

TABLE OF CONTENTS	I
LIST OF FIGURES	IV
LIST OF TABLES	IX
NOMENCLATURE	X
CHAPTER 1	1
INTRODUCTION AND LITERATURE REVIEW	1
1.1 GENERAL	1
1.2 LITERATURE REVIEW	2
1.3 INTERCONNECTED VEHICLE SUSPENSION	2
1.3.1 Passive Roll Plane Interconnected Suspension.....	8
1.1.2 Active Roll Plane Interconnected Suspension	16
1.1.3 Pitch Plane Interconnected Suspension	20
1.1.4 Experimental analysis of a hydro-pneumatic suspension	24
1.2 SCOPE OF THE INVESTIGATION	28
1.3 OBJECTIVE OF PRESENT INVESTIGATION	29
CHAPTER 2	30
DEVELOPMENT OF ANALYTICAL MODELS FOR THE ROLL PLANE INTERCONNECTED SUSPENSION	30
2.1 INTRODUCTION	30
2.2 HYDRO-PNEUMATIC SUSPENSION STRUTS	31
2.3 ROLL PLANE MODEL OF HYDRO-PNEUMATIC SUSPENSION STRUTS	31
2.4 SUSPENSION FORCES	35
2.4.1 Unconnected Suspension Struts.....	36
2.4.2 Roll Plane Interconnected Suspension (Type-I Struts).....	38
2.4.3 Effects of Compressibility and Floating Piston Dynamics	41
2.4.4 Roll Plane Interconnected Suspension (Type-II struts)	43
2.4.5 Effects of Compressibility and Floating Piston Dynamics	45
2.4.6 Roll Plane Interconnected Suspension (Type-IIa struts)	46
2.4.7 Effects of Compressibility and Floating Piston Dynamics	48
2.5 SUSPENSION PROPERTIES	50
2.5.1 Load Carrying Capacity.....	50

2.5.2 Suspension Rates	50
2.5.3 Vertical Damping Properties.....	52
2.5.4 Roll Stiffness for Different Strut Configurations.....	53
2.5.5 Roll Mode Damping Properties of Different Strut Configurations	57
2.6 ENHANCEMENT OF NEGATIVE DAMPING VIA INTERCONNECTING PIPES .	58
2.7 SUMMARY	61
CHAPTER 3	62
PROPERTY ANALYSIS OF DIFFERENT HYDRO-PNEUMATIC CONFIGURATIONS	62
3.1 INTRODUCTION.....	62
3.2 STATIC PROPERTIES OF THE STRUTS	62
3.2.1 Vertical and Roll Suspension Rates	68
3.3 VERTICAL DAMPING PROPERTIES	73
3.4 ENHANCEMENT OF NEGATIVE DAMPING AND DAMPING FORCE TUNING. 76	
3.4.1 Effect of Capillary Interconnecting Tubes.....	77
3.4.2 Effect of Normally Open Valves in the Interconnecting Pipes.....	79
3.5 ROLL DAMPING PROPERTIES	85
3.5 SUMMARY	87
CHAPTER 4.....	89
DYNAMIC RESPONSE CHARACTERISTICS OF DIFFERENT SUSPENSION CONFIGURATIONS	89
4.1 INTRODUCTION.....	89
4.2 DESCRIPTION OF EXCITATIONS	90
4.3 RESULTS AND DISCUSSIONS.....	92
4.3.1 Responses to Lateral Acceleration Excitation	92
4.3.2 Responses to Transient Pulse Excitations.....	96
4.5 VIBRATION TRANSMISSIBILITY CHARACTERISTICS.....	101
4.6 SUMMARY	109
CHAPTER 5	110
CONCLUSIONS AND RECOMMENDATIONS.....	110
5.1 MAJOR CONTRIBUTIONS	110
5.2 MAJOR CONCLUSIONS	110

5.3 RECOMMENDATIONS FOR THE FUTURE WORK	111
REFERENCES.....	113

LIST OF FIGURES

Figure 1.1: Schematics of passive mechanical interconnection [1].	3
Figure 1.2: Pneumatic interconnection in pitch plane: (a) constant effective area; and (b) variable effective area [1].	4
Figure 1.3: Hawley’s interconnected suspension arrangements [2].	4
Figure 1.4: Balance plate mechanism [11].	5
Figure 1.5: Schematic of the conceptual hydraulic scheme [12].	5
Figure 1.6: Semi active damping schematic [14].	6
Figure 1.7: Schematic of constant orifice and passive sequential damping [18].	7
Figure 1.8: Schematic of the suspension configurations: (a) Conventional anti-roll bar system; and (b) Mechanically coupled suspension system [24].	9
Figure 1.9: Schematic of an individual hydro pneumatic strut [3].	9
Figure 1.10: Schematic of a passive hydro-pneumatic suspension: (a) independent cylinder suspension; and (b) interconnected suspension [3].	10
Figure 1.11: Schematic of the hydro pneumatic strut [25].	11
Figure 1.12: Schematic of the interconnected hydro-pneumatic suspension [7, 26].	11
Figure 1.13: Schematic of the conventional interconnected hydro-pneumatic suspension [28].	12
Figure 1.14: Variable damping: (a) mechanism of the preset pressure relief valve; and (b) force-velocity characteristics of the IC hydro-pneumatic suspension [28].	13
Figure 1.15: Schematic of single gas chamber struts with shim-stack valves [32].	13
Figure 1.16: Schematic of the HIS system in a half-car vehicle model [33].	14
Figure 1.17: HIS roll-plane interconnection layout; (a) anti-synchronous arrangement; and (b) anti-oppositional arrangement [35, 36].	15
Figure 1.18: Schematic of twin gas chamber struts with shim-stack valves [37].	16
Figure 1.19: Schematic of the interconnected hydro-pneumatic twin gas chamber struts [39].	16
Figure 1.20: Schematic of an active roll control system [41].	17
Figure 1.21: Hydra-gas roll control system [43].	18
Figure 1.22: Schematic of the Hydra-gas roll control shuttle [43].	18
Figure 1.23: Schematic of the hydraulic and force control circuits of DDAS [45].	19
Figure 1.24: Schematic of the pitch-plane mechanically coupled suspension [50].	21
Figure 1.25: Schematic of the pitch plane interconnection layout of the hydrolastic and hydra gas suspension configurations [52, 53].	22

Figure 1.26: Free body diagram of the saloon car with its reaction forces [53].	22
Figure 1.27: Various pitch plane interconnected hydro-pneumatic suspension configurations [54].	24
Figure 1.28: Schematic of the interconnected Hydragas suspension test setup [58, 59].	25
Figure 1.29: Schematic of the anti-roll mode kinetic H2 suspension [61].	26
Figure: 1.30 Schematic of HIS interconnection arrangement: (a) anti-oppositional; and (b) anti-synchronous [10].	27
Figure 2.1: Schematics of the hydro-pneumatic suspension strut configurations: (a) Type-I; (b) Type-II; and (c) Type-II with additional flow orifices in the main piston.	31
Figure 2.2: Four-DOF roll plane model of the vehicle with roll-coupled hydro-pneumatic suspension struts (Type-I).	33
Figure 2.3: Four-DOF roll plane model of the vehicle with unconnected hydro-pneumatic suspension struts (Type-I) with an anti-roll bar.	34
Figure 2.4: Simplified roll plane model of the vehicle during turning maneuvers.	35
Figure 2.5: Reduced model of the unconnected struts used for deriving the strut forces: (a) Type- I; and (b) Type-II.	35
Figure 2.6: Interconnected strut model used for deriving the strut forces (Type-I).	38
Figure 2.7: Interconnected strut model used for deriving the strut forces (Type-II).	44
Figure 2.8: Interconnected strut model used for deriving the strut forces (Type-IIa).	46
Figure 2.9: Schematic of the multiple interconnection (Type-I strut).	59
Figure 2.10: Proposed variation in the valve opening as a function of the pressure differential across the interconnecting pipe.	60
Figure 3.1: Proposed schematic of the ride height valve.	66
Figure 3.2: Influence of variations in sprung weight on the suspension rates of type-I and type-II struts with the ride height control system.	68
Figure 3.3: (a) Effect of fluid compressibility on the vertical suspension rates of the hydro-pneumatic struts: (a) type-I strut (UC/IC); and (b) type-II and type-IIa struts (IC/UC).	69
Figure 3.4: Roll stiffness of interconnected suspension configurations and the effect of fluid bulk modulus: (a) IC- I configuration; and (b) IC-II and IC-IIa configurations.	70
Figure 3.5: Roll stiffness of the unconnected suspension configurations with and without antiroll bar, and the effect of fluid compressibility.	71

Figure 3.6: Effect of variation in main piston area on the roll stiffness of the interconnected suspension configurations: (a) IC- I configuration; and (b) IC-II and IC-IIa configurations.	72
Figure 3.7: Effect of main piston area (A_1) on the vertical suspension rates of the struts.	73
Figure 3.8: Variations in (a) total flow area and (b) force-velocity characteristics of the strut for different area ratios.	75
Figure 3.9: Total vertical mode force-velocity characteristics of each strut in different interconnected configurations.	76
Figure 3.10: (a) Schematic of the normally open valve; and (b) pressure drop in the interconnecting pipe with the valve.	80
Figure 3.11: Variation in opening area of the normally open valve with respect to strut velocities.	82
Figure 3.12: Variations in total damping force and force components developed by a strut in the IC-I and IC-II configurations with the strut velocity: (a) without valve; and (b) with normally open-valve.	83
Figure 3.13: Variations in total damping force and force components developed by a strut in the IC-IIa configurations with the strut velocity: (a) without valve; and (b) with normally open valve.	84
Figure 3.14: Comparisons of roll damping moment developed by of different interconnected and unconnected suspension configurations.	85
Figure 3.15: Roll damping moment –roll velocity characteristics of IC suspensions without and with valves in the interconnecting pipes: (a) IC-I/IC-II suspension; and (b) IC-IIa suspension. .	87
Figure 4.1: Rounded step lateral acceleration excitation.	91
Figure 4.2: Vertical displacement due to the pulse input applied at the tire-road interface.	91
Figure 4.3: Comparisons of sprung mass roll angle responses of the vehicle model employing different suspension configurations under a rounded-step lateral acceleration excitation: (a) unconnected (UC and UC-Rollbar) and connected (IC-I, IC-II and IC-IIa) suspensions; (b) unconnected and connected suspensions with damping valves; and (c) connected suspensions with interconnection valves.	93
Figure 4.4: Comparisons of sprung mass roll rate responses of the vehicle model employing different suspension configurations under a rounded-step lateral acceleration excitation: (a) unconnected (UC and UC-Rollbar) and connected (IC-I, IC-II and IC-IIa) suspensions; (b)	

unconnected and connected suspensions with damping valves; and (c) IC suspensions with interconnection valves.	94
Figure 4.5: Comparisons of unsprung mass roll angle responses of the vehicle model employing different suspension configurations under a rounded-step lateral acceleration excitation: (a) unconnected (UC and UC-Rollbar) and connected (IC-I, IC-II and IC-IIa) suspensions; (b) unconnected and connected suspensions with damping valves; and (c) IC suspensions with interconnection valves.	95
Figure 4.6: Comparisons of sprung mass vertical displacement responses of the vehicle model to an in-phase pulse excitation: (a) unconnected (UC and UC-Rollbar) and connected (IC-I, IC-II and IC-IIa) suspensions; (b) connected suspensions with damping valves; and (c) IC suspensions with interconnection valves.	97
Figure 4.7: Comparisons of sprung mass vertical acceleration responses of the vehicle model to an in-phase pulse excitation: (a) unconnected (UC and UC-Rollbar) and connected (IC-I, IC-II and IC-IIa) suspensions; (b) connected suspensions with damping valves; and (c) IC suspensions with interconnection valves.	98
Figure 4.8: Comparisons of sprung mass roll angle responses of the vehicle model to out-of-phase pulse excitation: (a) unconnected (UC and UC-Rollbar) and connected (IC-I, IC-II and IC-IIa) suspensions; (b) unconnected and connected suspensions with damping valves; and (c) IC suspensions with interconnection valves.	99
Figure 4.9: Comparisons of sprung mass roll acceleration responses of the vehicle model to out-of-phase pulse excitation: (a) unconnected (UC and UC-Rollbar) and connected (IC-I, IC-II and IC-IIa) suspensions; (b) unconnected and connected suspensions with damping valves; and (c) IC suspensions with interconnection valves.	100
Figure 4.10: Comparisons of vertical mode transmissibility responses of the vehicle model equipped with unconnected and connected suspension configurations: (a) sprung mass; and (b) unsprung mass.	102
Figure 4.11: Comparison of vertical mode transmissibility responses of the vehicle model with different suspension configurations with damping valves: (a) sprung mass responses; and (b) unsprung mass responses.	103
Figure 4.12: Comparison of vertical mode transmissibility responses of the vehicle model with IC suspensions employing interconnection valves: (a) sprung mass responses; and (b) unsprung mass responses.	104

Figure 4.13: Comparison of roll transmissibility responses of the vehicle model with UC and IC suspensions: (a) sprung mass responses; and (b) unsprung mass responses. 106

Figure 4.14: Comparison of roll transmissibility responses of the vehicle model with UC and IC suspensions with damping valves: (a) sprung mass responses; and (b) unsprung mass responses. 107

Figure 4.15: Comparison of roll transmissibility responses of the vehicle model with UC and IC suspensions with interconnection valves: (a) sprung mass responses; and (b) unsprung mass responses. 108

LIST OF TABLES

Table 3.1: Simulation parameters of the vehicle model.	63
Table 3.2: Strut parameters for different configurations.	64
Table 3.3: Static properties of different struts based on their configurations.	65
Table 3.4 Static properties of the different struts with and without ride height valves.	67
Table 3.5: Vertical mode damping force component ratios for different pipe diameters with low strut velocities.	79
Table 3.6: Vertical mode damping force component ratios for the struts in different IC suspension configurations employing normally open valves in the interconnecting pipes.	84
Table 4.1: Frequencies corresponding to peak sprung mass displacement transmissibility of the vehicle model with different suspension configurations.	105
Table 4.2: Frequencies corresponding to peak unsprung mass displacement transmissibility of the vehicle model with different suspension configurations.	105
Table 4.3: Frequencies corresponding to peak sprung mass roll displacement transmissibility of the vehicle model with different suspension configurations.	109
Table 4.4: Frequencies corresponding to peak unsprung mass displacement transmissibility of the vehicle model with different suspension configurations.	109

NOMENCLATURE

A	Effective orifice area.
A_1	Cross-sectional area of the main piston.
A_3	Annular area of the main piston
A_e	Effective area of the main piston.
A_{FP}	Area of the floating piston.
A_v	Instantaneous opening area of the normally open valve.
C_{ti}	Damping coefficients of the tires i ($i=l, r$).
C_d	Discharge coefficient.
D	Diameter of the interconnecting pipe.
D_v	Instantaneous diameter of the valve.
E	Bulk modulus of the hydraulic fluid.
F_i	Force developed by the suspension strut i ($i=l, r$).
$F_{d\phi}$	Roll mode force developed by the suspension strut.
F_{Si}	Restoring force developed by the suspension strut i ($i=l, r$).
FDS_i	Damping force developed due to the orifice flows with in the same strut i ($i=l, r$).
FDC_i	Damping force developed due to orifice flows in the connecting strut i ($i=l, r$).
FDL_i	Damping force developed due to flow across the struts i ($i=l, r$).
F_c	Magnitude of the friction force across the seals.
G	Damping valve area ratio.
I_s	Roll mass of inertia of the sprung mass.
I_u	Roll mass of inertia of the unsprung mass.
J	No. of interconnecting pipelines.
K	Severity parameter.
K_{ti}	Stiffness coefficient of the tires i ($i=l, r$).
K_{xi}	Vertical suspension rate of the strut i ($i=l, r$).
K_e	Equivalent stiffness coefficient of the anti-roll bar.
K_ϕ	Roll stiffness of the strut i ($i=l, r$).
K_{x0}	Static vertical stiffness of the suspension unit.

K_{ϕ}^o	Static roll stiffness of the suspension unit.
L	Length of the interconnecting pipe.
$L_{1,2}$	Constant length from the normally open valve constriction to the pressure tap location.
L_s	Lateral positions of the suspension struts with respect to c.g.
L_{ti}	Lateral positions of the left- and right-tires in the vehicle side i ($i=l, r$).
M_d	Roll damping moment.
M_s	Sprung mass of the vehicle.
M_u	Unsprung mass of the vehicle.
N	Smoothing parameter of the damping valve.
N_u	Number of the suspension units.
P_{jo}	Static equilibrium pressure of the fluid or gas chamber.
P_{jki}	Pressure differential between the chamber j and k of the strut i ($i=l, r$).
P_{ji}	Instantaneous pressure of the chamber j in strut i ($i=l, r$).
P_a	Atmospheric pressure.
P_c	Charge pressure of the gas chamber.
P_{jiki}	Pressure differential across the struts in chambers j and k ($j, k=1, 3$) in strut i ($i=l, r$).
P_{cl}	Pressure differential threshold where the valve initiates to operate in compression region.
P_{ch}	Pressure differential threshold where the valve completely closes in compression region.
P_{el}	Pressure differential threshold where the valve initiates to operate in extension region.
P_{eh}	Pressure differential threshold where the valve completely closes in extension region.
ΔP_{Total}	Pressure differential across the struts when normally open valves are employed in IC suspensions.
Q_{ji}	Rate of change of volume in chamber j ($j = 1, 2, 3$) of the strut i ($i=l, r$).
Q_{jki}	Fluid flow rate between the chambers j and k ($j, k = 1, 2, 3$) of the strut i ($i=l, r$).
Q_{jiki}	Fluid flow rate across the interconnecting pipelines j and k of the strut i ($i=l, r$).
Q	Total fluid flow rates across the interconnecting pipelines when multiple pipelines are involved.
R_m	Restoring rolling moment.
Re_D	Reynolds number.
T_R	Anti-roll moment due to anti-roll bar.

T_θ	Roll moment imposed on the sprung mass while vehicle experiencing lateral acceleration inputs.
T	Suspension track length.
V_{j0}	Static equilibrium volume of the chamber j ($j = 1, 2, 3, 4$).
ΔV_{2i}	Change in volume of chamber 2 of the strut i ($i=l, r$).
V_c	Charge volume of the gas chamber.
V_{ji}	Instantaneous volume of the fluid chamber j ($j = 1, 2, 3$) of the strut i ($i=l, r$).
V_{comp}	Change in volume of hydraulic chamber due to fluid compressibility.
W_i	Static load supported by the strut i ($i=l, r$).
X_{max}	steady state maximum amplitude of the lateral acceleration input.
a_y	Lateral acceleration.
a_{12}	Area of an individual orifice located across the chambers 1 and 2.
a_{13}	Area of an individual orifice located across the chambers 1 and 3.
a	Parameter used to determine height of the transient pulse excitation.
b	Parameter used to determine width of the transient pulse excitation.
b_o	Lapse time for the transient pulse excitation.
b_e	Time at wheels exit the bump excitation.
d	Minimal opening area of the normally-open valve.
$\frac{dv_{ji}}{dt}$	Rate of change of fluid volume in chamber j ($j = 1, 2, 3$) of strut i ($i=l, r$).
$\frac{dP_{ji}}{dt}$	Rate of change of fluid pressure in chamber j ($j = 1, 2, 3$) of strut i ($i=l, r$).
f	Oscillation frequency of the rounded step-lateral acceleration.
g	Acceleration due to gravity.
h_2	Distance between the c.g. of the sprung mass and roll center.
m_f	Mass of the floating piston.
n	Polytropic component.
x_s	Vertical displacement of the sprung mass.
\dot{x}_s	Absolute velocity of the sprung mass.
\ddot{x}_{2i}	Acceleration of the floating piston in strut i ($i=l, r$).
x_u	Vertical displacement of the unsprung mass.

\dot{x}_u	Absolute velocity of the unsprung mass.
x_{0i}	Road input on the wheels of the vehicle side i ($i=l, r$).
x_{1i}	Displacement of the main piston.
\dot{x}_{1i}	Absolute velocity of the main piston in strut i ($i=l, r$).
x_{2i}	Displacement of the floating piston.
\dot{x}_{2i}	Absolute velocity of the floating piston in strut i ($i=l, r$).
\ddot{x}_{2i}	Acceleration of the floating piston in strut i ($i=l, r$).
x_{j0i}	Initial length of the chamber j in strut i ($i=l, r$).
θ_s	Roll angle of the sprung mass.
θ_u	Roll angle of the unsprung mass.
$\dot{\theta}_s$	Roll velocity of the sprung mass.
$\dot{\theta}_u$	Roll velocity of the unsprung mass.
β	Diameter ratio.
σ	Smoothing parameter.
τ_s	Time constant.
γ	Pulse frequency.
ω	Excitation frequency.

CHAPTER 1

INTRODUCTION AND LITERATURE REVIEW

1.1 GENERAL

The design of a vehicle suspension system involves complex compromises among the ride, handling and directional control performance characteristics. A suspension design with a soft spring and light damping is desirable to achieve good ride performance by isolating the vehicle body from the road irregularities. Relatively stiff and well damped suspensions are desirable for improved cornering, acceleration, braking and directional control performance of the vehicle. Although high suspension damping provides better control of resonant oscillations, it deteriorates the ride performance in the frequency range considered significant in view of human comfort. Owing to conflicting design requirements, the vehicle suspensions are invariably designed to provide relatively low stiffness in the vertical mode and high stiffness in the lateral and roll modes. Mechanical interconnections between the axle wheels such as anti-roll and pan hard bars provide higher roll stiffness and thereby improved handling characteristics, although these may degrade the ride performance due to greater coupling among different modes [1, 2]. Mechanical interactions such as anti-roll bars also increase the warp mode stiffness. Such interconnections, however, do not help to increase effective damping, which is also essential for improved handling performance.

Alternatively, hydro-pneumatic interconnection between the left and right wheel suspensions in an axle offers enhanced roll stiffness and roll damping moment, while retaining low vertical stiffness. Such suspensions thus provide better compromise between the ride and handling performance of road vehicles. Moreover, the hydro-pneumatic coupled suspension struts can integrate restoring element in the form of air spring and damping valves within the same compact strut. Such struts also enable control of ride height with relative ease, which is especially vital for commercial vehicles that encounter considerable load variations. The high roll stiffness feature of the interconnected suspension struts also permits elimination of the bulky antiroll bar; thereby, the vehicle weight is reduced. The interconnections in the roll and pitch planes further offer potential to reduce the extent of coupling between the roll, pitch and warp modes of the vehicle [3-6].

Apart from the above, the hydraulic interconnections yield negative feedback damping effect, which has not yet been explored. The negative damping effect of such struts could facilitate realization of desired damping variation in an entirely passive manner and may help eliminate the

use of damping valves [7, 10]. In this study, different configurations of roll-coupled hydro-pneumatic suspension struts are investigated in view of their negative damping effects. The effects of valves or flow resistance in the interconnections are investigated with a goal to enhance the negative damping characteristics. The negative damping effect is enhanced to achieve variable suspension damping, namely a higher damping coefficient at low strut velocities and lower damping coefficient at higher strut velocities. This dissertation research particularly focuses on negative damping effect of interconnected suspension and its potential for realizing desired damping properties.

1.2 LITERATURE REVIEW

In last four decades, vast improvements in passive, semi-active, and active vehicle suspensions have been realized based on simulations as well as experimentations. Several studies can be found in the literature that explore the concept of interconnected suspension for enhancement of roll and pitch performance. While there are some early studies of mechanical and pneumatic interconnection, all recent studies explored interconnection using hydro-pneumatic struts. There are studies that focus on either roll or pitch interconnections as well as studies that explore combined roll and pitch interconnections. In view of the focus of present investigation on negative damping effects, a thorough review of literature is carried out on interconnected suspensions and its state of art.

1.3 INTERCONNECTED VEHICLE SUSPENSION

Mechanical Interconnections between conventional suspensions are used to enhance roll and lateral stiffness and thereby improve the handling performance of the passenger cars. An interconnection between the front and the rear suspensions can greatly affect the pitch motion of the vehicle, especially during acceleration or braking. Similarly, interconnection between the left and right suspensions would control the roll motion of the vehicle while permitting lower stiffness in the vertical mode.

Newton [1] described two different mechanical interconnection schemes which are shown in Figure 1.1.

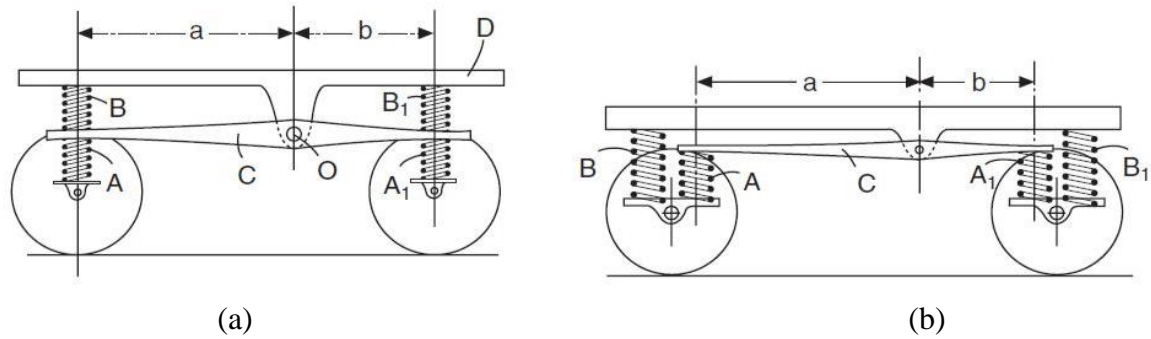


Figure 1.1: Schematics of passive mechanical interconnection [1].

In the scheme, shown in Figure 1.1(a), a mechanical link C in the form of a beam pivoted about O is introduced between the front and rear wheels to achieve higher pitch mode stiffness. The relatively soft vertical ride is achieved via softer springs A and A_1 , located between the sprung mass and the wheels. Relatively hard springs B and B_1 , located between the beam and the sprung mass, on the other hand, provide higher pitch mode stiffness. An alternate scheme shown in Figure 1.1(b) utilizing two sets of spring and a beam to realize similar characteristics for the suspension in the bounce and pitch modes.

Possible pitch plane interconnection for pneumatic suspensions, utilizing constant and variable piston area were also described in [1]. For constant effective area, as shown in Figure 1.2(a), the cg of the vehicle has to be located exactly at the center of vehicle, otherwise one of the pneumatic chamber piston will reach its extreme position. This is overcome by introducing variable effective area as shown in Figure 1.2(b). In this case, the pneumatic chambers having variable effective area will generate larger force P_2 to support larger load than the force P_1 at the other chamber, while the excess fluid could transfer to the other chamber via interconnecting pipe. It is further suggested that the pneumatic chambers could be filled with hydraulic fluid and an auxiliary chamber A (shown in Figure 1.2) filled with gas connected to interlink pipe, could replace both spring and damper of the suspension.

In 1927, Hawley [2] proposed few possible interconnections between and across the axles with hydraulic shock absorbers (Roll, Pitch, and Warp mode), as shown in Figure 1.3. However, the analytical models are not developed for the interconnection configurations.

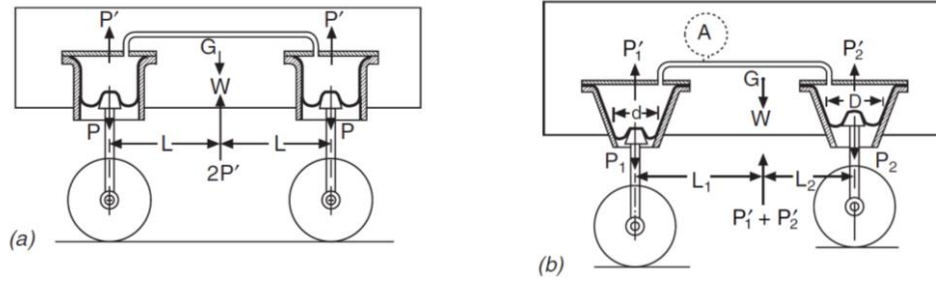


Figure 1.2: Pneumatic interconnection in pitch plane: (a) constant effective area; and (b) variable effective area [1].

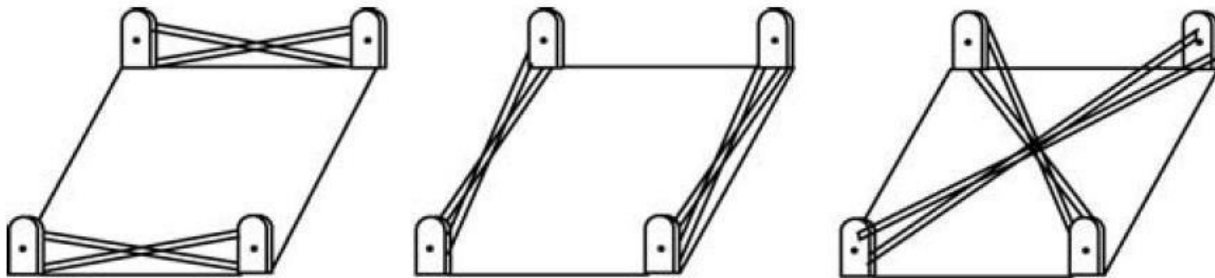


Figure 1.3: Hawley's interconnected suspension arrangements [2].

Zapletal [11] described a conceptual suspension system, in which a balance plate (75) is introduced at the rear side of vehicle to act as an anti-roll bar. It also carries the vertical (91) and pitch (90) springs, and the hydraulic pipelines are connected between front and rear, right and left wheels as shown in Figure 1.4. The study suggested that additional valves to be fitted in the hydraulic lines to increase damping.

Though the proposed scheme achieves full modal decoupling and eliminates the warp stiffness, but the mechanism of bounce mode damping is not explicitly revealed. Furthermore, the difference in unsprung masses between the front and rear causes significant inertial effect around the wheel hop frequencies. Buj [12] proposed a novel hydro-pneumatic interconnection scheme accompanied with a central unit. The central unit consists of spring and damper valves, which work only under when vehicle experiences pitch and bounce mode oscillations. In addition to central unit, hydro-pneumatic struts are located at each wheel stations and connected to the central unit via hydraulic lines, as shown in Figure 1.5. The experimental study discloses that complete modal decoupling is achieved due to interconnection layout and the central unit, but there was no analytical model investigated for this concept. The study also suggested that implementation of semi-active

damping module will improve the overall performance of vehicle and provide greater design flexibility.

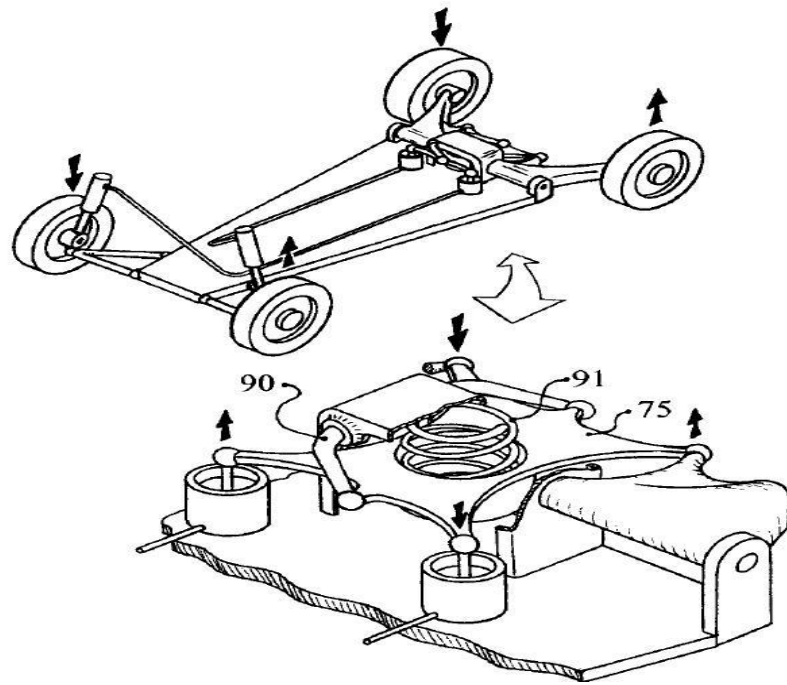


Figure 1.4: Balance plate mechanism [11].

Although above mentioned conceptual schemes are proposed with interconnection between the suspensions with either mechanical linkages or hydraulic pipelines, due to insufficient analysis on tuning damping characteristics— the significance of interconnected systems could not be analyzed much in detail.

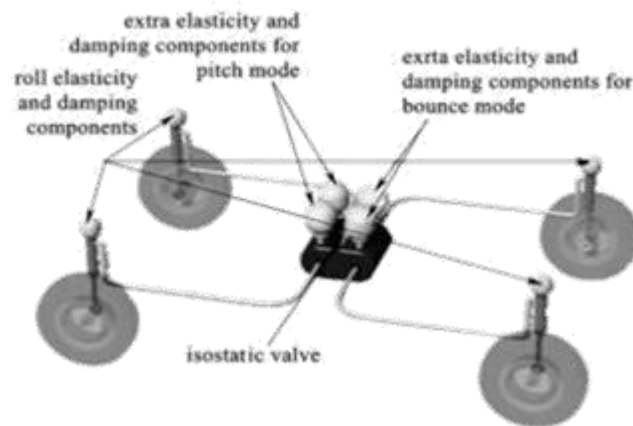


Figure 1.5: Schematic of the conceptual hydraulic scheme [12].

Several studies experimentally analyzed and simulated various damping schemes to enhance the shock attenuation and vibration isolation properties of a suspension, irrespective of the spring element (conventional or gas) considered.

Sharp et al. [13] simulated a quarter car model with conventional spring and damper for different road profiles at different speeds. The study suggested a relatively higher damping coefficient is essential to control the oscillations of vehicle model at lower speeds, whereas relatively light damping is needed for the vehicle when it travels at higher speeds to improve ride performance. Moreover, a higher damping coefficient at higher speeds deteriorates the vibration isolation performance of the vehicle. Karnoop et al. [14] investigated a Single Degree-of-Freedom (SDOF) system incorporated with active suspension and compared it with an equivalent active damper isolation system (semi-active), as shown in Figure 1.6, for the simple harmonic inputs.

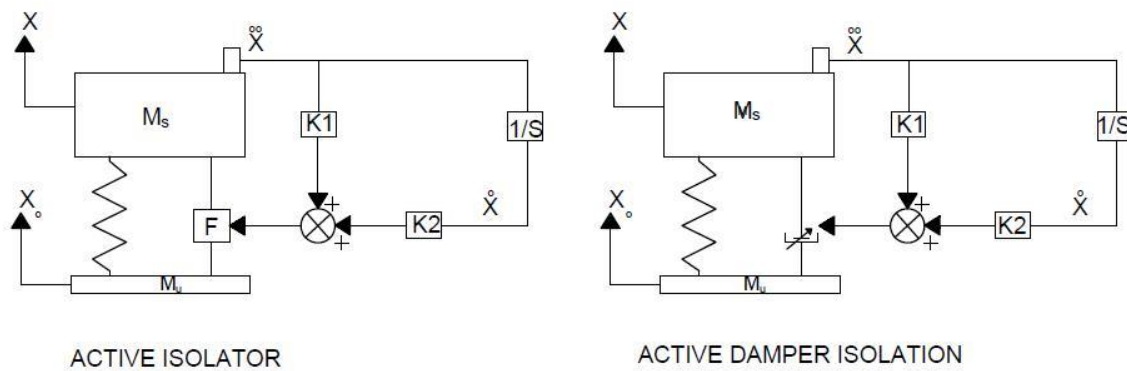


Figure 1.6: Semi active damping schematic [14].

The acceleration gain $K1$ and velocity gain $K2$ produce command signal in the active system. This command signal alters the resultant force of spring and damper units presented in the active suspension unit (F). Whereas in active damper isolation system, the instantaneous values of gain $K1$ and $K2$ change the damping ratio only. The study suggested that performance of an active damper isolation system is a compromised scheme based on cost as compared with the active system. Later, Krasnicki et al. [15] experimentally analyzed an on-off control damper scheme in a SDOF system and compared it with an equivalent passive conventional system. The result obtained from the harmonic analysis shows that on-off damper outperforms passive system only at lower frequencies. In contrast, a different on-off control scheme has proposed with relative velocity as a condition function to switch the modes of damper, but the time delay occurred while switching the modes of damper causes jerks and that could enhance instability of the system [16, 17].

In the meantime, a passive sequential damper model is proposed, as shown in Figure 1.7, and compared its time and frequency domain responses with a constant orifice damper in a quarter vehicle model [18]. Constant orifices progressively exhibit high damping coefficient as velocity increases and provide better shock attenuation performance, but light damping is needed for better vibration isolation performance. Sequential damping could be obtained by adding an external pressure relief valve to the constant orifice, in which preset pressure of the valve depends upon the relative velocity. Besides dissipative force, an additional restoring force is obtained from the proposed damper and gives design flexibility to alter the equivalent suspension rate of the system. Result shows that passive sequential damper provides better shock attenuation and vibration isolation characteristics than equivalent sequential semi-active and constant orifice dampers.

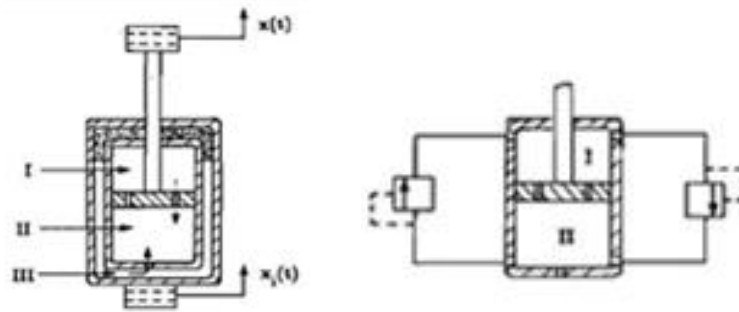


Figure 1.7: Schematic of constant orifice and passive sequential damping [18].

Apart from the above, studies suggested that asymmetric damping would enhance the ride performance of the heavy vehicle as compared with the symmetric damping in the compression and extension region. Asymmetric damping factor is defined as the ratio between the damping coefficient in the rebound and compression region [19]. The studies reveal that asymmetric damping factor should be nearly more than 5 to achieve better ride performance by controlling sprung mass acceleration of the heavy vehicle. Also, it reduces the Dynamic Load Coefficient (DLC) of the vehicle, which is a significant performance measure to avoid rutting of the pavements. [19, 20]. These studies have been further investigated with three different springs (Coil, Leaf and Air spring) in the quarter car model for various terrain conditions at different speeds. Based on simulation, air spring with asymmetrical damper reduces sprung mass acceleration and DLC of the vehicle considerably as compared with the other two springs accompanied with asymmetric dampers. Whereas, the ideal gas law is used to obtain the stiffness rate of air spring is isothermal rather than adiabatic. Besides damper, leaf spring itself creates

damping effect due to interlayer friction, and that changes the equivalent damping coefficient of the suspension.

By following this, Rakheja et al. [21] experimentally analyzed the damper performance of an urban bus to reduce DLC and weighted Root Mean Square (RMS) acceleration of the sprung mass. The laboratory tests for the damper were taken at various amplitudes with the frequency range of 0.5-12 Hz for 50°-70°C. The force-velocity characteristics exhibit higher force in rebound than in compression, irrespective of the excitation frequency. The hysteresis effect was found only at higher frequencies, which is attributed to inertia of the fluid. Additionally, the formulated mean force-velocity curve of the damper reveals that either one- or two stage damping in compression and two- or three-stage in rebound damping was giving optimal damping performance of the suspension for the velocity range from 0 to 0.8 m/s. It was concluded that asymmetric variable damping has improved the performance of the vehicle rather than considering symmetric variable damping. Nevertheless, asymmetric damping will change dynamic equilibrium position of the system and that affects rattle space of the suspension. Furthermore, a study reveals that relatively lower spring rate in extension with rebound biased variable asymmetric damping will improve the ride and handling qualities of a vehicle [22].

1.3.1 Passive Roll Plane Interconnected Suspension

Roll over propensity is mainly related to the off-road and commercial vehicles rather than passenger cars due to their high cg location. In addition to the cg location, the lateral compliance, effective roll stiffness, and tire properties are also to be considered when evaluating dynamic anti-roll performance of the vehicle [23]. The primary overturning moment experienced by the vehicle due to lateral acceleration is the major cause to initiate vehicle roll. In earlier passive suspension designs anti-roll bar and pan hard rod are used to improve the roll and lateral stability of the vehicle, respectively. However, these mechanical linkages only provide auxiliary stiffness, to deliver better stability, with the nominal suspension units employed in the vehicle. A simulation study [24] on the roll plane analysis with conventional springs in a heavy vehicle states that mechanically coupled springs with anti-roll bar, shown in Figure 1.8 (b), improves not only the design flexibility but also reduces the dynamic tire force effectively, as compared with the conventional anti-roll bar suspension system when vehicle experiences roll mode inputs. Though conventional anti-roll bar system yields relatively better anti-roll performance it deteriorates the ride performance at higher speeds due to its additional weight on unsprung masses.

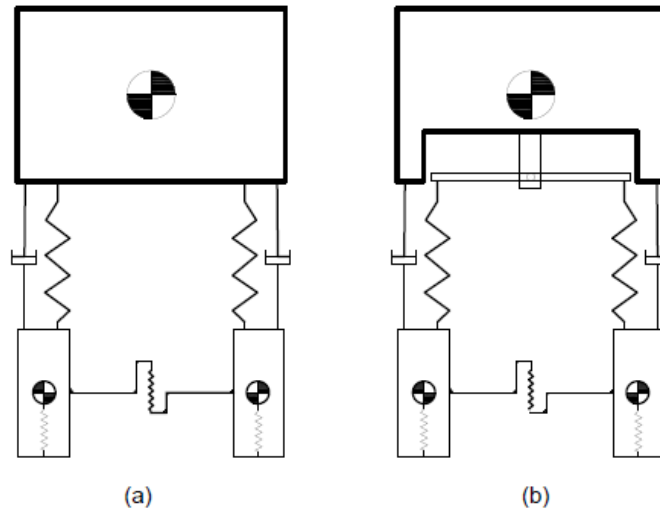


Figure 1.8: Schematic of the suspension configurations: (a) Conventional anti-roll bar system; and (b) Mechanically coupled suspension system [24].

On the other hand, fluidic coupling between the suspension units in the roll plane offers more design flexibility than the mechanically coupled suspension systems [7]. The major cause to opt passive hydro-pneumatic suspension is its variable stiffness attributed to the gas spring. The schematic of a conventional independent hydro-pneumatic strut is shown in Figure 1.9.

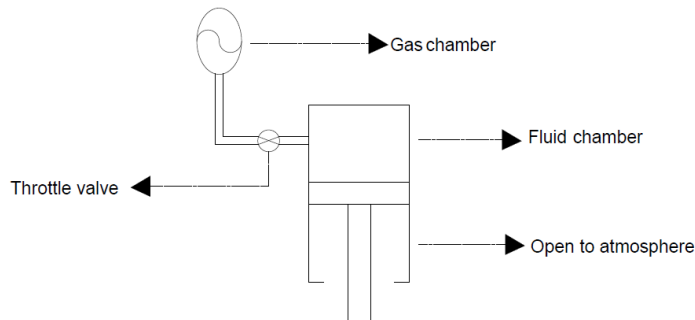


Figure 1.9: Schematic of an individual hydro pneumatic strut [3].

The gas chamber connected via the throttle valve acts as a gas spring, where the spring force could be calculated from the polytropic gas law. Owing to high compressibility of the gas, the spring rates are varied in the compression and extension region, and this would enhance the ride performance of the vehicle as compared with the passive conventional suspension systems [22]. Felez et al. [3] investigated independent and interconnected hydro-pneumatic suspensions in a crane vehicle, as shown in Figure 1.10. In interconnected configuration, the clockwise angular

movement of the sprung mass could be stabilized by the increase of pressure in the upper chamber of the right strut due to flow across the struts. Thus, the roll plane interconnected (IC) configuration offers better roll control performance than the independent configuration.

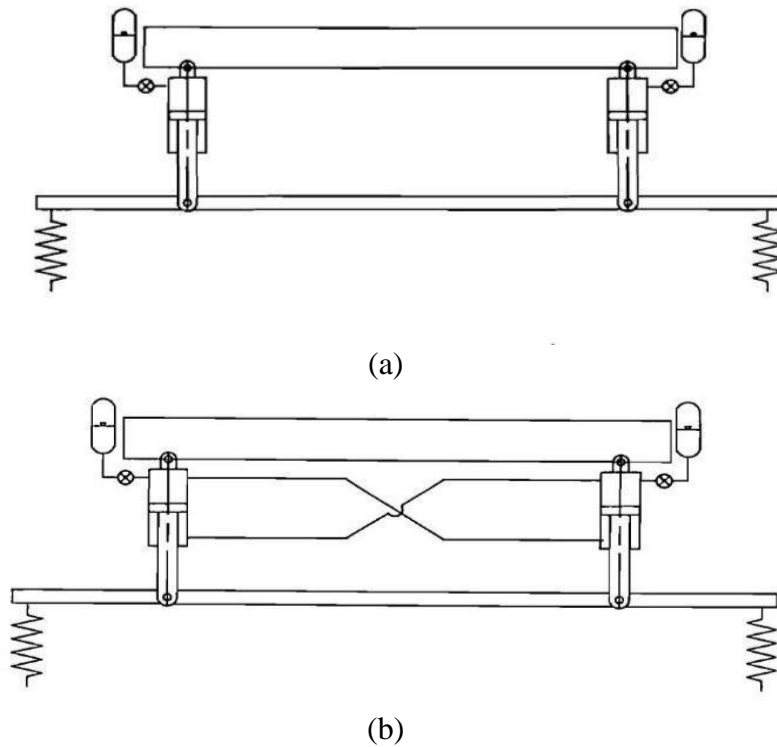


Figure 1.10: Schematic of a passive hydro-pneumatic suspension: (a) independent cylinder suspension; and (b) interconnected suspension [3].

A newer model of independent hydro-pneumatic strut has been investigated, to improve the roll stability of a tracked vehicle, as shown in Figure 1.11 [25]. Unlike the earlier studies [3], gas chamber volume has been varied by the displacement of the floating piston. Moreover, these independent hydro-pneumatic struts exhibit relatively larger effective area than the IC hydro-pneumatic suspension [4, 7, 25]. Thereby, the static equilibrium pressure of the suspension system has been reduced considerably. However, a newer model of interconnected hydro-pneumatic strut with comparatively larger effective area, shown in Figure 1.12, delivers more design flexibility in tuning the suspension properties [26].

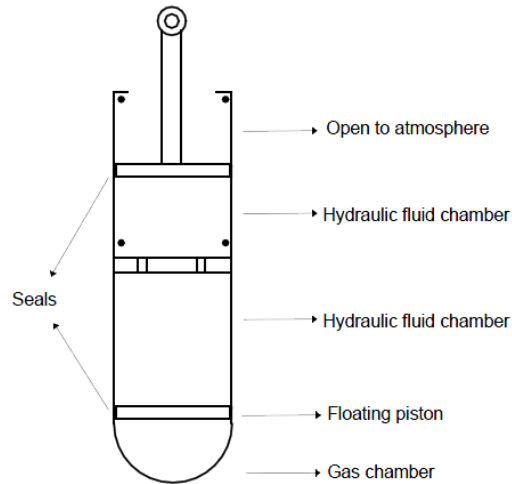


Figure 1.11: Schematic of the hydro pneumatic strut [25].

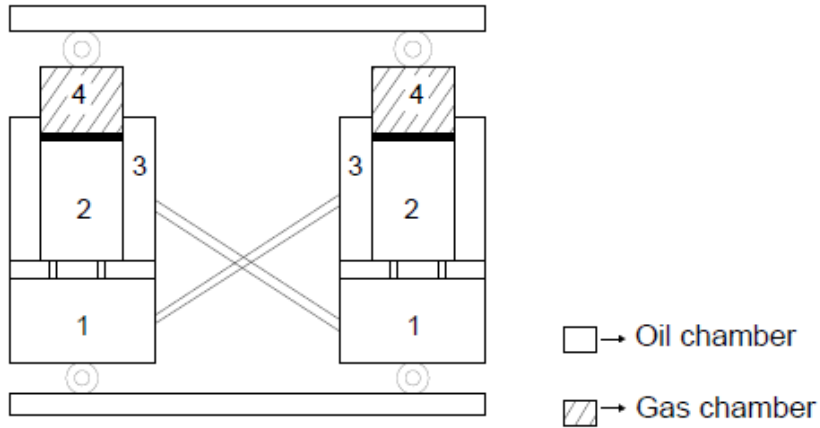


Figure 1.12: Schematic of the interconnected hydro-pneumatic suspension [7, 26].

Also, the studies [7, 26] suggested that interconnected hydro-pneumatic struts exhibit higher effective roll stiffness, as compared with the equivalent unconnected hydro-pneumatic suspension struts due to fluid flow across the struts. As a result, IC hydro-pneumatic suspensions possess better anti-roll performance when vehicle subjected to a lateral acceleration inputs. Furthermore, increase in annular area of the IC hydro-pneumatic strut enhances the effective roll stiffness of the suspension unit [4, 27].

The flow-resistance occurs across the orifices and struts is the prime cause to yield pressure differentials, and thus the resultant damping force. Liu et al. [28] investigated constant orifice and variable damping scheme in the conventional IC hydro-pneumatic struts, as shown in Figure 1.13. Firstly, the constant orifice damping scheme exhibits nearly quadratic force-velocity

characteristics; secondly, the variable damping scheme includes the passive preset pressure-relief valve which actuates under the thresholds of pressure differentials obtained across the valves. These valves are particularly used to reduce the high speed force-velocity characteristics and the schematic of pressure-relief valve mechanism is shown in Figure 1.14 (a).

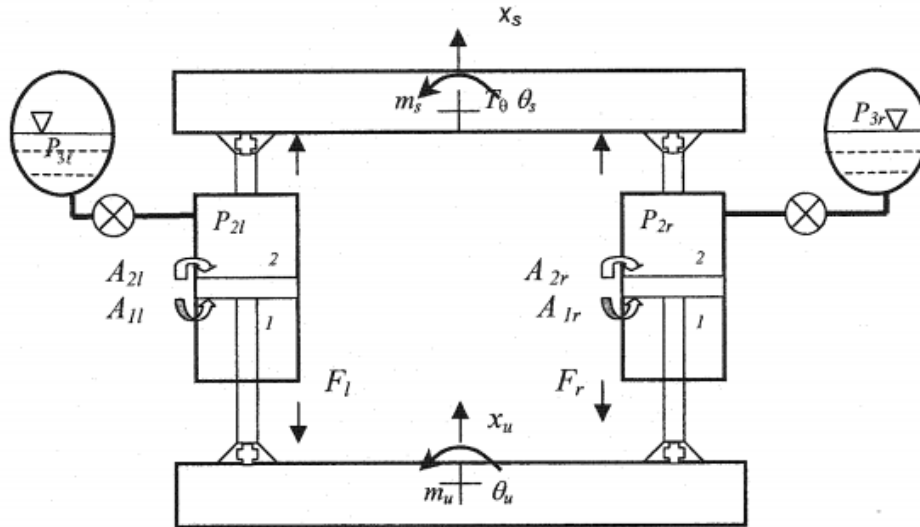
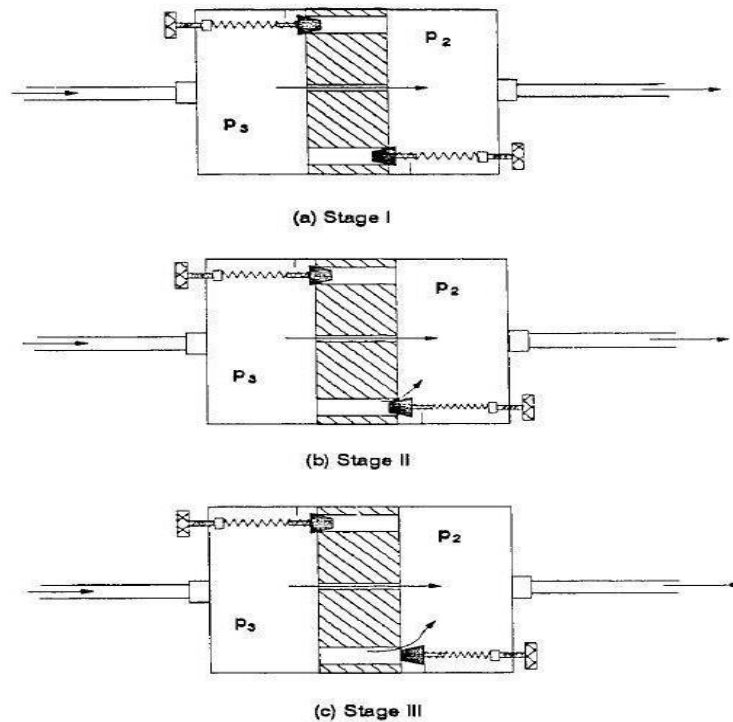
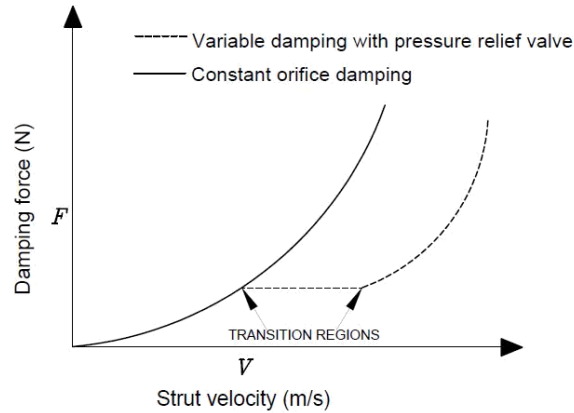


Figure 1.13: Schematic of the conventional interconnected hydro-pneumatic suspension [28].



(a)



(b)

Figure 1.14: Variable damping: (a) mechanism of the preset pressure relief valve; and (b) force-velocity characteristics of the IC hydro-pneumatic suspension [28].

As an example, the force-velocity characteristics of a hydro-pneumatic strut when equipped with passive pressure relief valve is shown in Figure 1.14(b). However, the presented analytical models were not provide the smooth transitions nearby the transition regions [28, 29, 30]. The result shows that constant orifice scheme exhibits better shock attenuation performance and the addition of pressure-relief valve improves the design flexibility in tuning the damping characteristics. Also, the addition of valves in interconnection reduces the total system mean pressure and stress between the hydraulic chambers as compared with the constant orifice damping [31]. A newer analytical model of a shim-stack valves employed in a hydro-pneumatic struts has been investigated to improve the damping characteristics especially near the transition regions to yield continuous damping force. The schematic of the single gas chamber hydro-pneumatic strut equipped with shim-stack valve is shown in Figure 1.15 [32].

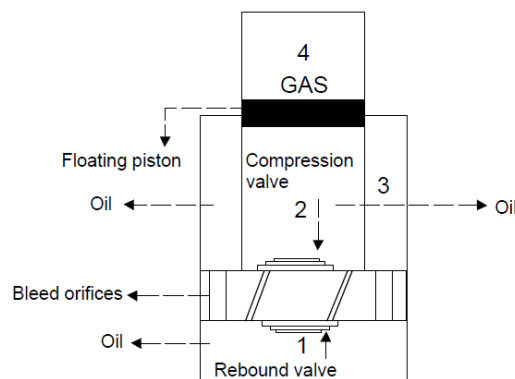


Figure 1.15: Schematic of single gas chamber struts with shim-stack valves [32].

However, the valve loss co-efficient and variation in discharge co-efficient of the shim-stack valve have not been explained in detail. A study stated that roll plane interconnected hydro-pneumatic struts (Figure 1.12) exhibit larger roll mode damping force than the equivalent unconnected configurations due to negative feedback effect in damping [26]. These negative damping force components chiefly depend on parameters, namely, orifice area, fluid flow rate, discharge co-efficient, interconnection pipe diameter and the hydraulic fluid density. It is also noted that vertical or roll stiffness of the interconnected struts are highly depends on the bulk modulus of the hydraulic fluid, when fluid compressibility is considered [8]. Smith et al. [33] investigated hydraulically interconnected suspension (HIS) system and simulated in a half car model, as shown in Figure 1.16.

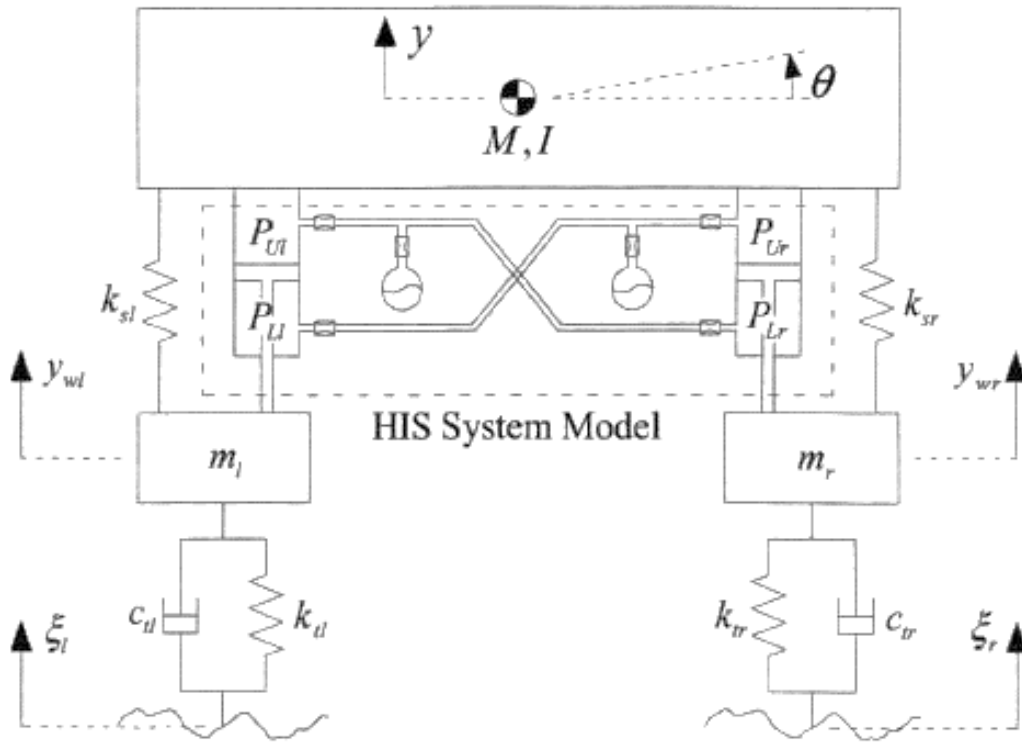


Figure 1.16: Schematic of the HIS system in a half-car vehicle model [33].

Unlike previous studies [eg 7, 26, 32], valves and gas units are located in the interconnection lines to provide restoring and dissipative forces with the conventional springs. The results from the simple harmonic analysis states that mean system pressure, position of the valve, valve loss co-efficient, gas egg volume and fluid viscosity are the essential parameters to tune the stiffness and damping properties of the suspension. However, there is no detail on estimating valve

characteristics and the valve loss co-efficient. In addition, the conventional springs accompanied with hydro-pneumatic suspension system could reduce the system pressure but the presence of conventional springs deteriorate the anti-roll performance of its counterpart, when vehicle experiences transient lateral acceleration inputs [6]. Smith et al. [34] suggested that valves located near the cylinders, in the HIS system, are highly effective when vehicle subjected to roll; thus, the relatively larger roll damping moment is obtained. Whereas, valves presented near the gas units are highly effective when vehicle experiences bounce mode inputs. As a result, roll mode damping property of the HIS system could be independently tuned without altering the vertical mode force-velocity characteristics. Furthermore, the two different roll-plane interconnection configurations of the HIS system, as shown in Figure 1.17, are investigated when the half-car vehicle model experiences transient roll inputs. The results suggested that anti-synchronous arrangement, as shown in Figure 1.17(a), enhances the vehicle to roll due to the configuration layout. When interconnection is being done across the pistons, the anti-oppositional arrangement reduces the roll motion of the vehicle effectively, as compared with the anti-synchronous configuration [35, 36].

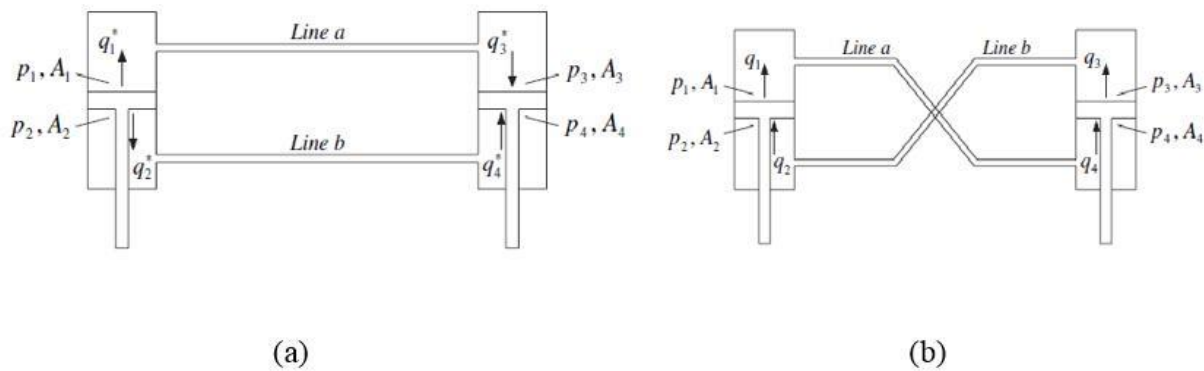


Figure 1.17: HIS roll-plane interconnection layout; (a) anti-synchronous arrangement; and (b) anti-oppositional arrangement [35, 36].

Cao et al. [37] analyzed interconnected twin gas chamber hydro-pneumatic struts in the half-car vehicle model to improve its anti-roll performance. Unlike single gas chamber hydro-pneumatic struts, the struts shown in Figure 1.18, exhibits nearly symmetrical suspension rate in the compression and extension regions. However, the gas chambers volumes should be adjusted, so as to yield the identical suspension rates based on the gas law considered. Due to the addition of gas chamber, the roll and vertical stiffness rates of the twin gas chamber struts are relatively lower than the struts as indicated in Figure 1.15 [38]. Moreover, the negative feedback coupling

effects between the twin gas IC hydro-pneumatic struts are relatively weaker when the pneumatic chambers are connected between each other, as shown in Figure 1.19 [39].

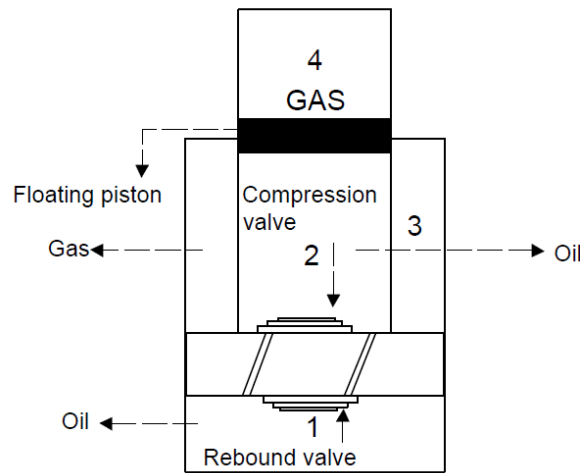


Figure 1.18: Schematic of twin gas chamber struts with shim-stack valves [37].

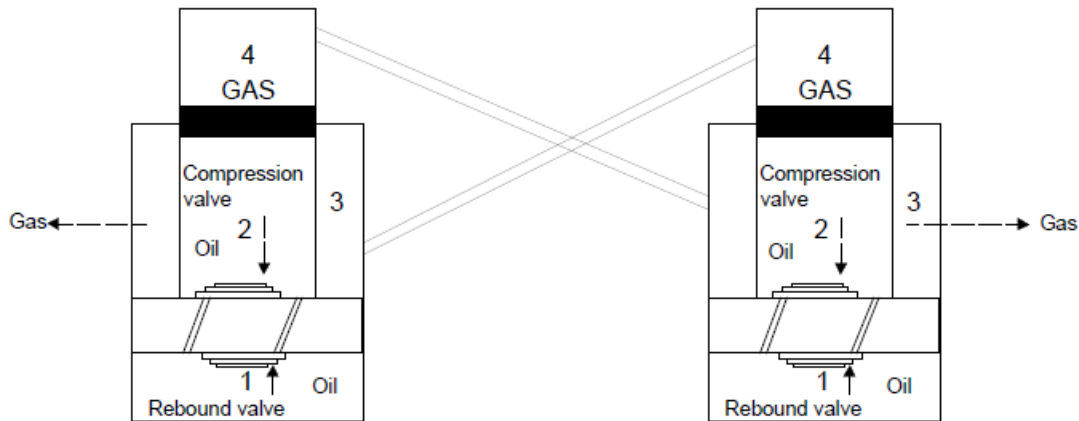


Figure 1.19: Schematic of the interconnected hydro-pneumatic twin gas chamber struts [39].

1.1.2 Active Roll Plane Interconnected Suspension

Active suspension systems are rarely investigated in a roll plane, as a benchmark prototype, due to its high operating and capital cost. Though active suspensions have many limitations in view of its application, the performance of these systems are relatively better under subjective analysis. Few studies [40, 41] investigated active anti-roll bar with a feedback control unit, as shown in Figure 1.20. The active anti-roll bars are connected to the rotary actuators, and its angular displacement is controlled by the hydraulic subsystem consisting of reservoir, pump and directional control valve. The lateral acceleration signal perceived by the sensors located at cg of

the vehicle, is send to the control unit and the control command is passed to the valve block which controls the rotational displacement of the actuator. The high operating and capital costs for the hydraulic pump and control unit, however, limits the application of such concept in mass produced vehicles.

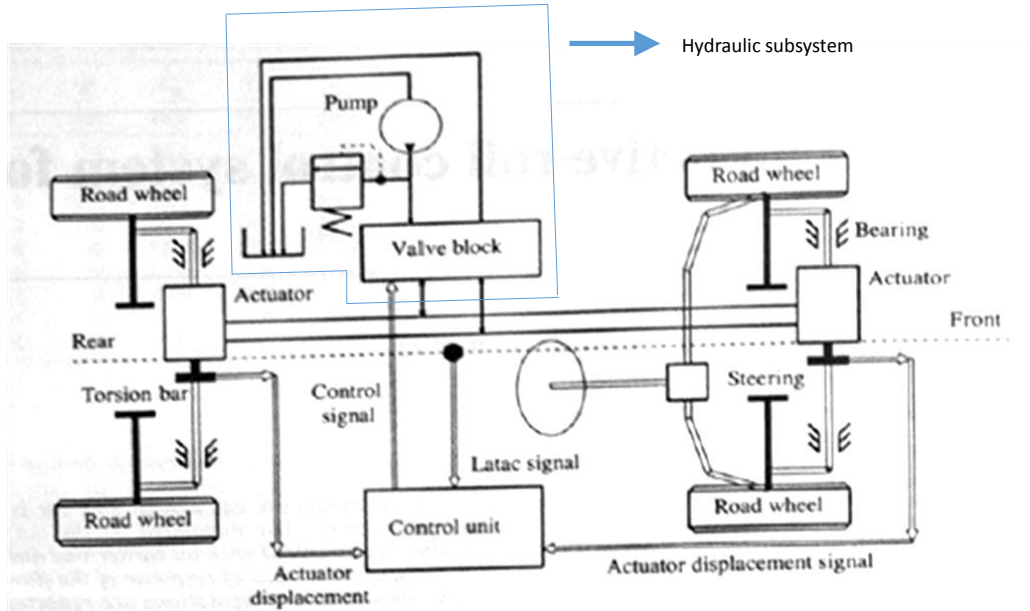


Figure 1.20: Schematic of an active roll control system [41].

As an improvement to the physical concept, the rotary actuators utilized above could be replaced by the linear actuators to reduce the cost of the hydraulic subsystem. It has also been shown in [42] that the presence of linear actuators enhance the design flexibility to improve the restoring roll moment for a given actuator pressure. The restoring roll moment M_A using linear actuators, can be easily controlled by changing the length of lever arm as illustrated by,

$$M_A = \frac{PL\pi d^2}{4} \quad (1.1)$$

where L is the length of the lever arm which connects the tie rod and actuator, d is the effective diameter of the actuator, and P refers to the operating pressure of the hydraulic system.

Rosam et al. [43] experimentally investigated active anti-roll bar with interconnected hydra-gas suspension units. While the primary interconnection layout, as shown in Figure 1.21, provides better anti-pitch performance, an addition of hydraulic subsystem and shuttle device connecting the left and right suspension form the active anti-roll control unit. The shuttle device, shown in Figure 1.22, provides a larger restoring rolling moment by displacing hydraulic fluid to one side

of the vehicle, based on the acceleration demand signal send through the control unit. Thereby, a relatively larger spring rate would be obtained due to the compression of gas chamber in the hydra-gas suspension units. Owing to progressive stiffness and damping characteristics, the performance of active anti-roll control unit in the hydra-gas suspension is highly economical, as compared with the other conventional active anti-roll bar systems [eg 40, 41].

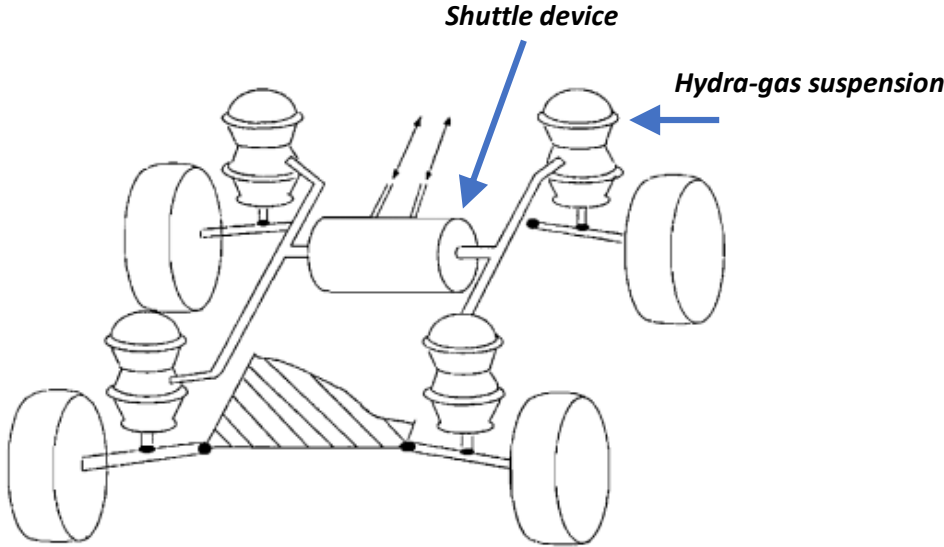


Figure 1.21: Hydra-gas roll control system [43].

However, in such system the inherent time delay attributed to hydraulic lines, produces jerks in the system. Furthermore, the leakage of oil in the shuttle device could form emulsion which is likely to make the device less effective to control roll of the vehicle.

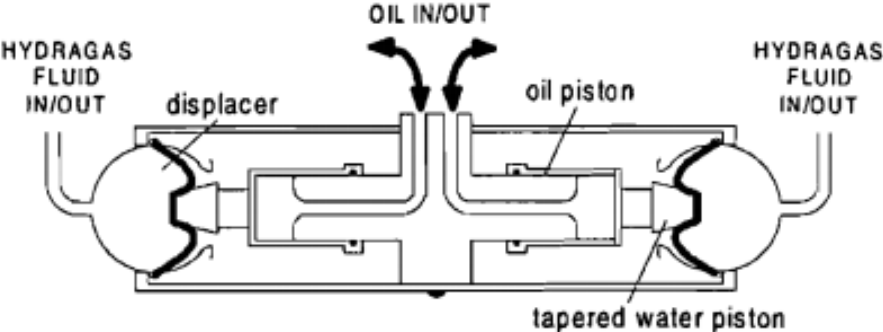


Figure 1.22: Schematic of the Hydra-gas roll control shuttle [43].

Cronje et al. [44] introduced an active anti-roll bar (AARB) system with four different suspension settings. The stiffness and damping characteristics of the suspension units are altered to provide better ride comfort without deteriorating the anti-roll performance of the AARB system. The study of an SUV claims that AARB system mitigates the roll angle considerably, while performing double lane change maneuver. The mechanism for suspension settings are not detailed or explained in the study. A new active roll control device in a half-car vehicle model, shown in Figure 1.23 was investigated by Wang et al. [45] is referred to as Demand Dependent Active System (DDAS). The DDAS consists of two different hydraulic circuits, namely, circuit I and circuit II. Circuit I consists of actuators and interconnection pipelines, and termed as mode-select circuit. The connections in the Circuit I could be altered to control the desired mode (roll or pitch) of the vehicle. Whereas, circuit II represents the force-control unit which consists of controllers and proportional pressure relief valve. The experimental results generated from the fishhook maneuver of a vehicle show that time delay inherent in the hydraulic system leads to increase in the roll mode natural frequency of the sprung mass from 2.5 to 3 Hz. To avoid this condition, a relatively higher proportional gain should be considered for the controller unit which in turn may lead to an increases in the response overshoot of the system. Also, the study suggests that circuit II could be replaced with an electrically controlled force unit in order to reduce the time delay, which may impose additional costs.

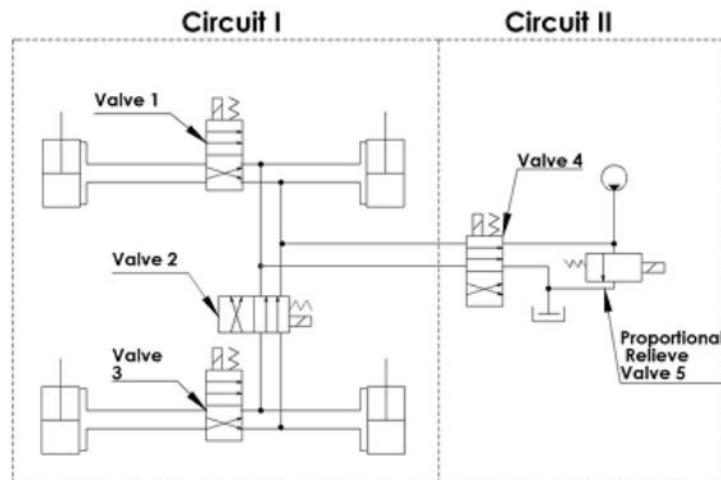


Figure 1.23: Schematic of the hydraulic and force control circuits of DDAS [45].

1.1.3 Pitch Plane Interconnected Suspension

Design and analysis of interconnected suspension in the pitch-plane are in general more cumbersome in comparison to the roll-plane interconnection due to the fact that the load distribution on the front and rear suspension units of road vehicles are not equal. Furthermore, difference in vertical input at the front and rear axle introduces pitch mode oscillations which if persists is considered annoying from passengers ride perspective. In practice, a limited control of the pitch vibrations is realized at low speeds by introducing different spring rate at the front and rear axles. Such design essentially attempts to increase the natural frequency of the rear sprung mass in comparison to the front end of the vehicle. Olley [46] suggested that the suspension rate of the front suspension should be 30% lower than the rear suspension rate in order to suppress the dominance of pitch motion by converting it to more tolerable bounce motion. Higher suspension rate at the rear on the other hand will not provide smoother ride, due to larger vertical accelerations of the sprung mass, when vehicle traveling at lower speeds (Less than 15 kmph) [47, 48]. Crolla et al. [49] investigated a four-DOF pitch-plane passenger vehicle model to improve its anti-pitch and ride performance. The results show that cg location and front/rear stiffness ratio are the prominent design parameters to improve anti-pitch performance, without affecting ride comfort of the vehicle when wheel base filtering effect is considered. Additionally, the front/rear stiffness ratio should be less than unity to reduce the pitch acceleration considerably. In brief, a relatively softer front suspension yields improved pitch mode oscillations. However, owing to lower suspension rate in the front necessitates an anti-roll bar to suppress the roll oscillations of the vehicle.

As an alternative to differential spring rate, as well as to control excessive pitch motions of road vehicles in braking and acceleration due to soft suspension, researchers have been exploring the interconnection of suspension in the pitch plane. Odhams et al. [50] analyzed a conventional mechanical pitch interconnection scheme in a passenger car to improve the ride comfort and reduce the pitch attitude of the passenger vehicle by evaluating different performance measures. The vertical and pitch mode suspensions are connected between the sprung mass and a rigid mechanical linkage, as seen in Figure 1.24. The value of the body mode coupling parameter, L_k determines the coupling effect of pitch and vertical mode oscillations of the vehicle model.

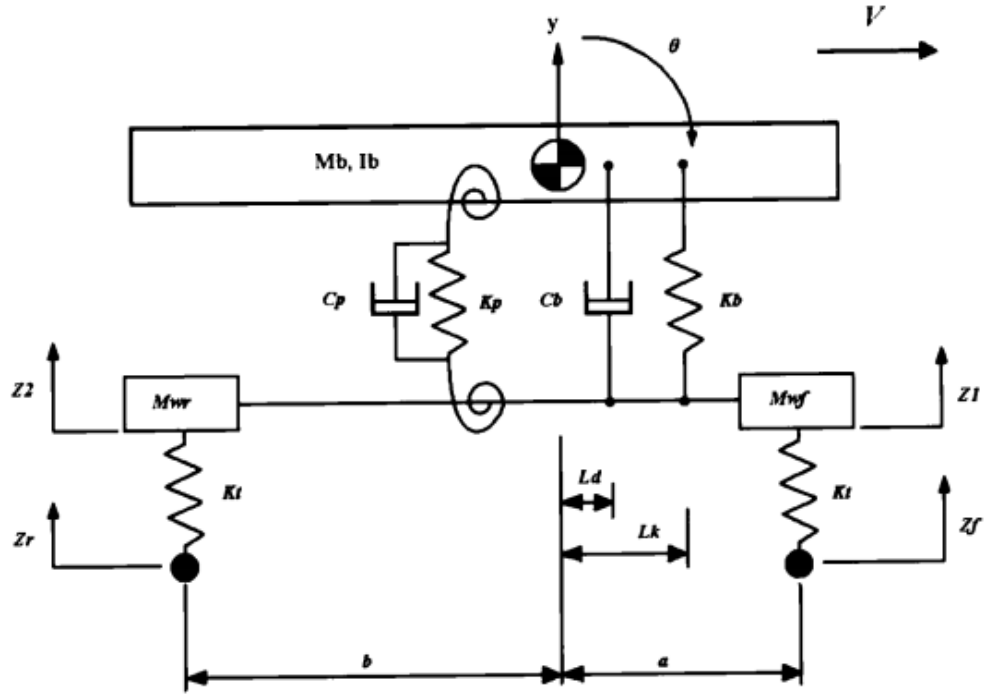


Figure 1.24: Schematic of the pitch-plane mechanically coupled suspension [50].

The study shows that bounce mode spring, (Kb) should be located near-midway between the front and rear axles to minimize dynamic tire force: whereas, vertical acceleration of the sprung mass could be minimized by placing the bounce mode spring near to front end of the car. Also, these performance measures could be calculated more precisely by considering the time delay (wheelbase filtering effect), experienced between the front and rear inputs of the vehicle [51].

Moulton et al. [52, 53] introduced two different fluidic pitch-plane interconnected suspension scheme in a saloon car to evaluate the suspension properties, as compared with passive conventional suspensions. The pitch plane interconnection layout of the two different configurations, namely, Hydrolastic and Hydragas under bounce and pitch motions are shown in Figure 1.25. In both the configuration, under pure roll or bounce excitation, there is no flow of working fluid between the chambers. Under pitch mode input, however, as shown, the front wheel causes the taper piston to transfer a large amount of hydraulic working fluid to the rear wheel; thereby, either rubber (hydrolastic) or gas spring (hydragas) units at the front suspension compress slightly as compared to the rear unit which expand significantly compensating for the pitch motion.

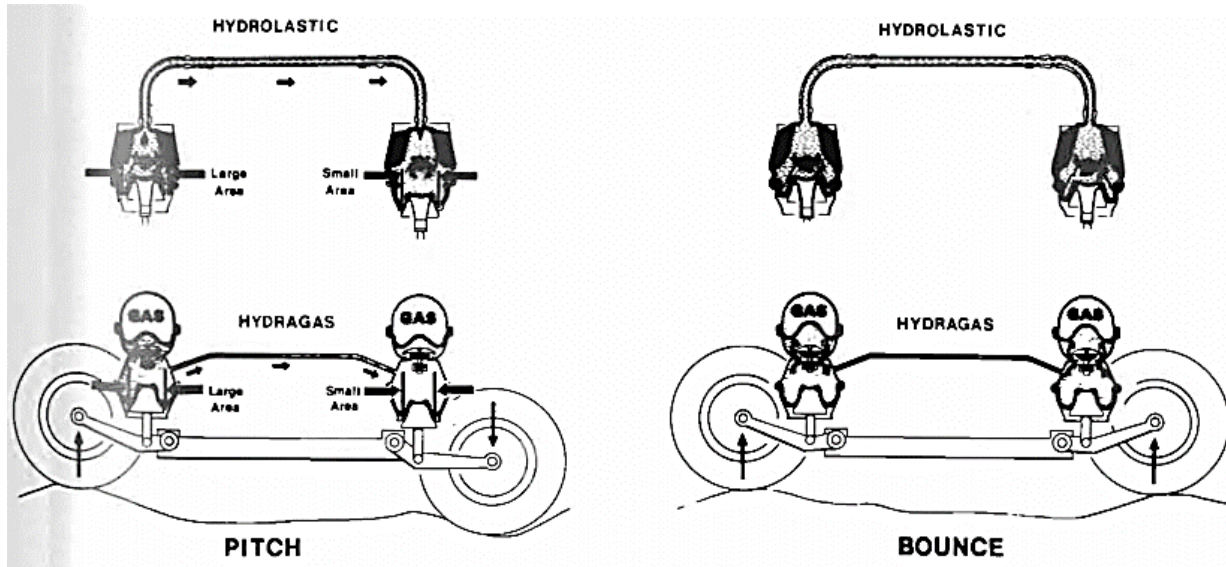


Figure 1.25: Schematic of the pitch plane interconnection layout of the hydrolastic and hydra gas suspension configurations [52, 53].

In addition such suspension mechanism exhibits progressive stiffness, and thus eliminates the need for anti-roll bar in the suspension design. Thus the fluidic pitch interconnections eliminate the addition of anti-roll bar in the suspension units. The interconnection in the hydrolastic suspension is above and the hydraulic lines and are connected in series with the rubber flap valves, which is employed to achieve variable damping characteristics in the individual suspension units. Whereas, in hydragas system, the interconnection is under port and in parallel with the dampers present in the suspension unit. Apart from this, the prime difference between the hydragas and hydrolastic is essentially the use of die-cast housings instead of pressed steel clips, respectively. The study further states that pitch plane interconnection with hydra-gas suspension units also decouples the pitch and bounce mode oscillations based on the pitch rate moment ratio defined in the following.

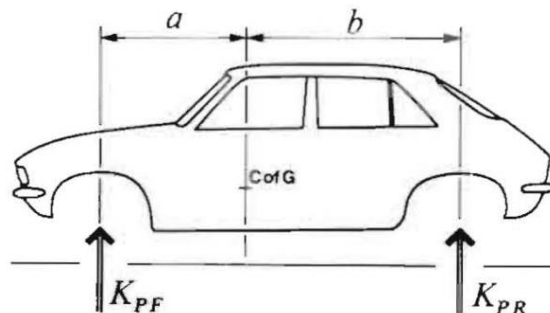


Figure 1.26: Free body diagram of the saloon car with its reaction forces [53].

The decoupling parameter, Pitch Rate Moment Ratio (PRMR) of the vehicle suspension unit could be calculated from the following:

$$PRMR = \frac{aK_{PF}}{bK_{PR}} \quad (1.2)$$

where K_{PF} and K_{PR} are the front and rear suspension rates of the suspension units, respectively. Whereas, a and b are the distances measured from the cg location of the vehicle to the front and rear wheel centers, as shown in Figure 1.26, respectively. The result obtained from the deterministic profile inputs shows that the vehicle predominantly experiences bounce mode oscillations if the PRMR is below 0.8. Whereas, a relatively larger suspension rate in the front yields excessive pitch mode oscillations with a PRMR greater than unity. Furthermore, the vehicle decouples the pitch and bounce mode oscillations when PRMR is equals to unity.

Cao et al. [54] investigated the properties of four different hydro-pneumatic suspension configurations with single and twin gas chamber struts in the pitch plane, as shown in Figure 1.27. The results show that configurations *A*, *B*, and *C* exhibit negative feedback effects of the couplings involving gas chambers 3 of the struts. Whereas, the configuration *D*, exhibit relatively lower pitch stiffness due to the positive feedback effects of the couplings. Furthermore, the hydraulic and hybrid coupling configurations (*B* and *D*) retain higher pitch damping moment and that offers benefits in reducing the pitch attitude and suspension travel when the vehicle experiencing straight-line braking inputs [55]. Later, Cao et al. [56] analyzed the twin gas chamber struts in a pitch plane interconnection layout. The results obtained from the braking torque inputs show that twin gas chamber struts could reduce the stopping distance effectively due to symmetrical pitch suspension rates in the compression and extension regions. On the other hand, tuning of pitch mode suspension properties does not affect the vertical mode restoring and damping properties of the interconnected struts [57]. This shows that fluidic interconnections reduce coupling between the bounce and pitch mode suspension properties and offer considerable design flexibility.

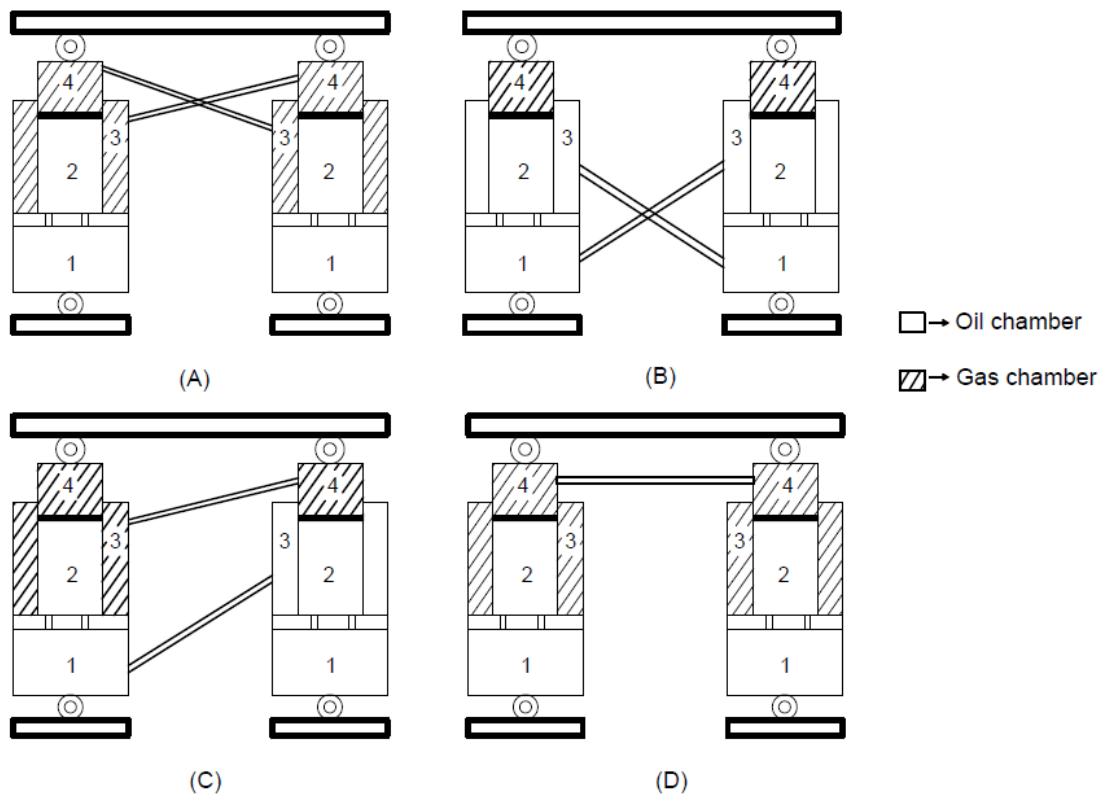


Figure 1.27: Various pitch plane interconnected hydro-pneumatic suspension configurations [54].

1.1.4 Experimental analysis of a hydro-pneumatic suspension

Though various analytical models of interconnected hydro-pneumatic suspension provided general insight and understanding of their potential performance, and theoretical characteristics of the suspension units, very few studies attempted experimental validation or evaluation. Among few, Rosam et al. [58] experimentally evaluated interconnected hydragas suspension units in a roll plane to improve the anti-roll performance of a saloon car. The test setup shown schematically in Figure 1.28, consists of accelerometers and transducers which are used to measure suspension accelerations (Roll, Yaw and Lateral) and deflections at each wheel stations. The roll angle of the vehicle body was determined by finding the difference between the suspension deflections on each side of the vehicle, and the suspension track width. The test results obtained from the steerpad maneuver at 30 *km/hr* show that interconnected hydragas suspension can limits the body roll angle and lateral oscillations. In addition, polytropic index of the gas process identified as 1.45 is shown to provide best fit for the experimental results. Further experiments were performed using the interconnected hydragas suspension units, for simple harmonic study to

characterize bilinear and linear stiffness/damping coefficients over the frequency range 0 to 10 Hz with the amplitude varying from 2 to 10 mm [59]. The results were obtained under both static and dynamic conditions using load cells and pressure gauges as shown in Figure 1.28.

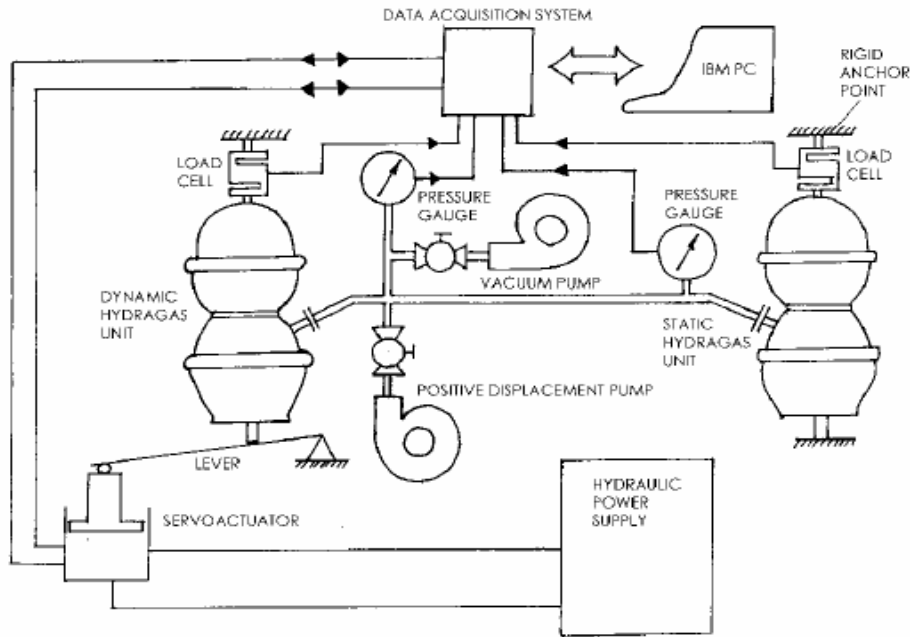


Figure 1.28: Schematic of the interconnected Hydragas suspension test setup [58, 59].

The experimental results show that bilinear model predicts the experimental behavior of the suspension units well at very low frequencies, however, at higher frequencies, fluid compressibility and inertial effects should be considered in the modeling to predict more accurate results. In addition, the force-velocity characteristics of the hydro-pneumatic strut could also vary with varying hydraulic oil temperature, especially when it lies above 75°C [60].

In another study, Wilde et al. [61] investigated anti-roll performance of the Honda CRV for different suspension settings by altering stiffness and force-velocity characteristics of the kinetic H2 suspension. The kinetic H2 system, as shown in Figure 1.29, consists of ten damper valves, four double acting hydraulic cylinder, two accumulators, and flexible hoses. These flexible hoses supersede hydraulic pipelines to allow free motion of the hydraulic cylinders.

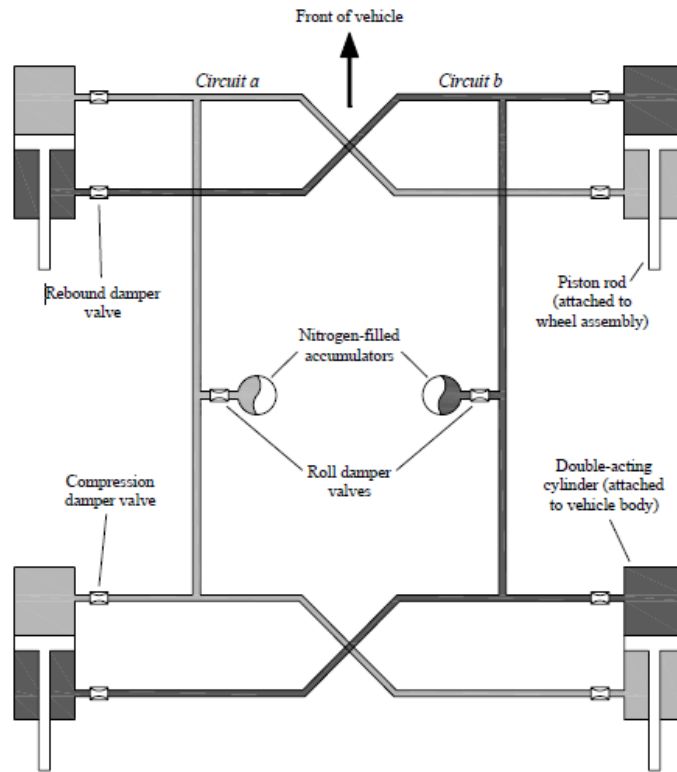


Figure 1.29: Schematic of the anti-roll mode kinetic H2 suspension [61].

Moreover, the damper valves located near the cylinders are mainly responsible to provide damping in bounce motion of the vehicle; whereas, the valves located near the accumulators are mainly active when the vehicle experiences roll mode inputs. The test results from the fishhook maneuver, at the vehicle speed of 70 km/hr , show that anti-roll performance of the kinetic H2 suspension is comparatively better than the conventional anti-roll bar system, and this is due to higher roll stiffness and damping inherent in the kinetic H2 suspension system. Smith et al. [10] experimentally analyzed hydraulically interconnected suspension (HIS) system, with two different interconnection layouts, namely, anti-opspositional and anti-synchronous, in a test rig by varying roll inertia and mean pressure of the system. The schematics shown in Figure 1.30 (a) and (b) give the layout for the actuators and their interconnections for the anti-opspositional and anti-synchronous configurations, respectively. Here, the pipelines with relatively smaller diameter is used to connect across the struts, while the damper valves and accumulators are located on the pipelines. The experimental results from the frequency domain study was used to illustrate the highly complex nature of the valve damping characteristics. Hence, the estimation of the roll and vertical damped natural frequencies of the sprung mass is also difficult. Simulation of flow through

valve using CFD package would yield appropriate valve characteristics, and thus used to predict the behavior of the HIS system.

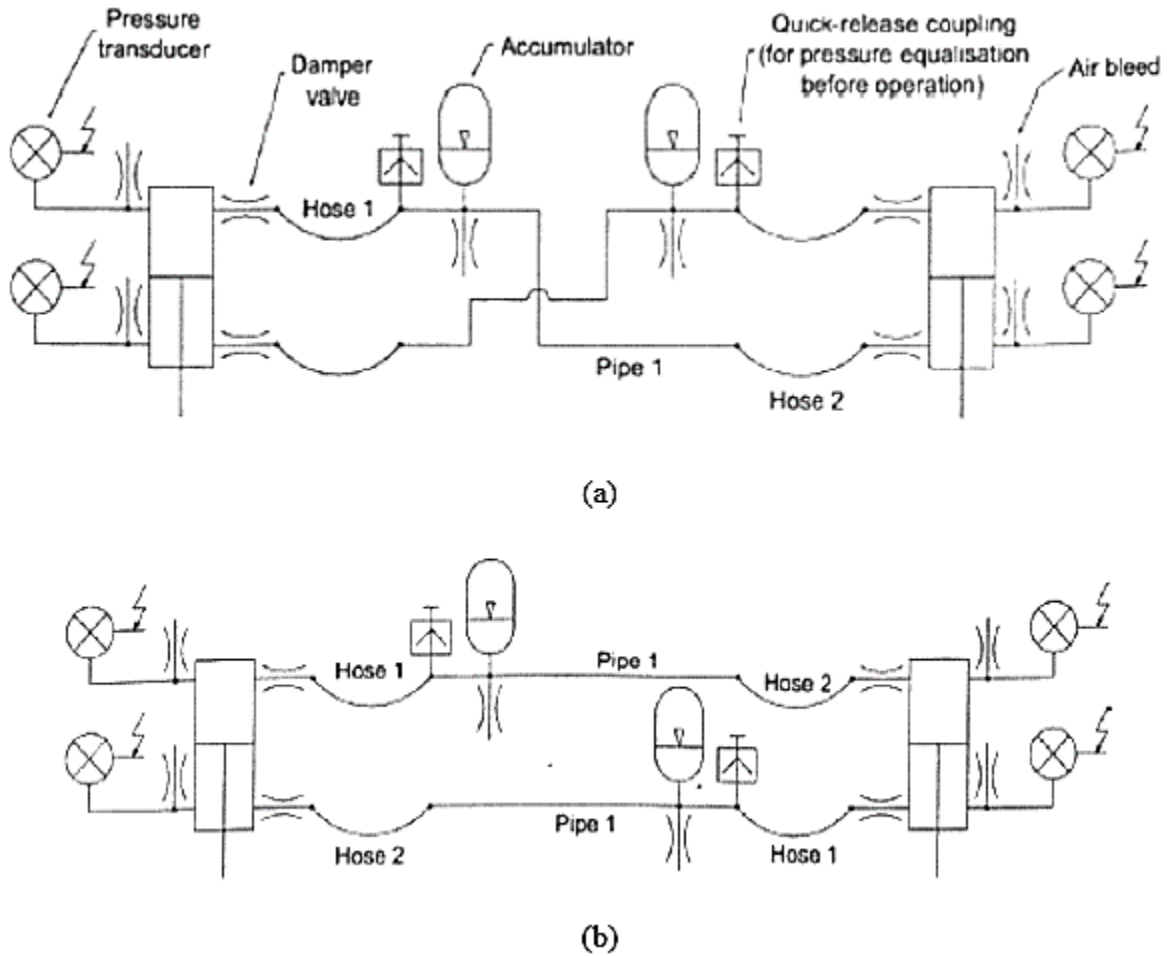


Figure: 1.30 Schematic of HIS interconnection arrangement: (a) anti-oppositional; and (b) anti-synchronous [10].

The results of the study also demonstrate that anti-oppositional arrangement provides better anti-roll performance than the anti-synchronous arrangement. This is attributed to larger fluid flow rate when the interconnection is across the piston of suspension units. It is thus concluded that the diameter of the connecting pipe influencing both damping and stiffness parameters of HIS system will play significant role in the design and performance.

Later, HIS system with anti-oppositional arrangement fitted in a SUV is experimentally investigated to evaluate its performance in a constant steer maneuver [62]. The test results show that HIS system with conventional springs can provide improved vehicle roll angle when compared

with conventional anti-roll bar systems. Moreover, the additional torsional stiffness due to the presence of anti-roll bar reduces the suspension travel and increases lateral oscillations, whereas, these oscillations could be eliminated when HIS system is installed in the vehicle. Furthermore, the reduction in suspension travel owing to anti-roll bar exhibits an increase in the dynamic tire load. Zhou et al. [63] investigated an anti-warp HIS system in an off-road vehicle in order to control lateral oscillations and dynamic tire load of the vehicle. The test results show that though anti-warp interconnection could mitigate the lateral oscillations and dynamic tire force without affecting the ride comfort, these performance measures could also be realized by employing anti-roll HIS system due to its relatively higher damping in the roll mode. Hua et al. [64] investigated air spring retained roll-plane interconnected HIS system in a coach bus to enhance the anti-roll performance and compared those results with the equivalent anti-roll bar system. The results from the pylon course slalom field test show that HIS system with air spring vary the roll natural frequency of the coach bus by varying the mean system pressure of the suspension.

In brief, HIS and Kinetic H2 suspensions offer the potentials to significantly improve road vehicle anti-roll performance. However, importance must be given in selecting the size of interconnecting pipes and the usage of external valves in the pipelines. It will also be necessary to characterize the valve loss coefficients appropriately in order to predict the system behavior, particularly at higher frequencies. Moreover, for practical applications, it may be necessary to reduce the effective area of the double acting hydraulic cylinders as compared with those investigated in [7, 32]. It may therefore be necessary to adopt additional spring element in order to carry the static load, particularly for the heavy vehicles.

1.2 SCOPE OF THE INVESTIGATION

The experimental and theoretical studies mentioned in the literatures expounded that roll plane IC hydro-pneumatic suspensions offer better anti-roll performance without compromising the ride comfort, particularly for the heavy vehicles. The properties of IC hydro-pneumatic suspensions could be further improved by altering stiffness and damping characteristics of the struts. Owing to progressive suspension properties, the characteristics of hydro-pneumatic suspension could be highly improved by tuning the design variables which are associated with the force components of the corresponding strut. Addition of valves could be used to tune the damping characteristics of the hydro-pneumatic struts. The valves installed in the pipelines could further enhance the

performance of interconnected hydro-pneumatic struts due to its inherent negative feedback effects. Alternatively, implementation of Ride Height Valves (RHV) in the hydro-pneumatic suspension would alter the restoring property of the struts owing to payload variations. Despite payload variation, the use of RHV will allow the suspensions to yield nearly constant sprung mass natural frequency as well as maintain a ride height irrespective of the variation in static load. Furthermore, an extensive parametric study of all the above parameters can be undertaken to realize desirable load carrying capacity and dynamic characteristics of the strut.

1.3 OBJECTIVE OF PRESENT INVESTIGATION

The roll-plane interconnected configurations, could be identified from the interconnection layouts, are evaluated and commented based on the deterministic and frequency responses of the system. The specific objectives of this thesis are:

1. To synthesize roll plane models of vehicle employing unconnected and interconnected hydro-pneumatic suspensions, in terms of their restoring and dissipative force components.
2. To analyze the effect of ride height valves and fluid compressibility while evaluating stiffness property of the corresponding suspension configurations.
3. To improve anti-roll and ride performance of the interconnected suspension configurations, negative feedback components could be further explored in terms of its design parameters; additionally, damping valves would be used in the unconnected struts to improve its ride performance.
4. To augment negative damping components, damping and interconnection valves would be utilized in interconnected configurations in view to enhance anti-roll without exploiting ride performance of the interconnected struts.

CHAPTER 2

DEVELOPMENT OF ANALYTICAL MODELS FOR THE ROLL PLANE INTERCONNECTED SUSPENSION

2.1 INTRODUCTION

The objective of a suspension system in a vehicle is to attain a satisfactory compromise among ride comfort, handling and directional control performance of the vehicle in the most economical and reliable manner. Good ride quality can be achieved by a suspension system with a soft spring and light damping, whereas hard spring and heavy damping are required to realize better directional stability and handling control. Hydro-pneumatic suspension systems offer considerable benefits over the conventional mechanical and purely pneumatic or hydraulic suspensions. These permit integration of the energy restoring and damping properties within a single unit and can provide ride height control with self-levelling in a relatively simple manner. Furthermore, variable stiffness could be achieved by nonlinear spring characteristics, which permits adequate natural frequency of the vehicle with varying loads. The hydro-pneumatic struts, proposed in earlier studies, encompassed an external accumulator to achieve desired restoring property and offered relatively lower effective area, which necessitated higher charge pressure for supporting the desired load. [3, 5]. The hydro-pneumatic struts with integrated accumulator and damping valves have been proposed to realize more compact design and damping tuning [8, 25]. Furthermore, Cao et al. [8] proposed a strut design with an enhanced effective area in order to reduce the operating pressure and thereby decrease the amount of seal friction. The hydro-pneumatic suspensions further offer flexibility to introduce either hydraulic or pneumatic couplings within or across the axle suspensions, which have shown to provide enhanced roll and pitch performance, while retaining relative soft vertical property [7, 32]. Such couplings or strut interconnections, however, yield negative feedback damping effect, which has not yet been explored. The negative damping effect may help achieve variable suspension damping and thereby permit elimination of the damping valves.

In this chapter, a four-degrees-of freedom (DOF) roll plane model of a vehicle with laterally interconnected hydro-pneumatic struts is formulated to analyze the roll and bounce mode properties of the suspension. The suspension model is analyzed to derive its roll and vertical mode suspension properties. The components of damping arising from hydraulic flows within and across the struts are derived to illustrate the negative feedback damping effect of the interconnected

suspension. The properties of the interconnected system are also compared with those of the unconnected system to demonstrate the significance of hydraulic interconnections.

2.2 HYDRO-PNEUMATIC SUSPENSION STRUTS

A hydro-pneumatic strut integrating a gas chamber, damping orifices and a floating piston, shown in Figure 2.1, is considered for the analysis. Three different configurations of the strut are considered for the analysis, which are denoted as type-I, type-II and type-IIa. The type-I strut comprises a gas chamber (4), a floating piston that separates the gas chamber from the oil chamber (2) and a main piston, as shown in Figure 2.1(a). The main piston comprises flow orifices that permit flows between chambers 1 and 2. This strut configuration provides larger effective area, thereby static equilibrium pressures are relatively low as compared with the conventional struts considering identical load carrying capacity. Type-II and type-IIa struts consist of a floating piston and the gas chamber (4), as shown in Figures 2.1(b) and (c). These configurations also include a fixed damping orifice plate that permits hydraulic flows between chambers 1 and 2. The type-II and type-IIa struts are identical except for additional orifices introduced between the chambers 1 and 3, which permit different interconnections, as described in the following sections.

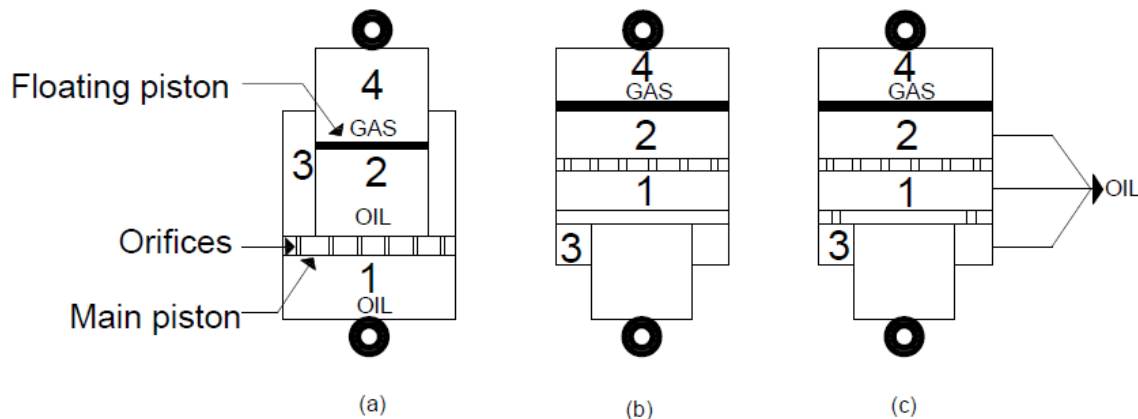


Figure 2.1: Schematics of the hydro-pneumatic suspension strut configurations: (a) Type-I; (b) Type-II; and (c) Type-II with additional flow orifices in the main piston.

2.3 ROLL PLANE MODEL OF HYDRO-PNEUMATIC SUSPENSION STRUTS

Hydraulic interconnections of the struts are conceived in the roll plane considering a four-DOF roll plane model of a vehicle, as shown in Figure 2.2. In this model, m_s represents the sprung mass of the entire vehicle and m_u is the unsprung mass due to the axles, which are lumped together in

the single roll plane. The roll mass of inertia of the sprung and unsprung masses are denoted by I_s and I_u , respectively. The tires are represented by their equivalent stiffness (K_{ti}) and damping (C_{ti}) constants using point-contact with the road. The vertical displacements of mass centers (cg) of the sprung and unsprung masses are denoted by x_s and x_u , respectively. Similarly, θ_s and θ_u describe the roll displacements of the sprung and unsprung masses, respectively, about their roll centers, assumed to be located at the respective cg. The roll-plane model of the vehicle with unconnected (UC) suspension struts is also formulated to study the effects of hydraulic interconnections. In this case, the hydraulic interconnections are replaced by a roll stiffener (K_e) representing the conventional anti-roll bar, as shown in Figure 2.3.

The equations of motion of the two vehicle models can be summarized as follows:

$$m_s \ddot{x}_s = F_l + F_r \quad (2.1)$$

$$I_s \ddot{\theta}_s = -F_l L_{sl} + F_r L_{sr} + T_\theta - T_R \quad (2.2)$$

$$m_u \ddot{x}_u = -K_{tl}(x_u - x_{ol} + L_{tl}\theta_u) - K_{tr}(x_u - x_{or} + L_{tr}\theta_u) - C_{tl}(\dot{x}_u - L_{tl}\dot{\theta}_u - \dot{x}_{ol}) - C_{tr}(\dot{x}_u - L_{tr}\dot{\theta}_u - \dot{x}_{or}) - F_l - F_r \quad (2.3)$$

$$I_u \ddot{\theta}_u = K_{tl}L_{tl}(x_u - x_{ol} + L_{tl}\theta_u) - K_{tr}L_{tr}(x_u - x_{or} + L_{tr}\theta_u) + C_{tl}L_{tl}(\dot{x}_u + L_{tl}\dot{\theta}_u - \dot{x}_{ol}) - C_{tr}L_{tr}(\dot{x}_u + L_{tr}\dot{\theta}_u - \dot{x}_{or}) - F_l L_{sl} + F_r L_{sr} + T_R \quad (2.4)$$

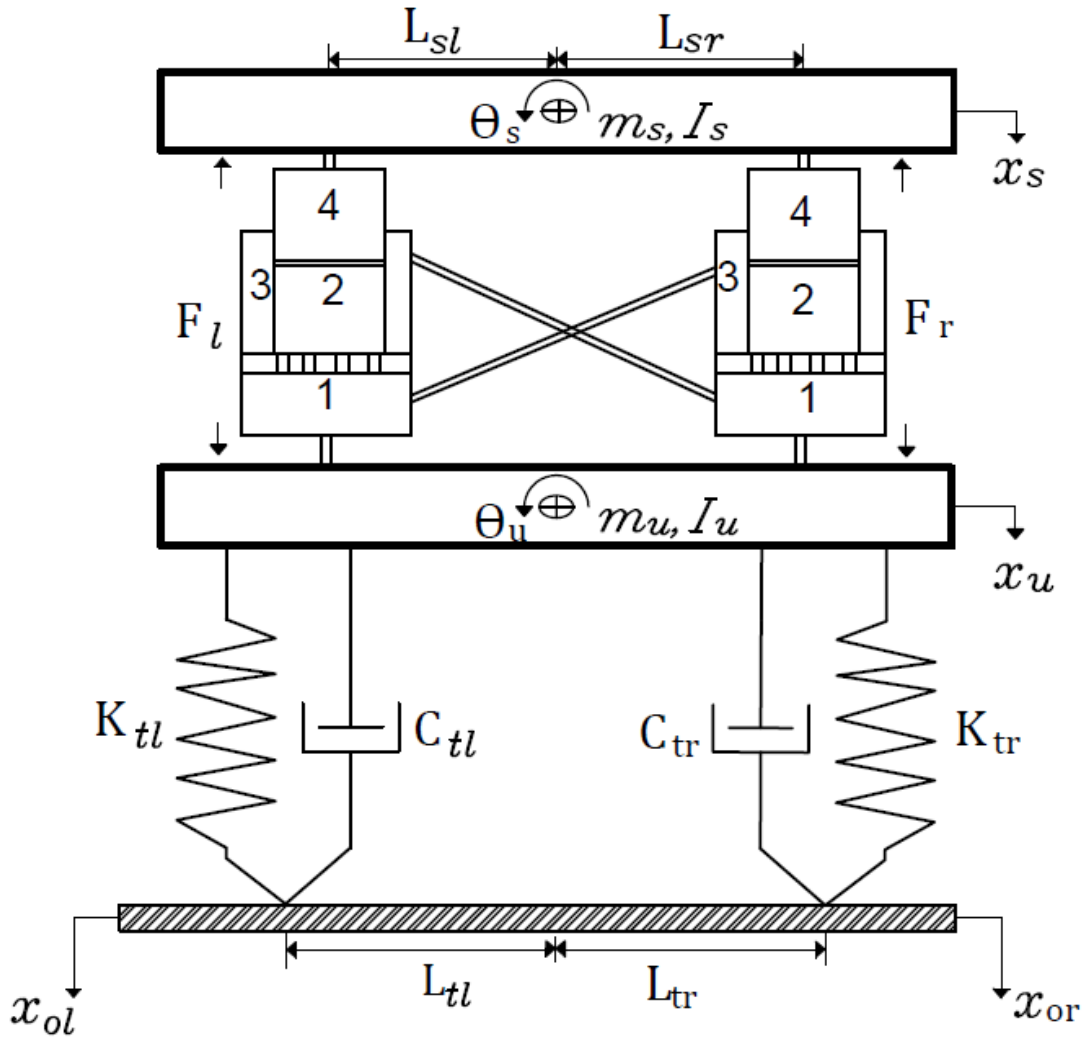


Figure 2.2: Four-DOF roll plane model of the vehicle with roll-coupled hydro-pneumatic suspension struts (Type-I).

In the above equations, L_{tl} and L_{tr} are lateral positions of the left- and right-tires, respectively, with respect to the unsprung mass cg. L_{sl} and L_{sr} are the lateral positions of the suspension struts with respect to the sprung mass cg. F_l and F_r are the forces developed by the left- and right-suspension struts, respectively, and T_R is the moment due to antiroll bar in case of the unconnected suspension. The road inputs at the left- and right-tires contact points are denoted as x_{ol} and x_{or} , respectively.

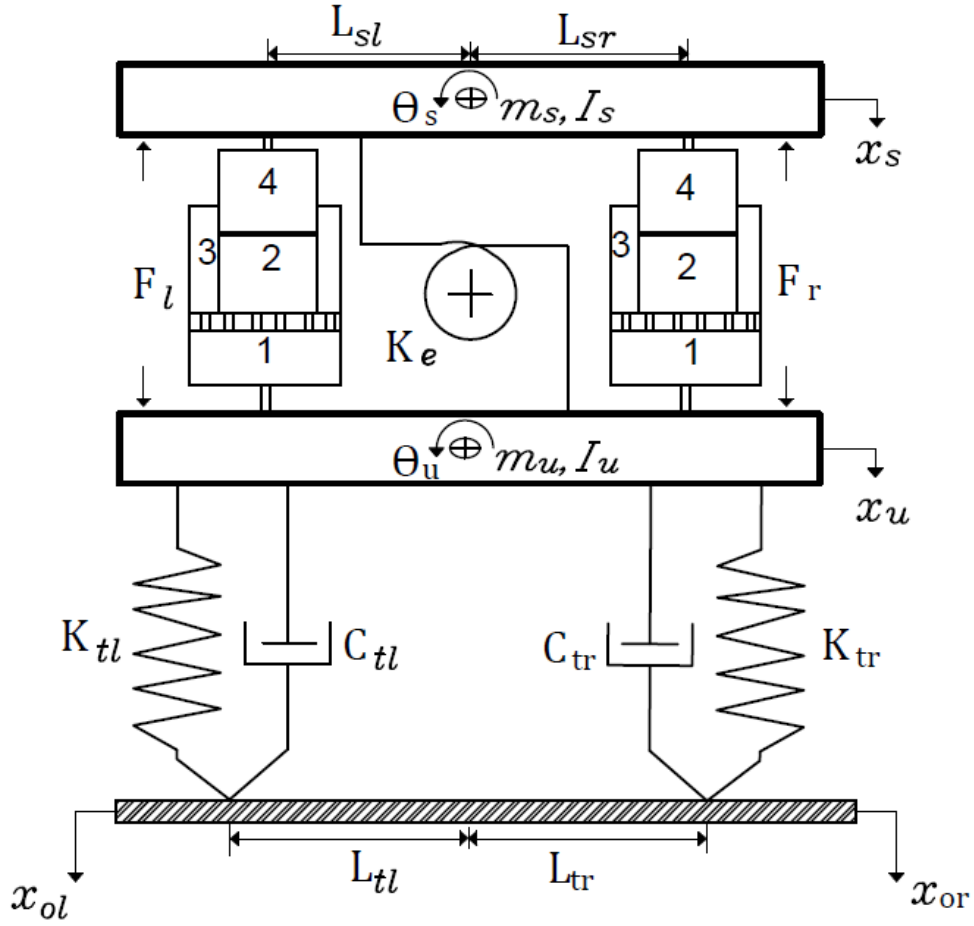


Figure 2.3: Four-DOF roll plane model of the vehicle with unconnected hydro-pneumatic suspension struts (Type-I) with an anti-roll bar.

Apart from the road input, the vehicle is subject to a lateral acceleration excitation during steering maneuvers. The roll moment T_θ imposed on the sprung mass may be defined using a simplified roll-plane schematic, shown in Figure 2.4, such that:

$$T_\theta = m_s a_y h_2 + m_s \theta_s h_2 g \quad (2.5)$$

In the above equation, the roll angle θ is assumed to be small, a_y is the lateral acceleration encountered during a steering maneuver, h_2 is the distance between cg of the sprung mass and the roll centre of unsprung mass, and g is acceleration due to gravity. However, the suspension roll center is assumed to be located at a fixed distance from the sprung mass cg.

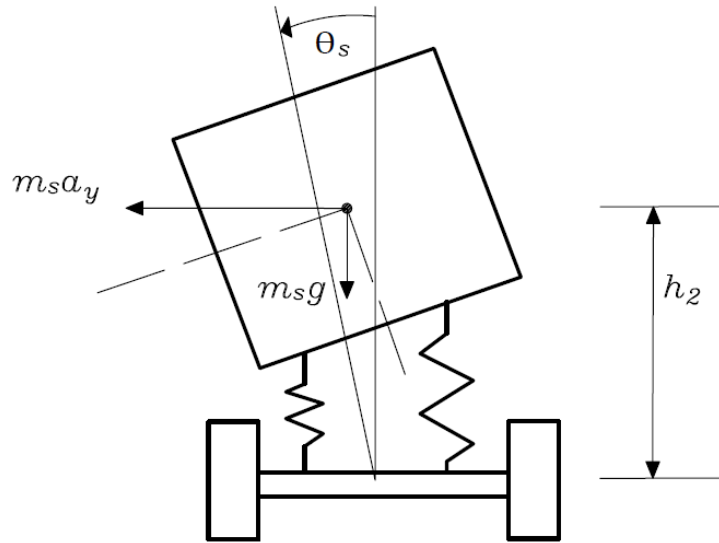


Figure 2.4: Simplified roll plane model of the vehicle during turning maneuvers.

2.4 SUSPENSION FORCES

The forces developed by the suspension struts in the UC configuration are derived from the flow continuity and fluid pressure relations. For this purpose, type-I, type-II and type-IIa unconnected strut models are reduced, as shown in Figure 2.5. It should be noted that struts used in UC configuration contain additional orifices in the main piston that permit flows between chambers 1 and 3. Furthermore, both the models consider struts with identical static pressures in the gas chamber, and thereby the identical load carrying capacity.

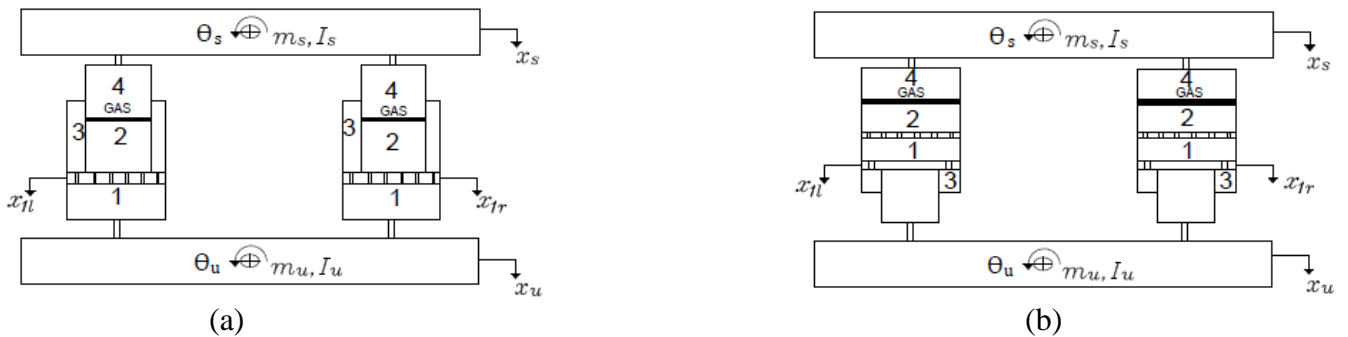


Figure 2.5: Reduced model of the unconnected struts used for deriving the strut forces:
 (a) Type- I; and (b) Type-II.

2.4.1 Unconnected Suspension Struts

Both, type-I and type-II, suspension struts yield identical force-displacement and force-velocity relationships, when unconnected, although the floating piston areas differ, as seen in Figure 2.5. The effective areas of both the struts are also identical. Identical static equilibrium pressures are thus selected to ensure same load carrying capacity of both types of struts. The charge pressure and static equilibrium fluid pressure of the struts are obtained for the given sprung weight of the vehicle. The static load W_i supported by strut i ($i=l, r$) is related to the effective strut area and the fluid pressure, such that:

$$W_i = (P_{4o} - P_a)A_e; \quad i=l, r \quad (2.6)$$

where P_{4o} refers to the absolute static equilibrium gas pressure in chamber 4, P_a is the atmospheric pressure, and l and r refer to left- and right-wheel struts, respectively. A_e is the effective area of the strut, which is equal to the floating piston area for type-I strut ($A_e = A_2$), and the rod area for type-II strut ($A_e = A_1 - A_3$). A_1 and A_3 are the cross-section areas of the main piston, and the annular region between the rod and the main piston. In static equilibrium condition, the fluid pressures in all the chambers ($P_{jo}; j = 1, 2, 3, 4$) are considered to be identical.

For the unconnected (UC) struts, the flow and pressure relations are initially derived assuming incompressible flows, negligible seals friction, negligible floating piston mass and turbulent flows through damping orifices. As referred from the Figure2.5, $x_{1i} = x_s \pm L_s\theta_s$ is the absolute displacement of the main piston in strut i ($i=l, r$). The rate of change of fluid volume in chamber 1 of strut i , Q_{1i} , is related to the strut velocity \dot{x}_i , which can also be expressed by the following flow continuity equation:

$$Q_{1i} = A_1\dot{x}_i = -Q_{12i} - Q_{13i}; \quad i=l, r \quad (2.7)$$

where Q_{1ki} refers to the fluid flow rate between chamber 1 and chamber k ($k= 2, 3$) of the same strut i ($i=l, r$). For turbulent flows through orifice restrictions, rates of fluid flows between chambers 1 and 2 as well as chambers 1 and 3 of strut i ($i=l, r$), can be expressed as:

$$Q_{12i} = C_d a_{12i} u_2 \sqrt{2(P_{12i})/\rho} \operatorname{sgn}(P_{12i}) \quad (2.8)$$

$$Q_{13i} = C_d a_{13i} u_3 \sqrt{2(P_{13i})/\rho} \operatorname{sgn}(P_{13i}) \quad (2.9)$$

where $P_{1ki} = P_{1i} - P_{ki}$ ($k = 2,3$) are the pressure differentials across the orifices in strut i ($i=l, r$), a_{12i} and a_{13i} are cross-section areas of each orifice separating chambers 1 from chambers 2

and 3, respectively, for the strut i . u_2 and u_3 are the number of orifices between chambers 1 and 2, and chambers 1 and 3, respectively, C_d is flow discharge coefficient and ρ is the fluid mass density. The sgn function ensures the direction of fluid flow in phase with the pressure difference.

Assuming polytropic gas process, the instantaneous pressure of gas in chamber 4 (P_{4i}) can be related to change in the gas volume, which further relates to strut displacement, x_i and the floating piston cross-section area A_{FP} . The instantaneous gas pressure is thus obtained, as:

$$P_{4i} = P_{40} V_{40}^n \frac{1}{(V_{40} - A_{FP} x_i)^n} \quad (2.10)$$

where V_{40} is the gas volume corresponding to static equilibrium position of the strut i and n is the polytropic constant. The floating piston area is also equal to A_4 , which is different for the two struts, as seen in Figure 2.5.

Considering incompressible fluid flows, the change in gas volume is identical to the change in volume of the oil in chamber (2), ΔV_{2i} , which can be related to the main piston and annular areas, as:

$$\Delta V_{2i} = A_2 x_i \quad (2.11)$$

In case of type-I strut, A_2 can be expressed as the difference between the main piston and annular areas,

$$A_1 - A_3 = A_2.$$

Dynamic strut forces

The dynamic force developed by a strut (F_i ; $i = l, r$) is directly related to the pressure forces acting on the main piston, such that:

$$F_i = N_u [P_{1i} A_1 - P_{3i} A_3 - (P_{40} - P_a) A_e] \quad (2.12)$$

where N_u refers to the number of struts used on each track of the vehicle. The strut force can be further expressed in terms of pressure differentials, P_{12i} and P_{13i} , as:

$$F_i = N_u [(P_{4i} - P_{40}) A_e + P_{12i} A_e + P_{13i} A_3 + P_a A_e] \quad (2.13)$$

In the above equation (2.13), $P_{4i} = P_{2i}$ is assumed by considering negligible seal friction and floating piston inertia. Upon substituting for pressure differentials P_{12i} and P_{13i} from equations (2.8) and (2.9), respectively, and P_{4i} from equation (2.10), the dynamic force developed by strut i can be expressed in the following manner:

$$F_i = N_u \left[P_{40} V_{40}^n \frac{1}{(V_{40} - A_{FP} x_i)^n} A_e + \frac{\rho}{2} \left(\frac{-A_e \dot{x}_i}{C_d u_2 a_{12i}} \right)^2 A_e sgn(\dot{x}_i) + \frac{\rho}{2} \left(\frac{-A_3 \dot{x}_i}{C_d u_3 a_{13i}} \right)^2 A_3 sgn(\dot{x}_i) - (P_{40} - P_a) A_e \right] \quad (2.14)$$

In the above equation, first term describes force due to gas spring, while the next two terms describe damping forces attributed to fluid flows between chambers 1 and 2, and 1 and 3, respectively. The last term, $(P_{4o} - P_a)A_e$ denotes the static load carried by the strut.

2.4.2 Roll Plane Interconnected Suspension (Type-I Struts)

Figure 2.6 illustrates schematic of the type-I struts connected in the roll plane of the vehicle, where chambers 1 and 3 of the left-strut are connected to chambers 3 and 1 of the right-strut, respectively, via hydraulic lines. Unlike the unconnected struts, the flow orifices between chambers 1 and 3 are eliminated. The equation of static equilibrium for the interconnected struts are identical to those of the UC struts, as described in equation (2.6).

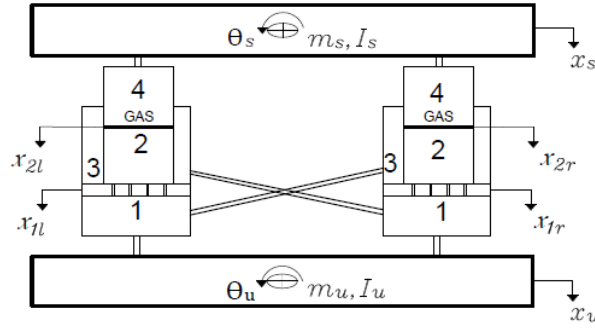


Figure 2.6: Interconnected strut model used for deriving the strut forces (Type-I).

Assuming incompressible fluid flow, the rate of change of volume in chamber 1 of the left-strut (Q_{1l}) is related not only to the flow between chambers 1 and 2 of the same strut (Q_{12l}) but also the fluid flows to chamber 3 of the right-strut through the interconnecting pipe (Q_{1l3r}). The flow continuity equation for the left-strut can thus be expressed as:

$$Q_{1l} = -Q_{12l} - Q_{1l3r} = -A_1 \dot{x}_l \quad (2.15)$$

Similarly, the rate of change of fluid volume in chamber 1 of the right-strut (Q_{1r}) is related to the flows between chambers 1 and 2 of the right-strut (Q_{12r}) and to chamber 3 of the left-strut (Q_{1r3l}), such that:

$$Q_{1r} = -Q_{12r} - Q_{1r3l} = -A_1 \dot{x}_r \quad (2.16)$$

Similar to the UC struts, assuming turbulent flows through orifice restrictions between chambers 1 and 2 of the strut i ($i=l, r$), the pressure differentials across the orifices can be obtained from:

$$Q_{12i} = C_d a_{12i} u_2 \sqrt{2(P_{12i})/\rho} \operatorname{sgn}(P_{12i}) \quad (2.17)$$

The fluid flows across the two struts via the interconnecting lines are considered to be laminar. Using the *Hagen-Poiseuille* relation, the flow rates through the lines can be expressed as:

$$Q_{1l3r} = \frac{\pi D^4 P_{1l3r}}{128 \mu L}; \quad Q_{1r3l} = \frac{\pi D^4 P_{1r3l}}{128 \mu L} \quad (2.18)$$

In equation (2.18), L and D are the length and diameter of the interconnecting pipes, μ denotes the dynamic viscosity of fluid, and $P_{1l3r} = P_{1l} - P_{3r}$ and $P_{1r3l} = P_{1r} - P_{3l}$ are the differential pressures due to flows through the interconnecting pipes.

The instantaneous pressure of gas in chamber 4 of strut i , which is identical to the oil pressure in chamber 2 (P_{2i}), is related to deflection of the floating piston (x_{2i}), in the same strut i . Assuming polytropic process of the gas, the gas pressures in the left- and right-struts are obtained from:

$$P_{4l} = P_{4o} V_{4o}^n \frac{1}{(V_{4o} - A_{FP} x_{2l})^n} \quad (2.19)$$

$$P_{4r} = P_{4o} V_{4o}^n \frac{1}{(V_{4o} - A_{FP} x_{2r})^n} \quad (2.20)$$

In above relations, the static equilibrium gas pressures (P_{4o}) and volumes (V_{4o}) are considered to be identical for both the struts. It should be noted that the change in volume of the gas chambers in left- and right-struts are related to deflections of floating pistons (x_{2l} and x_{2r}) of both the struts, such that:

$$A_{FP} x_{2l} = (A_1 x_l - A_3 x_r); \quad A_{FP} x_{2r} = (A_1 x_r - A_3 x_l) \quad (2.21)$$

Dynamic strut forces

The dynamic force F_i developed by the strut i ($i = l, r$) can be related to the pressure forces, as:

$$F_i = N_u [(P_{1i} - P_{1o}) A_1 - (P_{3i} - P_{3o}) A_3 - P_a A_2] \quad (2.22)$$

It should be noted that the static equilibrium pressures of fluids within all the chambers are identical, such that $P_{1o} = P_{2o} = P_{3o} = P_{4o}$. The above relation can also be expressed in terms of gas pressure, and pressure differentials across the orifices (P_{12i}) and the interconnecting lines (P_{1r3l} and P_{1l3r}), such that:

$$F_l = N_u [(P_{4l} - P_{4o}) A_1 - (P_{4r} - P_{4o}) A_3 + P_{12l} A_1 - P_{12r} A_3 - P_{1r3l} A_3 - P_a A_2]$$

$$F_r = N_u [(P_{4r} - P_{4o}) A_1 - (P_{4l} - P_{4o}) A_3 + P_{12r} A_1 - P_{12l} A_3 - P_{1l3r} A_3 - P_a A_2] \quad (2.23)$$

Upon substituting for P_{4i} from equations (2.19) and (2.20), and for the pressure differentials from equations (2.17) and (2.18), the dynamic forces developed by the left- and right-struts can be obtained, as:

$$F_l = N_u \left[P_{4o} V_{4o}^n \left\{ \frac{A_1}{(V_{4o} - A_1 \dot{x}_l + A_3 \dot{x}_r)^n} - \frac{A_3}{(V_{4o} - A_1 \dot{x}_r + A_3 \dot{x}_l)^n} \right\} - (P_{4o} - P_a) A_2 + \right. \\ \left. \frac{\rho}{2C_d^2} \left\{ \left(\frac{A_1 \dot{x}_l - A_3 \dot{x}_r}{u_2 a_{12l}} \right)^2 A_1 \operatorname{sgn}(\dot{x}_l) - \left(\frac{A_1 \dot{x}_r - A_3 \dot{x}_l}{u_2 a_{12r}} \right)^2 A_3 \operatorname{sgn}(\dot{x}_r) \right\} - \frac{A_3^2 \dot{x}_l 128 \mu L}{\pi D^4} \right] \quad (2.24)$$

$$F_r = N_u \left[P_{4o} V_{4o}^n \left\{ \frac{A_1}{(V_{4o} - A_1 \dot{x}_r + A_3 \dot{x}_l)^n} - \frac{A_3}{(V_{4o} - A_1 \dot{x}_l + A_3 \dot{x}_r)^n} \right\} - (P_{4o} - P_a) A_2 + \right. \\ \left. \frac{\rho}{2C_d^2} \left\{ \left(\frac{A_1 \dot{x}_r - A_3 \dot{x}_l}{u_2 a_{12r}} \right)^2 A_1 \operatorname{sgn}(\dot{x}_r) - \left(\frac{A_1 \dot{x}_l - A_3 \dot{x}_r}{u_2 a_{12l}} \right)^2 A_3 \operatorname{sgn}(\dot{x}_l) \right\} - \frac{A_3^2 \dot{x}_r 128 \mu L}{\pi D^4} \right] \quad (2.25)$$

The above relations show that dynamic force developed by a strut is dependent not only on its own motion but also the motion of the connected strut. This is due to fluid coupling between the two struts. The dynamic force developed by each strut comprises following force components:

(a) Gas spring force, F_{si}

The gas spring force developed by each strut is related to motions of both the struts (x_l, x_r) , as seen from first two terms in equations (2.24) and (2.25). The gas spring force due to left- and right-struts can be expressed as:

$$F_{sl} = N_u \left\{ P_{4o} V_{4o}^n \left\{ \frac{A_1}{(V_{4o} - A_1 \dot{x}_l + A_3 \dot{x}_r)^n} - \frac{A_3}{(V_{4o} - A_1 \dot{x}_r + A_3 \dot{x}_l)^n} \right\} - (P_{4o} - P_a) A_2 \right\} \quad (2.26)$$

$$F_{sr} = N_u \left\{ P_{4o} V_{4o}^n \left\{ \frac{A_1}{(V_{4o} - A_1 \dot{x}_r + A_3 \dot{x}_l)^n} - \frac{A_3}{(V_{4o} - A_1 \dot{x}_l + A_3 \dot{x}_r)^n} \right\} - (P_{4o} - P_a) A_2 \right\} \quad (2.27)$$

(b) Damping force due to orifice flows within the same strut, FDS_i

The dynamic force components in equations (2.24) and (2.25) are attributed to flows through orifices within the same strut and flows across the struts through interconnecting lines, respectively. The damping force components related to flows within the same strut are given by:

$$FDS_l = \frac{\rho N_u}{2C_d^2} \left(\frac{A_1 \dot{x}_l - A_3 \dot{x}_r}{u_2 a_{12l}} \right)^2 A_1 \operatorname{sgn}(\dot{x}_l) \quad (2.28)$$

$$FDS_r = \frac{\rho N_u}{2C_d^2} \left(\frac{A_1 \dot{x}_r - A_3 \dot{x}_l}{u_2 a_{12r}} \right)^2 A_1 \operatorname{sgn}(\dot{x}_r) \quad (2.29)$$

From the above relation, it is evident that the fluid flows within the same strut are affected by relative velocities across both the struts.

(c) Damping force due to orifice flows in the connecting strut, FDC_i

The orifice flows within the left-strut contribute to a negative damping component in the dynamic force developed by the right-strut. This coupling effect is evident from terms $-P_{12r}A_3$ and $-P_{12l}A_3$ in the forces developed by the left- and right-struts, respectively, given in equation (2.23). Negative feedback damping components for the left- and right-struts are also evident from the 5th terms in equations (2.24) and (2.25), given by:

$$FDC_l = -\frac{\rho N u}{2C_d^2} \left(\frac{A_1 \dot{x}_r - A_3 \dot{x}_l}{u_2 a_{12r}} \right)^2 A_3 \operatorname{sgn}(\dot{x}_r) \quad (2.30)$$

$$FDC_r = -\frac{\rho N u}{2C_d^2} \left(\frac{A_1 \dot{x}_l - A_3 \dot{x}_r}{u_2 a_{12l}} \right)^2 A_3 \operatorname{sgn}(\dot{x}_l) \quad (2.31)$$

(d) Damping force due to flows across the struts, FDL_i

The damping force component attributed to laminar flows through the interconnecting lines is related to motion of the same strut alone, such that:

$$FDL_i = -\frac{A_3^2 \dot{x}_i 128 \mu L}{\pi D^4} \quad (2.32)$$

The damping force components, described in (c) and (d), constitute the negative effects on the damping force developed by each strut, which is attributed to flows across the two struts.

2.4.3 Effects of Compressibility and Floating Piston Dynamics

The dynamic forces formulated in the previous section consider negligible contribution due to fluid compressibility, seals friction and floating piston dynamics. Considering high pressure requirements, especially for heavy vehicles applications, both the seals friction and fluid compressibility may exhibit notable effects on the dynamic forces developed by the struts. In this section, the dynamic forces are derived considering fluid compressibility, the friction due to floating piston seals and the floating piston mass.

For the compressible hydraulic fluid, the rate of change of fluid volume in chamber 1 of the left-strut (Q_{1l}) is related to flow rates through orifices (Q_{12l}) and the interconnecting pipe (Q_{1l3r}), and the fluid compressibility effect. The flow rate (Q_{1l}) is further related to velocity of the strut \dot{x}_i . The flow continuity equation for the left-strut can thus be expressed as:

$$Q_{1l} = -Q_{12l} - Q_{1l3r} + \frac{dV_{1l}}{dt} = -A_1 \dot{x}_l \quad (2.33)$$

where the term $\frac{dV_{1l}}{dt}$ relates to the rate of change of fluid volume in chamber 1 of strut l due to compressibility, which is related to fluid bulk modulus E , and the rate of change of fluid pressure in chamber 1 of the left-strut, such that:

$$\frac{dP_{1l}}{dt} = -E \frac{dV_{1l}}{V_{1l}} \quad (2.34)$$

Equations (2.33) and (2.34) yield the following relation for the rate of change of pressure of the fluid in chamber 1 of the left-strut:

$$\frac{dP_{1l}}{dt} = -E \left(\frac{Q_{1l} + Q_{12l} + Q_{1l3r}}{A_1 x_{10l} + A_1 x_l} \right) \quad (2.35)$$

The flow continuity equation for the right-strut is obtained in the similar manner, as:

$$Q_{1r} = -Q_{12r} - Q_{1r3l} + \frac{dV_{1r}}{dt} = -A_1 \dot{x}_r \quad (2.36)$$

The rate of change of pressure in chamber 1 of the right-strut is also derived in a similar manner, as:

$$\frac{dP_{1r}}{dt} = -E \left(\frac{Q_{1r} + Q_{12r} + Q_{1r3l}}{A_1 x_{10r} + A_1 x_r} \right) \quad (2.37)$$

In equations (2.35) and (2.37), x_{10i} is the initial length of chamber 1 of strut i ($i = l, r$) corresponding to the static equilibrium condition, which determines the instantaneous volume of the fluid in chamber 1.

The dynamic force developed by a strut is obtained from the pressure forces, as:

$$F_i = N_u [(P_{1i} - P_{1o}) A_1 - (P_{3i} - P_{3o}) A_3 - (P_{4o} - P_a) A_2]; \quad i=l, r \quad (2.38)$$

The above equation can also be expressed in terms of pressure differentials and gas pressures, as:

$$\begin{aligned} F_l &= N_u [P_{2l} A_1 - P_{2r} A_3 + P_{12l} A_1 - P_{12r} A_3 - P_{1r3l} A_3 - (P_{4o} - P_a) A_2] \\ F_r &= N_u [P_{2r} A_1 - P_{2l} A_3 + P_{12r} A_1 - P_{12l} A_3 - P_{1l3r} A_3 - (P_{4o} - P_a) A_2] \end{aligned} \quad (2.39)$$

Apart from the above, the inertia force due to the floating piston mass and the seal friction force lead to difference in pressures of fluid in chambers 2 and 4. This is evident from equation of motion for the floating piston, given by:

$$m_f \ddot{x}_{2i} + m_f g + P_{4i} A_2 + F_c \operatorname{sgn}(\dot{x}_{2si}) = P_{2i} A_2 \quad (2.40)$$

where m_f is the floating piston mass and g is acceleration due to gravity, and $\dot{x}_{2si} = \dot{x}_{2i} - \dot{x}_{1i}$ denotes the relative velocity of the floating piston with respect to that of the rod. \dot{x}_{1i} is the absolute velocity of the main piston in strut i . F_c is the magnitude of friction across the floating piston seals. The dynamic force developed by each strut is obtained upon substituting for the gas pressures from equations (2.19) to (2.21), pressure differentials from equations (2.17) and (2.18), and P_{2i} from equation (2.40) into equation (2.39), such that:

$$\begin{aligned} F_l = N_u \left[P_{4o} V_{4o}^n \left\{ \frac{A_1}{(V_{4o} - A_1 \dot{x}_l + A_3 \dot{x}_r)^n} - \frac{A_3}{(V_{4o} - A_1 \dot{x}_r + A_3 \dot{x}_l)^n} \right\} - (P_{4o} - P_a) A_2 + \right. \\ \left. \frac{\rho}{2C_d^2} \left\{ \left(\frac{-A_1 \dot{x}_l + A_3 \dot{x}_r}{u_2 a_{12l}} \right)^2 A_1 \operatorname{sgn}(\dot{x}_l) - \left(\frac{-A_1 \dot{x}_r + A_3 \dot{x}_l}{u_2 a_{12r}} \right)^2 A_3 \operatorname{sgn}(\dot{x}_r) \right\} - \frac{A_3^2 \dot{x}_l 128 \mu L}{\pi D^4} + (\ddot{x}_{2l} A_1 - \right. \\ \left. \ddot{x}_{2r} A_3) \frac{m_f}{A_2} - (A_1 \operatorname{sgn}(\dot{x}_{2sl}) - A_3 \operatorname{sgn}(\dot{x}_{2sr})) \frac{F_c}{A_2} + m_f g \right] \quad (2.41) \end{aligned}$$

$$\begin{aligned} F_r = N_u \left[P_{4o} V_{4o}^n \left\{ \frac{A_1}{(V_{4o} - A_1 \dot{x}_r + A_3 \dot{x}_l)^n} - \frac{A_3}{(V_{4o} - A_1 \dot{x}_l + A_3 \dot{x}_r)^n} \right\} - (P_{4o} - P_a) A_2 + \right. \\ \left. \frac{\rho}{2C_d^2} \left\{ \left(\frac{-A_1 \dot{x}_r + A_3 \dot{x}_l}{u_2 a_{12r}} \right)^2 A_1 \operatorname{sgn}(\dot{x}_r) - \left(\frac{-A_1 \dot{x}_l + A_3 \dot{x}_r}{u_2 a_{12l}} \right)^2 A_3 \operatorname{sgn}(\dot{x}_l) \right\} - \frac{A_3^2 \dot{x}_r 128 \mu L}{\pi D^4} + (\ddot{x}_{2r} A_1 - \right. \\ \left. \ddot{x}_{2l} A_3) \frac{m_f}{A_2} - (A_1 \operatorname{sgn}(\dot{x}_{2sr}) - A_3 \operatorname{sgn}(\dot{x}_{2sl})) \frac{F_c}{A_2} + m_f g \right] \quad (2.42) \end{aligned}$$

Comparison of above two equations with equations (2.24) and (2.25) suggests additional coupling terms attributed due to the floating piston inertia and the seal friction.

2.4.4 Roll Plane Interconnected Suspension (Type-II struts)

Figure 2.7 illustrates schematic of the roll-plane connected type-II struts. Similar to type-I configuration, chambers 1 and 3 of the left-strut are connected to chambers 3 and 1 of the right-strut, respectively, while the orifice flows are eliminated across chambers 1 and 3.

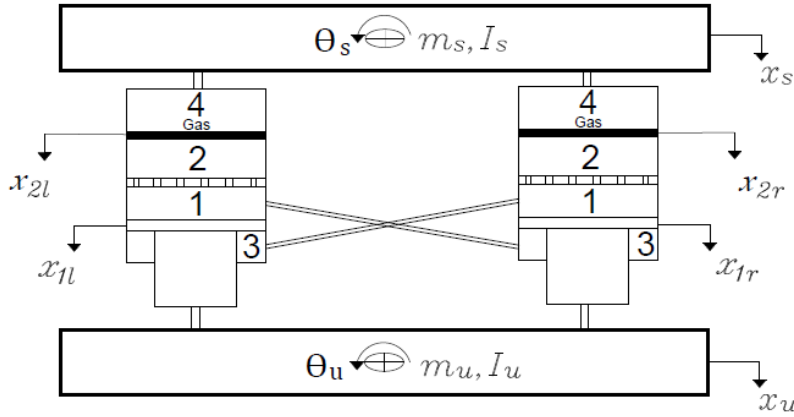


Figure 2.7: Interconnected strut model used for deriving the strut forces (Type-II).

Assuming incompressible hydraulic fluid, the rate of change of volume in chamber 1 of the left-strut (Q_{1l}) is related to the fluid flows across the orifices between chambers 2 and 1 of the same strut (Q_{21l}), and the flows from chamber 3 of the right-strut via interconnecting pipe (Q_{3r1l}), such that:

$$Q_{1l} = Q_{21l} + Q_{3r1l} = A_1 \dot{x}_l \quad (2.43)$$

Similarly, the rate of change of volume in chamber 1 of the right-strut (Q_{1r}) is related to the flows across the fixed orifices between chambers 2 and 1 of the same strut (Q_{21r}) and fluid flows from chamber 3 of the left-strut through the connecting pipe (Q_{3l1r}). The flow continuity equation for the right-strut can thus be described as:

$$Q_{1r} = Q_{21r} + Q_{3l1r} = A_1 \dot{x}_r \quad (2.44)$$

The above equations, (2.43) and (2.44), are identical to equations (2.15) and (2.16), respectively, derived for roll-connected type-I struts, with the exception of direction of flows due to strut geometry. The flow rates across the orifices and the interconnecting pipes are also identical to the relations obtained for type-I struts, defined in equations (2.17) and (2.18).

Although, the expressions for instantaneous gas pressures in chambers 4 of the connected struts are identical to those obtained for type-I struts, the gas volume V_{4o} in type-II struts is greater than that used in type-I struts. Owing to larger floating piston area, initial gas charge pressure (P_c) in type-II struts is lower than that used in type-I struts, given by:

$$P_c = P_{4o} \left(\frac{V_{4o}}{V_c} \right)^n \quad (2.45)$$

The above equations suggest that type-I and type-II roll interconnections would yield identical force-velocity characteristics in the roll and vertical modes, when contributions due to floating

piston inertia and seals friction are neglected. The force-displacement properties are also identical in the vertical mode due to identical effective area, while those differ in the roll mode.

2.4.5 Effects of Compressibility and Floating Piston Dynamics

The dynamic forces developed by roll-connected type-II struts are also influenced by the fluid compressibility, friction due to floating piston seals and floating piston dynamics. The equation of motion for the floating piston mass is obtained as:

$$m_f \ddot{x}_{2i} + P_{2i} A_1 + F_c \operatorname{sgn}(\dot{x}_{2si}) = P_{4i} A_1 + m_f g \quad (2.46)$$

The above equation is identical to that derived for type-I struts, described in equation (2.40), except for the relatively larger floating piston area, A_1 . The dynamic force developed by each strut is obtained upon substituting for the gas chamber pressures from equations (2.19) and (2.20), pressure differentials due to orifice flows and flow across the pipes from equations (2.17) and (2.18), and P_{2i} from the above equation (2.46) into equation (2.39), such that:

$$\begin{aligned} F_l = N_u \left[P_{4o} V_{4o}^n \left\{ \frac{A_1}{(V_{4o} - A_1 x_l + A_3 x_r)^n} - \frac{A_3}{(V_{4o} - A_1 x_r + A_3 x_l)^n} \right\} - (P_{4o} - P_a) A_2 + \right. \\ \left. \frac{\rho}{2C_d^2} \left\{ \left(\frac{-A_1 \dot{x}_l + A_3 \dot{x}_r}{u_2 a_{12l}} \right)^2 A_1 \operatorname{sgn}(\dot{x}_l) - \left(\frac{-A_1 \dot{x}_r + A_3 \dot{x}_l}{u_2 a_{12r}} \right)^2 A_3 \operatorname{sgn}(\dot{x}_r) \right\} - \frac{A_3^2 \dot{x}_l 128 \mu L}{\pi D^4} - \left(\ddot{x}_{2l} + \right. \right. \\ \left. \left. \frac{A_3}{A_1} \ddot{x}_{2r} \right) m_f - \left(\operatorname{sgn}(\dot{x}_{2sl}) + \frac{A_3}{A_1} \operatorname{sgn}(\dot{x}_{2sr}) \right) F_c + m_f g \left(1 - \frac{A_3}{A_1} \right) \right] \quad (2.47) \end{aligned}$$

$$\begin{aligned} F_r = N_u \left[P_{4o} V_{4o}^n \left\{ \frac{A_1}{(V_{4o} - A_1 x_r + A_3 x_l)^n} - \frac{A_3}{(V_{4o} - A_1 x_l + A_3 x_r)^n} \right\} - (P_{4o} - P_a) A_2 + \right. \\ \left. \frac{\rho}{2C_d^2} \left\{ \left(\frac{-A_1 \dot{x}_r + A_3 \dot{x}_l}{u_2 a_{12r}} \right)^2 A_1 \operatorname{sgn}(\dot{x}_r) - \left(\frac{-A_1 \dot{x}_l + A_3 \dot{x}_r}{u_2 a_{12l}} \right)^2 A_3 \operatorname{sgn}(\dot{x}_l) \right\} - \frac{A_3^2 \dot{x}_r 128 \mu L}{\pi D^4} - \left(\ddot{x}_{2r} + \right. \right. \\ \left. \left. \frac{A_3}{A_1} \ddot{x}_{2l} \right) m_f - \left(\operatorname{sgn}(\dot{x}_{2sr}) + \frac{A_3}{A_1} \operatorname{sgn}(\dot{x}_{2sl}) \right) F_c + m_f g \left(1 - \frac{A_3}{A_1} \right) \right] \quad (2.48) \end{aligned}$$

Comparisons of the dynamic forces developed by type-II configuration with those derived for type-I configuration in equations (2.41) and (2.42), show that the contribution due to floating piston seals and dynamics is related to the area ratio A_3/A_1 . Since this area ratio for type-II struts is relatively small compared to type-I struts, the effect of the floating piston seals and dynamics is expected to be lower.

2.4.6 Roll Plane Interconnected Suspension (Type-IIa struts)

The effective roll stiffness and damping properties of an interconnecting hydro-pneumatic suspension are strongly dependent upon the fluid volume in the interconnecting chambers and the interconnection layout. Figure 2.8 illustrates an alternate interconnection of the type-II struts, where chambers 2 and 3 of the left-strut are coupled with chambers 3 and 2 of the right-strut, respectively. This configuration is analyzed to study the effect of variations in the interconnection arrangement on the resulting roll mode suspension properties.

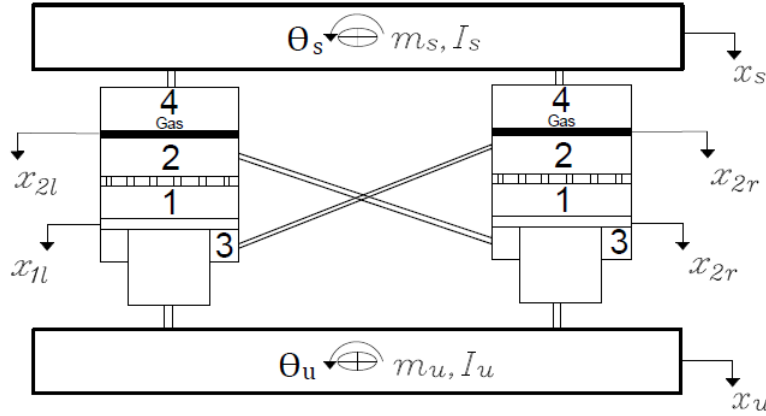


Figure 2.8: Interconnected strut model used for deriving the strut forces (Type-IIa).

The fluid flow rates and pressure relations are initially derived assuming incompressible hydraulic fluid, turbulent flows through damping orifices between chambers 1 and 2, and laminar flows through interconnecting pipes. Unlike type-I and type-II struts, the rate of change of fluid volume in chamber 1 (Q_{1i}) is related only to the flow rate from chamber 2 through the orifices, Q_{21i} , derived as:

$$Q_{1i} = Q_{21i} = A_1 \dot{x}_i; \quad i=l,r \quad (2.49)$$

Similarly, the flow continuity equations for chamber 3 of the left- and right-struts involves the flows through the interconnecting pipes alone, given by:

$$Q_{3l} = -Q_{3l2r} = -A_3 \dot{x}_l; \quad Q_{3r} = -Q_{3r2l} = -A_3 \dot{x}_r \quad (2.50)$$

The fluid flows across the two struts via interconnecting pipes, are obtained assuming Q_{3l2r} and Q_{3r2l} , as laminar flows, such that:

$$Q_{3l2r} = \frac{\pi D^4 P_{3l2r}}{128 \mu L}, \quad Q_{3r2l} = \frac{\pi D^4 P_{3r2l}}{128 \mu L} \quad (2.51)$$

Dynamic strut forces

The dynamic suspension forces produced by left- and right-struts can be expressed in terms of gas pressures and pressure differentials, as:

$$\begin{aligned}
F_l &= N_u [P_{2l} A_1 - P_{2r} A_3 - P_{21l} A_1 - P_{3l2r} A_3 - (P_{4o} - P_a) A_e] \\
F_r &= N_u [P_{2r} A_1 - P_{2l} A_3 - P_{21r} A_1 - P_{3r2l} A_3 - (P_{4o} - P_a) A_e]
\end{aligned} \tag{2.52}$$

For the incompressible fluid flow and negligible seal friction, $P_{2i} = P_{4i}$. The relationships between the strut forces and motions are thus obtained upon substituting for the gas pressure and pressure differentials, as:

$$\begin{aligned}
F_l &= N_u \left[P_{4o} V_{4o}^n \left\{ \frac{A_1}{(V_{4o} - A_1 x_l + A_3 x_r)^n} - \frac{A_3}{(V_{4o} - A_1 x_r + A_3 x_l)^n} \right\} - (P_{4o} - P_a) A_2 - \right. \\
&\quad \left. \frac{\rho}{2C_d^2} \left\{ \left(\frac{A_1 \dot{x}_l}{u_2 a_{12l}} \right)^2 A_1 \operatorname{sgn}(\dot{x}_l) \right\} - \frac{A_3^2 \dot{x}_l 128 \mu L}{\pi D^4} \right]
\end{aligned} \tag{2.53}$$

$$\begin{aligned}
F_r &= N_u \left[P_{4o} V_{4o}^n \left\{ \frac{A_1}{(V_{4o} - A_1 x_r + A_3 x_l)^n} - \frac{A_3}{(V_{4o} - A_1 x_l + A_3 x_r)^n} \right\} - (P_{4o} - P_a) A_2 - \right. \\
&\quad \left. \frac{\rho}{2C_d^2} \left\{ \left(\frac{A_1 \dot{x}_r}{u_2 a_{12r}} \right)^2 A_1 \operatorname{sgn}(\dot{x}_r) \right\} - \frac{A_3^2 \dot{x}_r 128 \mu L}{\pi D^4} \right]
\end{aligned} \tag{2.54}$$

The above equations reveal that damping force components of the type-IIa configuration are different from those derived for the type-I and type-II configurations, presented in equations (2.24) and (2.25). The gas spring force developed by each strut is identified from first two terms in equations (2.53) and (2.54). It is concluded that all three interconnected (IC) configurations exhibit identical force-displacement relationship in the vertical mode, while type-II and type-IIa struts possess lower spring rates in roll mode due to the larger gas volume. Three different dynamic force components of an interconnecting strut may be identified excluding the static force component, which are described below.

(a) Damping force due to orifice flows within the same strut, FDS_i

The damping force component, which is a function of same strut velocity (\dot{x}_i) in equations (2.53) and (2.54), is attributed to flows through orifices within the same strut and expressed as:

$$FDS_l = \frac{\rho N_u}{2C_d^2} \left(\frac{A_1 \dot{x}_l}{u_2 a_{12l}} \right)^2 A_1 \operatorname{sgn}(\dot{x}_l) \tag{2.55}$$

$$FDS_r = \frac{\rho N_u}{2C_d^2} \left(\frac{A_1 \dot{x}_r}{u_2 a_{12r}} \right)^2 A_1 \operatorname{sgn}(\dot{x}_r) \tag{2.56}$$

Equations (2.55) and (2.56) reveal that FDS of a type-IIa strut is larger than the other two IC configurations, presented in equations (2.28) and (2.29), for the identical strut velocity \dot{x}_i . This is due to different fluid flow rates across the orifices in the same strut.

The damping force due to orifice flow in the connected strut FDC , is absent in type-IIa IC configuration. This is because of interconnection layout, described in Figure 2.8, and fluid flow rates across the orifices, and flows through interconnecting pipes. In other words, damping obtained through orifices could be tuned independently in type-IIa without affecting the orifice flows in the connecting strut.

(b) Damping force due to flows across the struts, FDL_i

The damping force component attributed to laminar flows through the interconnecting lines is related to the velocity of same strut alone, such that:

$$FDL_i = -\frac{A_3^2 \dot{x}_i 128 \mu L}{\pi D^4} \quad (2.57)$$

The above equation constitutes the negative effect on the damping force developed by each strut, due to flows across the pipelines. This negative damping component (FDL) is identical to that obtained for the other two interconnected configurations, and it is significant for tuning of damping properties of a strut, where the damping valves may be eliminated.

2.4.7 Effects of Compressibility and Floating Piston Dynamics

In consideration of compressible hydraulic fluid, the rate of change in fluid volume in chamber 3 of the left-strut (Q_{3l}) is related to flow rates through the interconnecting pipe (Q_{3l2r}), and the fluid compressibility effect. The flow rate is further related to velocity of the same strut \dot{x}_l . The flow continuity equation for the left strut can thus be expressed as:

$$Q_{3l} = -Q_{3l2r} - \frac{dP_{3l}}{dt} \left(\frac{E}{V_{3l}} \right) = -A_3 \dot{x}_l \quad (2.58)$$

Similarly, the flow continuity equation for chamber 3 of the right-strut (Q_{3r}) can be expressed as:

$$Q_{3r} = -Q_{3r2l} - \frac{dP_{3r}}{dt} \left(\frac{E}{V_{3r}} \right) = -A_3 \dot{x}_r \quad (2.59)$$

where the term $\frac{dP_{3i}}{dt}$ relates to the rate of change of fluid pressure in chamber 3 due to fluid compressibility of the strut $i(i = l, r)$.

The dynamic force F_i developed by the strut i can be expressed as functions of the pressure forces, as:

$$F_i = N_u [(P_{1i} - P_{1o}) A_1 - (P_{3i} - P_{3o}) A_3 - (P_{4o} - P_a) A_e] \quad (2.60)$$

The above equation can also be expressed in terms of pressure differentials, static force and gas pressures, as:

$$\begin{aligned} F_l &= N_u [P_{2l} A_1 - P_{2r} A_3 - P_{21l} A_1 - P_{3l2r} A_3 - (P_{4o} - P_a) A_e] \\ F_r &= N_u [P_{2r} A_1 - P_{2l} A_3 - P_{21r} A_1 - P_{3r2l} A_3 - (P_{4o} - P_a) A_e] \end{aligned} \quad (2.61)$$

Apart from the above, the inertia force due to floating piston mass and the seal friction force also contributes to difference in fluid pressures between chambers 2 and 4. This can be realized from equation of motion for the floating piston which is given by:

$$m_f \ddot{x}_{2i} + P_{2i} A_1 + F_c \operatorname{sgn}(\dot{x}_{2si}) = P_{4i} A_1 + m_f g \quad (2.62)$$

Equation (2.62) is identical to the equation (2.46), which suggests that type-II and type-IIa configurations hold identical force-displacement characteristics in roll and vertical modes. The dynamic force developed by each strut is obtained upon substituting for the gas chamber pressures from equations (2.19) and (2.20), pressure differentials due to orifice flows and flow across the pipes from equations (2.17) and (2.51), and P_{2i} from the equation (2.62) into equation (2.61), such that:

$$\begin{aligned} F_l &= N_u \left[P_{4o} V_{4o}^n \left\{ \frac{A_1}{(V_{4o} - A_1 x_l + A_3 x_r)^n} - \frac{A_3}{(V_{4o} - A_1 x_r + A_3 x_l)^n} \right\} - (P_{4o} - P_a) A_e + \right. \\ &\quad \frac{\rho}{2C_d^2} \left\{ \left(\frac{A_1 \dot{x}_l}{u_2 a_{12l}} \right)^2 A_1 \operatorname{sgn}(\dot{x}_l) \right\} - \frac{A_3^2 \dot{x}_l 128 \mu L}{\pi D^4} - \left(\dot{x}_{2l} + \frac{A_3}{A_1} \dot{x}_{2r} \right) m_f - \left(\operatorname{sgn}(\dot{x}_{2sl}) + \right. \\ &\quad \left. \left. \frac{A_3}{A_1} \operatorname{sgn}(\dot{x}_{2sr}) \right) F_c + m_f g \left(1 - \frac{A_3}{A_1} \right) \right] \end{aligned} \quad (2.63)$$

$$\begin{aligned} F_r &= N_u \left[P_{4o} V_{4o}^n \left\{ \frac{A_1}{(V_{4o} - A_1 x_r + A_3 x_l)^n} - \frac{A_3}{(V_{4o} - A_1 x_l + A_3 x_r)^n} \right\} - (P_{4o} - P_a) A_e + \right. \\ &\quad \frac{\rho}{2C_d^2} \left\{ \left(\frac{A_1 \dot{x}_r}{u_2 a_{12r}} \right)^2 A_1 \operatorname{sgn}(\dot{x}_r) \right\} - \frac{A_3^2 \dot{x}_r 128 \mu L}{\pi D^4} - \left(\dot{x}_{2r} + \frac{A_3}{A_1} \dot{x}_{2l} \right) m_f - \left(\operatorname{sgn}(\dot{x}_{2sr}) + \right. \\ &\quad \left. \left. \frac{A_3}{A_1} \operatorname{sgn}(\dot{x}_{2sl}) \right) F_c + m_f g \left(1 - \frac{A_3}{A_1} \right) \right] \end{aligned} \quad (2.64)$$

Comparisons of equations (2.63) and (2.64) with those obtained for type-II struts in equations (2.47) and (2.48) suggest that type-IIa struts yield considerably different damping force component FDS due to difference in the damping plate geometry.

2.5 SUSPENSION PROPERTIES

The static and dynamic suspension properties for the UC and IC configurations are derived in terms of load carrying capacity, and vertical and roll modes stiffness and damping properties. These are described in the following subsections.

2.5.1 Load Carrying Capacity

The load carrying capacity of the UC and IC struts are related to effective area A_e , the static gas charge pressure (P_{4o}), and gas volume (V_{4o}) of the strut. The rod area serves as the effective area for supporting the vehicle's load, and it is identical for both the IC and UC struts, irrespective of the configuration. Owing to relatively larger rod area as compared with conventional struts [4], the static equilibrium pressure of the strut has been reduced considerably. The load carrying capacity of the UC and IC configurations is given by:

$$W = N_u(P_{4o} - P_a)A_e \quad (2.65)$$

The initial gas charge pressure, P_C , and the static deflection of the suspension (x_o) are determined from the initial charge volume of the strut, such that:

$$P_C = P_{4o} \left(\frac{V_C - A_e x_o}{V_C} \right)^n \quad (2.66)$$

In above equation, P_C and V_C are the initial charge pressure and initial charge volume of gas chambers in the strut.

2.5.2 Suspension Rates

Type-I struts

The suspension rate of an interconnected hydro-pneumatic suspension is derived from its dynamic force components, which are functions of gas and fluid pressures of the strut i , as described in the section 2.4.2. The spring rate of the strut can be obtained from the restoring force component attributed to the gas pressure, F_{si} , such that:

$$K_{xi} = \frac{dF_{si}}{dx_i} \quad (2.67)$$

Where K_{xi} is the vertical spring rate of strut i ($i=l, r$). Under a pure vertical relative displacement input ($x_l = x_r = x_i$), the displacements of floating pistons are identical in the left- and right-struts. In addition, the restoring force of strut i could be derived from equation (2.22) as:

$$F_{si} = (P_{1i} - P_a)A_1 - (P_{3i} - P_a)A_3 = P_{2i}A_e; \quad i=l, r \quad (2.68)$$

For the identical vertical displacement inputs, the difference between the displacements of the floating and main pistons are related to the fluid compressibility, such that:

$$\frac{V_{2i}}{E}(P_{2i} - P_{2o}) = A_e(x_{1i} - x_{2i}) \quad (2.69)$$

where V_{2i} is the instantaneous hydraulic fluid volume in chamber 2 of strut i and P_{2i} is the instantaneous pressure of fluid in strut i ($i=l, r$). $A_e x_{1i}$ refers to the total hydraulic fluid volume displaced by the main piston when the strut is subjected to a vertical displacement. Substituting for x_{2i} from equation (2.69) into equation (2.19), yields following relationship for fluid pressure:

$$P_{4i} \left[V_{4o} - A_e x_{1i} + \frac{V_{2i}}{E}(P_{2i} - P_{2o}) \right]^n = P_{4o} V_{4o}^n \quad i=l, r \quad (2.70)$$

The above relation is the function of instantaneous fluid pressure P_{2i} and main piston displacement x_{1i} . The derivative of P_{2i} with respect to x_{1i} is subsequently obtained as:

$$\frac{dP_{2i}}{dx_{1i}} = \frac{\partial \phi / \partial x_{1i}}{\partial \phi / \partial P_{2i}} = \frac{n P_{4i} A_e}{V_{4o} - A_e x_{1i} + \frac{V_{2i}}{E} [P_{2i} - P_{2o}]} \quad (2.71)$$

where V_{4o} refers to the volume of gas chamber (4) under the static equilibrium condition in strut i . Furthermore, the suspension rate in equation (2.67) can be directly related to the rate of change of fluid pressure with respect to the piston motion, such that:

$$K_{xi} = A_e \frac{dP_{2i}}{dx_{1i}} \quad (2.72)$$

The vertical suspension rate of the type-I strut is thus be obtained from equations (2.71) and (2.72), as:

$$K_{xi} = \frac{n P_{4i} A_e^2}{V_{4o} - A_e x_{1i} + \frac{V_{2i}}{E} [P_{2i} - P_{2o}]} \quad (2.73)$$

Likewise, assuming incompressible hydraulic fluid, the suspension rate of the type-I strut in connected as well as unconnected configurations is related to the function of strut displacement, x_i as:

$$K_{xi} = \frac{n P_{4o} V_{4o}^n A_e^2}{(V_{4o} - A_e x_i)^{n+1}} \quad (2.74)$$

Type-II and Type-IIa struts

For type-II struts (Figure 2.1), the vertical spring rate is derived in a similar manner. The spring rate is related to change in fluid pressure P_{2i} with respect to the main piston deflection x_{1i} , such that:

$$K_{xi} = A_{FP} \frac{dP_{2i}}{dx_{1i}} \quad (2.75)$$

It should be noted that A_{FP} in type-II struts differ from that of type-I struts. Under pure vertical displacement inputs ($x_l = x_r = x_i$), the change in volume of the fluid in chamber 2 is also related to fluid compressibility and expressed as:

$$\frac{V_{2i}}{E}(P_{2i} - P_{2o}) = A_e x_{1i} - A_{FP} x_{2i} \quad (2.76)$$

In the above equation, term $A_{FP} x_{2i}$ refers to total volume change in the gas chamber of strut i , which is evidently larger than that in type-I struts. Equations (2.76) and (2.19) yield the following relationship, for the fluid pressure as a function of the piston deflection:

$$P_{4i} \left[V_{4o} - A_e x_{1i} + \frac{V_{2i}}{E}(P_{2i} - P_{2o}) \right]^n = P_{4o} V_{4o}^n \quad i=l,r \quad (2.77)$$

The rate of change of fluid pressure in strut i , with respect to the relative vertical displacement of the main piston can be derived as:

$$\frac{dP_{2i}}{dx_{1i}} = \frac{\partial \phi / \partial x_{1i}}{\partial \phi / \partial P_{2i}} = \frac{n P_{4i} A_e}{V_{4o} - A_e x_{1i} + \frac{V_{2i}}{E A_e} [P_{2i} - P_{2o}]} \quad (2.78)$$

Equation (2.78) is identical to equation (2.73), but the static equilibrium volume of gas chamber in type-II strut is larger than the type-I strut. The vertical suspension rate K_{xi} , for the type-II and type-IIa struts is subsequently obtained as:

$$K_{xi} = \frac{n P_{4i} A_e A_{FP}}{V_{4o} - A_e x_{1i} + \frac{V_{2i}}{E A_e} [P_{2i} - P_{2o}]} \quad (2.79)$$

Like type-I struts, the vertical suspension rates of type-II and type-IIa strut configurations are also obtained considering incompressible hydraulic fluid, as:

$$K_{xi} = \frac{n P_{4o} V_{4o}^n A_{FP} A_e}{(V_{4o} - A_{FP} x_i)^{n+1}} \quad (2.80)$$

2.5.3 Vertical Damping Properties

The vertical damping properties of different strut configurations are obtained assuming turbulent flows through damping orifices and laminar flow across the interconnecting pipes. For type-I connected struts, the damping force components developed by the strut have been described in equations (2.28) to (2.32), when the fluid compressibility effect is considered negligible. The total damping force developed by the strut is the sum of force components attributed to flows through orifices within the strut (FDS_i), flows through orifices in the connecting strut (FDC_i) and flows across the struts (FDL_i), such that:

$$F_{Dxi} = FDS_i + FDC_i + FDL_i \quad (2.81)$$

where F_{Dxi} is the total damping force. Under pure vertical motion ($\dot{x}_i = \dot{x}_r = \dot{x}_l$), the vertical damping force developed by type-I IC struts can be expressed as:

$$F_{Dxi} = N_u \left[\frac{\rho}{2} \left(\frac{A_2 \dot{x}_i}{C_d u_2 a_{12i}} \right)^2 A_1 \text{sgn}(\dot{x}_i) - \frac{\rho}{2} \left(\frac{A_2 \dot{x}_i}{C_d u_2 a_{12i}} \right)^2 A_3 \text{sgn}(\dot{x}_i) - \frac{A_3^2 \dot{x}_i 128 \mu L}{\pi D^4} \right] \quad (2.82)$$

From equation (2.82), it is evident that last two terms are significant in view of the negative damping effect due to interconnection in roll plane. Since type-I and type-II exhibit identical dynamic force components, as described in equations (2.24) and (2.25), the vertical mode damping force components of the type-II are identical to those of the type-I configuration.

The damping force developed by type-IIa struts, however, differ from those of type-I and type-II configurations due to absence of the coupling component FDC_i , as described in section 2.4.6. The vertical damping force due to type-IIa struts is thus obtained from equations (2.55) to (2.57), as:

$$F_{Dxi} = N_u \left[\frac{\rho}{2} \left(\frac{A_1 \dot{x}_i}{C_d u_2 a_{21i}} \right)^2 A_1 \text{sgn}(\dot{x}_i) - \frac{A_3 \dot{x}_i 128 \mu L}{\pi D^4} A_3 \right] \quad (2.83)$$

Comparison of equations (2.82) and (2.83) suggests that type-IIa struts may yield higher damping force than type-I and type-II struts for a given relative velocity, \dot{x}_i .

Unconnected configurations

All three UC configurations yield identical fluid flow rates across the orifices; therefore, the vertical mode damping properties are identical. Similar to IC configuration, the total vertical mode damping force of the UC configurations is given by:

$$F_{Dxi} = N_u \left[\frac{\rho}{2} \left(\frac{-A_2 \dot{x}_i}{C_d u_2 a_{12i}} \right)^2 A_2 \text{sgn}(\dot{x}_i) + \frac{\rho}{2} \left(\frac{-A_3 \dot{x}_i}{C_d u_3 a_{13i}} \right)^2 A_3 \text{sgn}(\dot{x}_i) \right] \quad (2.84)$$

It is observed that by comparing equations (2.82) to (2.84), the negative damping force components could be obtained only when the struts are interconnected, which indicates the enhanced design flexibility in tuning the vertical damping force components for IC configurations than the unconnected configurations.

2.5.4 Roll Stiffness for Different Strut Configurations

Interconnected configuration (Type-I)

The sprung mass of a vehicle experiences roll motion due to external rolling moment, which yields relative vertical and roll displacements between the sprung and unsprung masses, given by $x_i = (x_s - x_u \pm L_s \theta)$ and $\theta = (\theta_s - \theta_u)$. Suspension roll stiffness could be derived from restoring rolling moment, (R_m), developed by suspension subject to a static roll angle, such that:

$$K_\theta = \frac{dR_m}{d\theta} \quad (2.85)$$

The roll deflection across the suspension is considered by applying out-of-phase pure vertical displacement inputs ($x_l = -x_r$) and $\theta = 0$. For the type-I configuration, the volume of fluid in chambers 1, 2 and 3 of the left strut and chamber 1 of the right strut yields the following relationship:

$$x_l A_1 - x_r A_3 = x_{2l} A_e + \Delta V_{Comp} \quad (2.86)$$

The above equation satisfies the change in gas chamber volume of the strut l , when main piston undergoes extension, whereas $x_{2l} A_e$ refers to the change in volume of the gas chamber in strut l due to the displacement of floating piston. ΔV_{Comp} in the above equation relates to change in volume due to fluid compressibility. The restoring rolling moment imposed by the struts in the left- and right-tracks can be computed from:

$$R_m = (F_{sl} - F_{sr}) L_s \quad (2.87)$$

where L_s refers to half the suspension track width or the horizontal spacing between the suspension strut mount and projection of the cg of the sprung mass on the lateral axis, which is identical for both left- and right-struts in the roll plane. The change in volume of the left strut due to fluid compressibility could be written as:

$$x_{2l} A_e - \frac{V_{4l}}{E} (P_{4l} - P_{4o}) = x_{1l} A_e - L_s \theta (A_1 + A_3) \quad (2.88)$$

When the suspension experiences a roll mode input, $x_{1l} A_e$ term in equation (2.88), refers to the total fluid volume change due to vertical displacement of the main piston in strut l . V_{4i} is the instantaneous fluid volume of the strut i ($i = l, r$). Similarly, chambers 1, 2 and 3 of the right strut and chamber 1 of the left strut, are related to the fluid compressibility, which can be expressed as:

$$x_{2r} A_e - \frac{V_{4r}}{E} (P_{4r} - P_{4o}) = x_{1r} A_e + L_s \theta (A_1 + A_3) \quad (2.89)$$

Under pure roll motion of the struts, $x_{1l} A_e - x_{1r} A_e = 0$, the equations (2.88) and (2.89) have been manipulated, which is a function of angular deflection, θ and thus can be expressed as:

$$\psi(P_{4l}, \theta) = \left[\left(\frac{P_{4o}}{P_{4l}} \right)^{1/n} - \left(\frac{P_{4o}}{2P_{4o} - P_{4l}} \right)^{1/n} \right] V_{4o} + 2L_s \theta (A_1 + A_3) = \frac{2V_{4l}}{E} (P_{4l} - P_{4o}) \quad (2.90)$$

In equation (2.90), P_{4r} has been expressed in terms of P_{4l} by using static equilibrium equation (2.6) of the connected left- and right-strut. In other words, the equation (2.6) has been transformed as:

$$2P_{4o} A_e = (P_{4l} + P_{4r}) A_e \quad (2.91)$$

The change in gas pressure of the left strut with respect to roll deflection can thus be derived as:

$$\frac{dP_{4l}}{d\theta} = \frac{\partial\psi/\partial\theta}{\partial\psi/\partial P_{4l}} = \frac{2L_s(A_1+A_3)}{\left[(2P_{40}-P_{4l})^{-\left(\frac{1}{n}+1\right)} - (P_{4l})^{-\left(\frac{1}{n}+1\right)} \right] \frac{V_{40} \sqrt[n]{P_{40}} + 2V_{4l}}{n} + \frac{2V_{4l}}{E}} \quad (2.92)$$

The roll stiffness of the hydraulically interconnected suspension is subsequently obtained from equations (2.85), (2.87) and (2.92), such that:

$$K_{\theta} = 2L_s(A_1 + A_3) \frac{dP_{4l}}{d\theta} = \frac{4L_s^2(A_1+A_3)^2}{\left[(2P_{40}-P_{4l})^{-\left(\frac{1}{n}+1\right)} - (P_{4l})^{-\left(\frac{1}{n}+1\right)} \right] \frac{V_{40} \sqrt[n]{P_{40}} + 2V_{4l}}{n} + \frac{2V_{4l}}{E}} \quad (2.93)$$

The roll stiffness of the unconnected configurations is derived in a similar manner, such that:

$$K_{\theta} = 2L_s(A_1 - A_3) \frac{dP_{4l}}{d\theta} = \frac{4L_s^2(A_e)^2}{\left[(2P_{40}-P_{4l})^{-\left(\frac{1}{n}+1\right)} - (P_{4l})^{-\left(\frac{1}{n}+1\right)} \right] \frac{V_{40} \sqrt[n]{P_{40}} + 2V_{4l}}{n} + \frac{2V_{4l}}{E}} \quad (2.94)$$

Similarly, roll stiffness for the interconnected suspension struts with incompressible fluid is given by [7]:

$$K_{\theta} = nN_u P_{40} V_{40}^n (A_1 + A_3) L_s \left\{ \frac{(A_1+A_3)L_s - (A_1-A_3)\frac{dx}{d\theta}}{[V_{40}+(x-L_s\theta)A_1 - (x+L_s\theta)A_3]^{n+1}} + \frac{(A_1+A_3)L_s + (A_1-A_3)\frac{dx}{d\theta}}{[V_{40}+(x+L_s\theta)A_1 - (x-L_s\theta)A_3]^{n+1}} \right\} \quad (2.95)$$

Likewise, the roll stiffness for the incompressible unconnected suspension struts is given by [7]:

$$K_{\theta} = nN_u P_{40} V_{40}^n A_{FP}^2 L_s^2 \left\{ \frac{1 - \frac{dx}{d\theta}/L_s}{[V_{40}+(x-L_s\theta)A_{FP}]^{n+1}} + \frac{1 + \frac{dx}{d\theta}/L_s}{[V_{40}+(x+L_s\theta)A_{FP}]^{n+1}} \right\} \quad (2.96)$$

At static equilibrium, the vehicle experiences zero roll displacement ($\theta = 0$), the static roll stiffness of the suspension can thus be obtained from equation (2.95), and expressed as:

$$K_{\theta}^o = \frac{2nP_{40}(A_1+A_3)^2 L_s^2}{V_{40}} \quad (2.97)$$

Similarly, the static roll stiffness of the UC configuration from equation (2.96) has been obtained as:

$$K_{\theta}^o = \frac{2nP_{40}(A_e)^2 L_s^2}{V_{40}} \quad (2.98)$$

In the above equations (2.95) and (2.96), the term x refers to the relative displacement of the sprung and unsprung masses in vertical direction and θ is the relative angular displacement between the sprung and unsprung masses. The ratio between the static roll stiffness for the interconnected configuration and the unconnected configuration has been expressed as roll stiffness amplification factor (RSAF), which emphasizes the enhanced roll stiffness property of the interconnected over the unconnected configuration [5]. Equations (2.97) and (2.98) show that

type-I strut exhibits higher roll stability than its corresponding UC configuration for the given identical static charge pressure and volume of the gas chamber.

Interconnected configurations (Type-II and Type-IIa)

Type-II and type-IIa configurations have been shown in Figures 2.7 and 2.8, respectively. Under extension of each strut, the volume of fluid in chambers 1, 2, 3 of the left strut and chamber 3 of the right strut yields the following relationship:

$$x_l A_1 - x_r A_3 = x_{2l} A_{FP} + \Delta V_{Comp} \quad (2.99)$$

Similar to the equations (2.88) and (2.89), the relationship between the fluid compressibility and deflections of the left- and right-struts can be expressed as:

$$\begin{aligned} x_{2l} A_{FP} - \frac{V_{4l}}{E} (P_{4l} - P_{4o}) &= x_{1l} A_e - L_s \theta (A_1 + A_3) \\ x_{2r} A_{FP} - \frac{V_{4r}}{E} (P_{4r} - P_{4o}) &= x_{1r} A_e + L_s \theta (A_1 + A_3) \end{aligned} \quad (2.100)$$

Rearranging equations (2.91) and (2.100) yield following expression as a function of angular deflection θ :

$$\psi(P_{4l}, \theta) = \left[\left(\frac{P_{4o}}{2P_{4o} - P_{4l}} \right)^{1/n} - \left(\frac{P_{4o}}{P_{4l}} \right)^{1/n} \right] V_{4o} - \frac{2V_{4l}}{E} (P_{4l} - P_{4o}) + 2L_s \theta (A_1 + A_3) = 0 \quad (2.101)$$

The change in instantaneous gas pressure of the left strut can be derived by solving equation (2.101) with respect to its roll deflection, such that:

$$\frac{dP_{4l}}{d\theta} = \frac{\partial \psi / \partial \theta}{\partial \psi / \partial P_{4l}} = \frac{2L_s (A_1 + A_3)}{\left[(P_{4l} - 2P_{4o})^{-\left(\frac{1}{n} + 1\right)} + (P_{4l})^{-\left(\frac{1}{n} + 1\right)} \right] \frac{V_{4o} \frac{n}{\sqrt{P_{4o}}} + \frac{2V_{4l}}{E}}{n}} \quad (2.102)$$

The restoring roll moment for the IC configuration could be expressed in terms of pressure forces, as described in equation (2.52), such that:

$$R_m = (P_{4l} - P_{4r}) (A_1 + A_3) L_s \quad (2.103)$$

The roll stiffness of the type-II and type-IIa interconnected suspensions is thus obtained as:

$$K_\theta = 2L_s (A_1 + A_3) \frac{dP_{4l}}{d\theta} = \frac{4L_s^2 (A_1 + A_3)}{\left[(P_{4l} - 2P_{4o})^{-\left(\frac{1}{n} + 1\right)} + (P_{4l})^{-\left(\frac{1}{n} + 1\right)} \right] \frac{V_{4o} \frac{n}{\sqrt{P_{4o}}} + \frac{2V_{4l}}{E}}{n}} \quad (2.104)$$

The roll stiffness for the compressible and incompressible type-II configurations is identical as that of the type-IIa configuration. The relatively larger gas volume of type-II and type-IIa configurations, however, yields lower dynamic roll stiffness, which will be discussed in the following chapter.

2.5.5 Roll Mode Damping Properties of Different Strut Configurations

The roll mode damping forces for different suspension configurations could be derived upon considering out-of-phase ($\dot{x}_l = -\dot{x}_r = \dot{x}_i$) velocity inputs for the left- and right-struts. The roll mode damping property of the suspension can be presented in terms of the damping moment (M_d), where F_{dl} and F_{dr} are the damping forces developed by the strut i ($i=l, r$). The significance of interconnection in the roll mode is mainly illustrated by its enhanced roll mode damping property. The fluid flows across the connected struts enhance the roll mode damping property of the interconnected struts. The relative velocities across the two struts are related to vertical and roll deflections of the sprung and unsprung masses in the following manner:

$$\begin{aligned}\dot{x}_l &= (\dot{x}_s - \dot{x}_u) - L_s(\dot{\theta}_s - \dot{\theta}_u); \\ \dot{x}_r &= (\dot{x}_s - \dot{x}_u) + L_s(\dot{\theta}_s - \dot{\theta}_u); \end{aligned} \quad (2.105)$$

Unconnected configurations

The suspension struts employed in UC configurations generate damping force due to fluid flows through bleed orifices between chambers 1 and 2, and 1 and 3. The total roll mode damping force ($F_{d\phi}$) of a UC strut could be obtained as:

$$F_{d\phi} = \frac{\rho}{2} \left(\frac{(\dot{x}_s - \dot{x}_u - L_s \dot{\theta}) A_e}{C_d u_2 a_{12i}} \right)^2 A_e \operatorname{sgn}(\dot{x}_i) + \frac{\rho}{2} \left(\frac{A_3 (\dot{x}_s - \dot{x}_u - L_s \dot{\theta})}{C_d u_3 a_{13i}} \right)^2 A_3 \operatorname{sgn}(\dot{x}_i) \quad (2.106)$$

The above relation is obtained by substituting equation (2.105) into equation (2.14), where the damping force components are functions of the relative velocity, \dot{x}_i and $\dot{\theta}$. Since, the inputs are out-of-phase, the total roll damping moment for the unconnected strut could be expressed in terms of angular velocity, which can be obtained by substituting $\dot{x}_s - \dot{x}_u = 0$ in equation (2.106), such that:

$$M_d = \frac{\rho}{2} \left(\frac{L_s \dot{\theta}}{C_d u_2 a_{12i}} \right)^2 (A_e + A_3)^3 \operatorname{sgn}(\dot{x}_i) \quad (2.107)$$

The above equation is valid only if the total orifice area between the chambers 1 and 2 are identical to the total orifice area between the chambers 1 and 3 ($u_2 a_{12i} = u_3 a_{13i}$).

Type-I Configuration

Unlike unconnected struts, the total roll mode damping force of the interconnected configuration ($F_{d\phi}$) consists of coupled damping components, as described in equations (2.24) and (2.25), such that:

$$F_{d\phi} = N_u \left[\frac{\rho}{2} \left(\frac{A_1(\dot{x}_s - \dot{x}_u - L_s \dot{\theta}) - A_3(\dot{x}_s - \dot{x}_u + L_s \dot{\theta})}{C_d u_2 a_{12i}} \right)^2 A_1 \operatorname{sgn}(\dot{x}_i) - \frac{\rho}{2} \left(\frac{A_1(\dot{x}_s - \dot{x}_u + L_s \dot{\theta}) - A_3(\dot{x}_s - \dot{x}_u - L_s \dot{\theta})}{C_d u_2 a_{12i}} \right)^2 A_3 \operatorname{sgn}(\dot{x}_i) - \frac{A_3^2 (\dot{x}_s - \dot{x}_u - L_s \dot{\theta}) 128 \mu L}{\pi D^4} \right] \quad (2.108)$$

Considering a pure roll motion across the struts ($\dot{x}_s - \dot{x}_u = 0$), the roll damping moment in terms of angular velocity can be obtained as:

$$M_d = N_u \left[\frac{\rho}{2} \left(\frac{L_s \dot{\theta}}{C_d u_2 a_{12i}} \right)^2 (A_{1i} + A_{3i})^3 \operatorname{sgn}(\dot{x}_i) + \frac{A_3^2 L_s \dot{\theta} 128 \mu L}{\pi D^4} \right] \quad (2.109)$$

The first term in the above equation represents the damping moment due to flows through the orifices, while the second term denotes the contribution due to flows across the two struts. The type-II configuration also yields identical expressions for the total roll mode damping force and roll damping moment.

Type-IIa configuration

The total roll mode damping force and roll damping moment for the type-IIa strut is given as:

$$F_{d\phi} = N_u \left[\frac{\rho}{2} \left(\frac{A_1(\dot{x}_s - \dot{x}_u - L_s \dot{\theta})}{C_d u_2 a_{12i}} \right)^2 A_1 \operatorname{sgn}(\dot{x}_i) - \frac{A_3(\dot{x}_s - \dot{x}_u - L_s \dot{\theta}) 128 \mu L}{\pi D^4} A_3 \right] \quad (2.110)$$

The above equation has been obtained from equation (2.53), by substituting the relative velocities of the strut as described in equation (2.105). Similar to type-I configuration, the roll mode damping moment of the type-IIa strut could be described as:

$$M_d = N_u \left[\frac{\rho}{2} \left(\frac{L_s \dot{\theta}}{C_d u_2 a_{12i}} \right)^2 (A_1)^3 \operatorname{sgn}(\dot{x}_i) + \frac{A_3^2 L_s \dot{\theta} 128 \mu L}{\pi D^4} \right] \quad (2.111)$$

From equations (2.109) and (2.111), it is evident that the roll damping moment for the type-IIa configuration is lower than the type-I and type-II configurations. Furthermore, the roll mode damping does not exhibit the negative damping effect. The negative damping force components yield only positive damping moment. The result of substantially higher roll mode damping of IC suspension could help enhance the roll stability and handling quality of the vehicle.

2.6 ENHANCEMENT OF NEGATIVE DAMPING VIA INTERCONNECTING PIPES

As illustrated in section 2.4.2, the interconnection between the struts in roll plane yield negative damping force components due to flows across the struts. The force component due to flows through interconnecting pipes, FDL enhances roll mode damping moment and could help tune the bounce mode damping properties for a better ride comfort without deploying valves inside the interconnected struts. The negative damping effect of the IC suspension may be emphasized by introducing multiple interconnecting pipes of relatively small size opening area, as shown in

Figure 2.9. Based on the *Hagen-Poiseuille* relation, differential pressures across the struts is given by:

$$\Delta P = \frac{128\mu L Q J}{\pi D^4} \quad (2.112)$$

where Q denotes the fluid flow rate across the interconnecting pipes and J refers to the number of interconnecting pipes in the configuration.

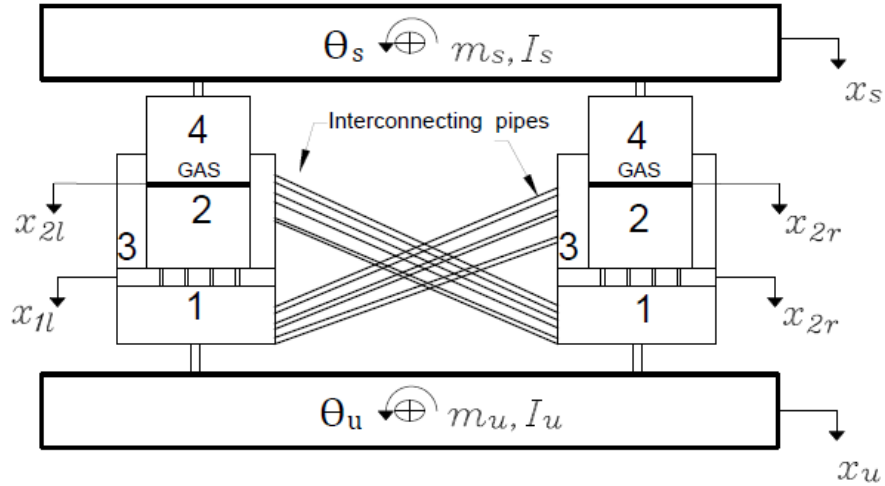


Figure 2.9: Schematic of the multiple interconnection (Type-I strut).

Implementation of large number of interconnecting pipes of relatively small opening area, however, may pose certain design complexities. The small size pipes may limit the fluid flows and cause hydraulic lock under a relatively high velocity. Moreover, multiple pipes also increase the potential for leakage. Alternatively, flow valves may be employed to achieve variable pressure drop across the interconnecting pipe and thereby greater flow resistance and negative damping effect.

A normally open valve is proposed so as to realize greater flow area under low magnitude motions. The opening area is gradually decreased with increasing pressure differential in order to enhance the negative damping effect under high magnitude motions. The schematic of the effective valve diameter is shown in Figure 2.10.

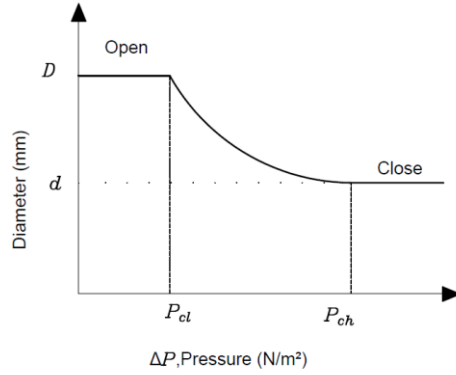


Figure 2.10: Proposed variation in the valve opening as a function of the pressure differential across the interconnecting pipe.

Figure 2.10 illustrates the proposed variation in the valve diameter as a function of the pressure differential ΔP . The saturation of the valve opening corresponding to the higher pressure differential, P_{ch} , is denoted as the ‘closed’ portion of the valve.

The normally open valve permits effective flow diameter D at relatively low motions when the pressure differential is less than a preset low limit, P_{cl} ($\Delta P < P_{cl}$). The valve opening decreases gradually when pressure differential exceeds P_{cl} and saturates near d as the pressure differential approaches the upper limit P_{ch} . The variations in the flow area of the valve may be realized in a linear manner, such that:

$$D = \begin{cases} D & 0 \leq \Delta P < P_{cl} \\ D - (D - d) \left(\frac{\Delta P - P_{cl}}{P_{ch} - P_{cl}} \right) & P_{cl} \leq \Delta P < P_{ch} \\ d & P_{ch} \leq \Delta P \end{cases} \quad (2.113)$$

Identical valve characteristics are considered for the compression as well as extension modes, such that $P_{el} = P_{cl}$ and $P_{eh} = P_{ch}$. It is also recognized that linear variations in the valve opening may cause sudden variations in the negative damping forces in the vicinity of the transition regions ($\Delta P \approx P_{cl}$ or P_{el}). An alternative function is thus proposed to realize somewhat smoother variations in the valve opening, given by:

$$D = \begin{cases} D & 0 \leq \Delta P < P_{cl} \\ \frac{(D-d)}{2} \cos\left(\frac{2\pi}{K(P_{ch}-P_{cl})}\right) (\Delta P - P_{cl}) + \frac{(D+d)}{2} & P_{cl} \leq \Delta P < P_{ch} \\ d & P_{ch} \leq \Delta P \end{cases} \quad (2.114)$$

In equation (2.118), K is the severity parameter by which valve openings could be adjusted to yield smooth transition and provide continuous damping force. The above relationship between the valve opening and the pressure differential is also illustrated in Figure 2.10.

2.7 SUMMARY

A new strut design is proposed to enhance the effects of negative damping when struts are interconnected in the roll-plane. Three different interconnected and their corresponding unconnected configurations are analytically described by their spring and damping forces. In addition to the floating piston dynamics, fluid compressibility effect has been introduced to derive the suspension forces. The dynamic suspension force components for all suspension configurations are derived based on flow and pressure equations, and their static and dynamic properties are formulated. Though suspension configurations vary in their dynamic properties, the strut geometry, load carrying capacity and static equilibrium pressures are maintained identical in order to compare the relative merits and demerits of the suspension units. Due to larger floating piston area, a large amount of gas volume is needed for type-II and type-IIa as compared with type-I configuration. All three unconnected configurations provide identical vertical and roll mode suspension properties.

Damping force components of the interconnected configurations are expressed in terms of roll and bounce modes separately. Type-I and type-II configurations possess three different damping force components, which are named as FDS (damping force attributed to orifice flows within the same strut), FDC (coupling component due to orifice flows from the connected strut) and FDL (linear damping component due to flows across the struts). The type-IIa configuration possesses only FDS and FDL damping force components. It is proposed that the negative damping effect of the interconnection may be emphasized by increasing the pressure differential across the interconnecting pipes via a flow control valve, the formulation derived in this chapter are used to study the vertical and roll mode stiffness and damping properties of different configurations in the following chapter.

CHAPTER 3

PROPERTY ANALYSIS OF DIFFERENT HYDRO-PNEUMATIC CONFIGURATIONS

3.1 INTRODUCTION

The analytical models of the hydro-pneumatic suspension struts and interconnection arrangements, presented in the previous chapter, revealed design flexibility in view of load carrying capacity, roll mode stiffness and damping characteristics. Moreover, the strut design offers relatively large working area compared to those in the reported studies [3, 5, 6]. The charge pressure required for a given load capacity could thus be reduced, and the design of seals may be simplified. Roll plane interconnections offer not only enhanced roll stiffness and roll damping but also reduce the coupling between the vertical and roll mode motions of the vehicle.

Analytical models also revealed negative damping force components due to flows through roll-plane interconnections. This has been cited as negative feedback damping [7], although the significance of these components for suspension tuning has not been explored. In this chapter, analytical formulations are used to evaluate relative vertical and roll mode stiffness properties of the proposed configurations, in addition to the load carrying capacity of the suspension. The negative damping force arising from the interconnection flows is evaluated and its potential for tuning of the damping properties is explored. The ride height leveling feature of the hydro-pneumatic suspension struts is further discussed considering the design of a ride-height valve. Apart from the ride height control, it is shown that the ride-height valve could minimize variations in the vertical mode frequency under varying loads.

3.2 STATIC PROPERTIES OF THE STRUTS

The static properties of the strut designs, described in chapter 2, are evaluated considering identical working area and load carrying capacity. This also implies identical fluid pressure corresponding to the static equilibrium condition. Furthermore, identical static deflections of the selected strut designs are assumed to ensure same ride height of different suspension configurations. Table 3.1 summarizes the simulation parameters for the roll plane vehicle model with different suspension configurations, presented in Figure 2.3. The simulation parameters are taken as those of a highway bus reported in [65], while the hydraulic fluid properties are adopted from an earlier study [7]. Table 3.2 presents the geometric parameters of the struts employed in unconnected (UC) and connected (IC-I, IC-II and IC-IIa) suspension configurations.

Table 3.1: Simulation parameters of the vehicle model.

Symbols	Description	Parameter values
m_s	Sprung mass	17748 kg
m_u	Unsprung mass	2500 kg
I_s	Roll mass moment of inertia of the sprung mass	32000 kgm ²
I_u	Roll mass moment of inertia of the unsprung mass	3050 kgm ²
K_{tl}, K_{tr}	Stiffness coefficients of the left and right tires	3574800 N/m
C_{tl}, C_{tr}	Damping coefficients of the left and right tires	12000 Ns/m
L_{sl}, L_{sr}	Lateral distances from left and right struts to sprung mass cg	0.8 m
L_{tl}, L_{tr}	Lateral distances from left and right tires to unsprung mass cg	1.03 m
h_2	Vertical distance between sprung mass roll center to the ground	1.179 m
C_d	Discharge coefficient	0.7
n	Polytropic constant	1.38
N_u	Number of struts used on each side	2
p_a	Atmospheric pressure	101325 Pa
μ	Dynamic viscosity of the fluid	0.082 Ns/m ²
ρ	Mass density of the fluid	912 kg/m ³
D	Interconnecting pipe diameter	0.03 m

Owing to the differences in the floating piston area, the struts used in the proposed suspension configurations employ different initial charge volume of the gas (V_c). It is ensured that all the configurations yield identical fluid pressure corresponding to static equilibrium so as to evaluate their relative properties under identical load carrying capacity. The suspension strut parameters are also chosen to ensure identical static deflections under the given load.

Table 3.2: Strut parameters for different configurations.

Strut Specifications	UC/IC-I	UC/IC-II	UC/IC-IIa
Main piston area, $A_1(m^2)$	0.01434	0.01434	0.01434
Annular area, $A_3(m^2)$	0.0024	0.0024	0.0024
Rod area, $A_e(m^2)$	0.01194	0.01194	0.01194

The volume of gas corresponding to static equilibrium and initial charge pressure (P_C) thus differ for different suspension configurations. The gas chamber volume at static equilibrium (V_{4o}) is obtained from:

$$V_{4o} = V_C \left(\frac{P_C}{P_{4o}} \right)^{\frac{1}{n}} \quad (3.1)$$

where the static equilibrium gas volume is related to static deflection x_o of the strut, such that $V_{4o} = V_C - A_{FP}x_o$. The initial charge pressure for different configurations is chosen to achieve identical static deflection, such that:

$$P_C = P_{4o} \left(\frac{V_C - A_{FP}x_o}{V_C} \right)^n \quad (3.2)$$

In the above equation, $A_{FP} = A_e$ for type-I struts. The polytropic process of the gas yields progressively hardening property of the suspension struts in compression and softening force-deflection property in extension, as it is evident in Equations (2.74) and (2.80). The equivalent linear vertical mode static stiffness (K_{x_o}) of the struts is obtained from the first-order *Taylor* series approximation about x_o , as:

$$K_{x_o} = \frac{n P_{4o} A_{FP} A_e}{V_{4o}} \quad (3.3)$$

The static deflection of the strut is subsequently obtained from Equations (3.2) and (3.3), as:

$$x_o = \frac{V_{4o}}{n A_{FP}} \quad (3.4)$$

The selected parameters yield identical static stiffness and thus the vertical mode natural frequency of the sprung mass, which is obtained as 1.5 Hz. The static suspension rates of different configurations in vertical and roll modes are listed in the Table 3.3. The static roll stiffness values of the unconnected configurations are relatively lower than corresponding roll mode interconnected configurations due to hydraulic coupling across the struts. The static roll stiffness of the UC-Roll bar is made identical with the IC-II and IC-IIa, in order to compare the relative merits and demerits over the suspension configurations.

Table 3.3: Static properties of different struts based on their configurations.

Property	UC	UC-Roll bar	IC- I	IC- II and IC- IIa
Load carrying capacity (kg)	4437.04	4437.04	4437.04	4437.04
Suspension rate (kN/m)	406.7	406.7	406.7	406.7
Roll stiffness (kNm/rad)	520.6	851.8	1023	851.8

On the other hand, variations in the payload would yield different ride height of the vehicle and thereby the static equilibrium pressure of the gas chamber (P_{4o}) and vertical mode natural frequency. Ride height valves can be conveniently implemented in the hydro-pneumatic suspensions to ensure constant static ride height of the vehicle, irrespective of the load.

Figure 3.1 illustrates the roll-plane model of the vehicle with a hydro-pneumatic suspension, where each strut is equipped with a ride-height control valve. The control valve is regulated by a leveling link BH, coupling the sprung mass with the valve housing mounted on the axle. The valve consists of a beam pivoted at K. An increase in the payload causes the beam to rotate clockwise about the pivot K, which permits the flow of air from the reservoir to the gas chamber of the strut. The gas volume in chamber 4 increases to raise the sprung mass until the valve beam approaches a horizontal position. The static equilibrium pressure of the gas chamber also increases to support the higher vehicle load. Similarly, a reduction in the payload causes the beam to rotate in the counter-clockwise direction, which permits the flow of air from chamber 4 to the ambient through a check valve until the beam approaches a horizontal position. The gas pressure decreases, while the gas volume is held to the nominal value. The ride-height valve (RHV), shown in Figure 3.1, provides control of static height alone and cannot compensate for height changes induced by dynamic motion of the vehicle.

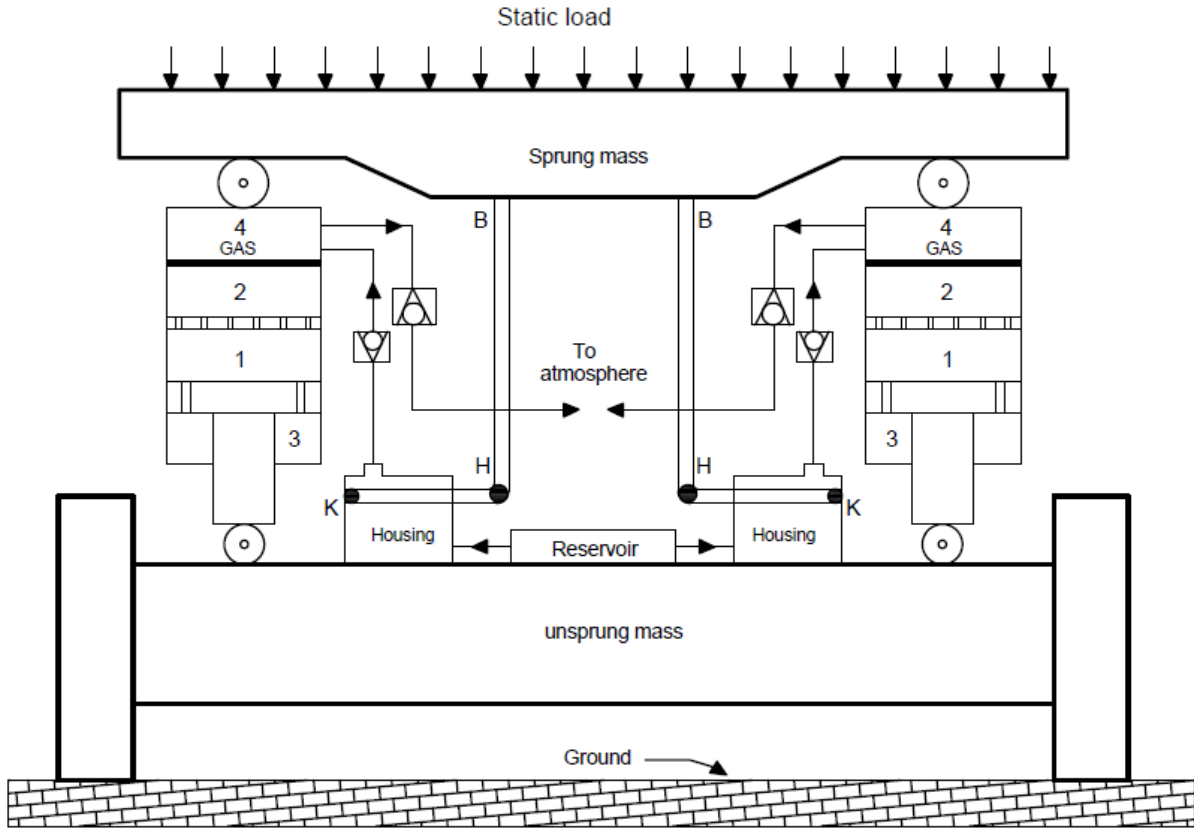


Figure 3.1: Proposed schematic of the ride height valve.

The influence of variations in the vehicle load acting on a single strut is evaluated to identify static stiffness by considering $\pm 25\%$ and $\pm 50\%$ variations about the nominal load W . The change in gas pressure with varying static load alters the static stiffness of the strut. Assuming a single-degree-of-freedom (DOF) representation of a strut supporting one-quarter of the sprung mass, it can be shown that the natural frequency remains constant, irrespective of the vehicle load. The natural frequency of the single DOF system can be obtained from the static stiffness, defined in Equation (3.5), as:

$$f_n = \frac{1}{2\pi} \sqrt{\frac{nA_{FP}g}{V_{40}}} \quad (3.5)$$

The above equation suggests that vertical mode natural frequency is independent of the vehicle mass, while the static equilibrium volume of the gas chamber V_{40} remains constant when a RHV is used. Table 3.4 compares the variations in static stiffness of the strut with and without the RHV and the vertical mode natural frequency, when the sprung weight is varied by $\pm 25\%$ and $\pm 50\%$ about the nominal weight.

Table 3.4 Static properties of the different struts with and without ride height valves.

Static load (kN)	With RHV			Without RHV		
	Natural frequency (rad/s)	Static stiffness (kN/m)	Static deflection (m)	Natural frequency (rad/s)	Static stiffness (kN/m)	Static deflection (m)
65.3	9.44	604.5	0.11	10.90	805.7	0.08
54.4	9.44	505.6	0.11	10.21	592.0	0.09
43.5	9.44	406.7	0.11	9.44	406.7	0.11
32.6	9.44	307.7	0.11	8.53	251.4	0.13
21.8	9.44	208.8	0.11	7.41	128.8	0.17

The results are obtained considering nominal static deflection of the strut as 0.11 m and corresponding gas volume of 0.0018 m^3 for type-I struts, and 0.0022 m^3 for type-II struts. It is evident that the natural frequency remains constant for the entire range of variations in the mass, when RHV is employed. In the absence of the RHV, the natural frequency increases by nearly 15% with 50% increase in the vehicle mass. The natural frequency decreases by nearly 20% with 50% reduction in the vehicle mass, which is attributed to softening tendency of the strut under extension. It is further seen that static stiffness of the strut increases with increasing vehicle mass. The change in stiffness with the mass, however, is considerably large in the absence of the RHV. The nominal value of static stiffness increases by nearly 98% with 50% increase in the vehicle mass and decreases by nearly 68% with 50% decrease in the nominal weight, when RHV is not installed in the vehicle. This is due to variations in the gas volume V_{40} with change in the vehicle mass.

The suspension rate in the vertical mode varies by nearly 24% symmetrically for every 25% change in vehicle load when RHV is deployed in the vehicle, as shown in Figure 3.2. In brief, presence of RHV in the vehicle, symmetrically shifts the suspension rate in the compression and extension regions, with respect to the load variation considered from the nominal load condition. Furthermore, the use of ride-height control system ensures identical suspension travel in compression and rebound. In the absence of RHV, the strut yields unequal travel in compression and rebound, and may encounter bump stop impacts. For instance, a 50% increase in the sprung mass causes static deflection of 0.08 m as opposed to 0.11 m for the nominal mass, as seen in Table 3.4. This will reduce effective suspension travel during compression and extension by 3cm.

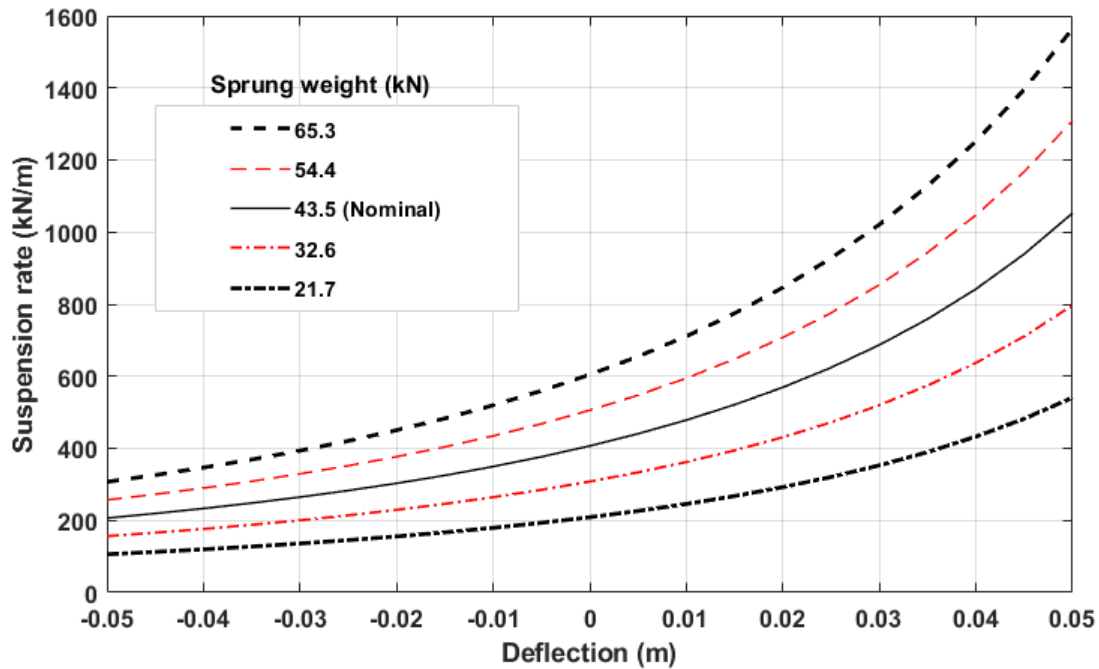


Figure 3.2: Influence of variations in sprung weight on the suspension rates of type-I and type-II struts with the ride height control system.

3.2.1 Vertical and Roll Suspension Rates

The vertical suspension rates of type-I and type-II (type-IIa) struts are depicted in Figures 3.3(a) and 3.3(b), respectively. The suspension rates are obtained for incompressible and compressible hydraulic fluids. Moreover, the effect of fluid compressibility on the vertical suspension rates is also presented by considering two different values of the fluid bulk modulus (E): $7e+08 N/m^2$ (nominal); and $7e+07 N/m^2$. Besides the smaller gas volume, the area ratio of the main and floating pistons is larger in type-I strut compared to the type-II strut. As a result, the instantaneous fluid volume in chamber 2 of type-I struts is comparatively larger than the type-II and type-IIa struts. The type-II and type-IIa struts thus exhibit relatively higher suspension rates than type-I strut, when the hydraulic fluid compressibility is considered. This is also evident from Equations (2.73) and (2.79). The results suggest highly asymmetric spring rates in compression and extension for both types of struts, which is attributed to compressibility of the gas. Reducing the fluid bulk modulus, however, mitigates the degree of asymmetry in the gas spring force, as seen in Figures 3.3.

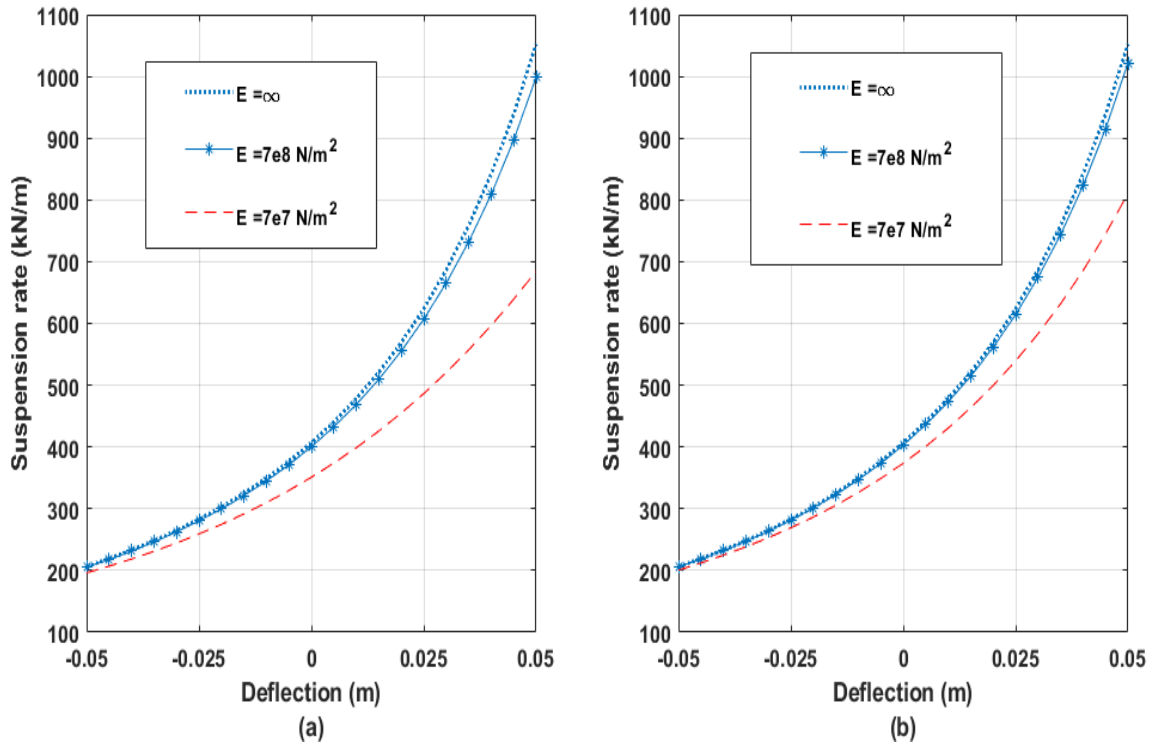


Figure 3.3: (a) Effect of fluid compressibility on the vertical suspension rates of the hydro-pneumatic struts: (a) type-I strut (UC/IC); and (b) type-II and type-IIa struts (IC/UC).

The vertical suspension rates, shown in Figures 3.3(a) and 3.3(b), have been evaluated considering a single strut. The vertical spring rates remain identical for both unconnected (UC) as well as interconnected struts. The interconnections, however, yield significant roll stiffness of the suspension, as discussed in section 2.5.4. The effective roll stiffness characteristics of different interconnected struts are evaluated under out-of-phase deflections of the right- and left-struts, as described in section 2.5.4. The suspension roll stiffness is subsequently obtained from the roll moment, using Equations (2.87) and (2.103). Figure 3.4 (a) shows the roll stiffness of IC-I configuration considering incompressible and compressible hydraulic fluids.

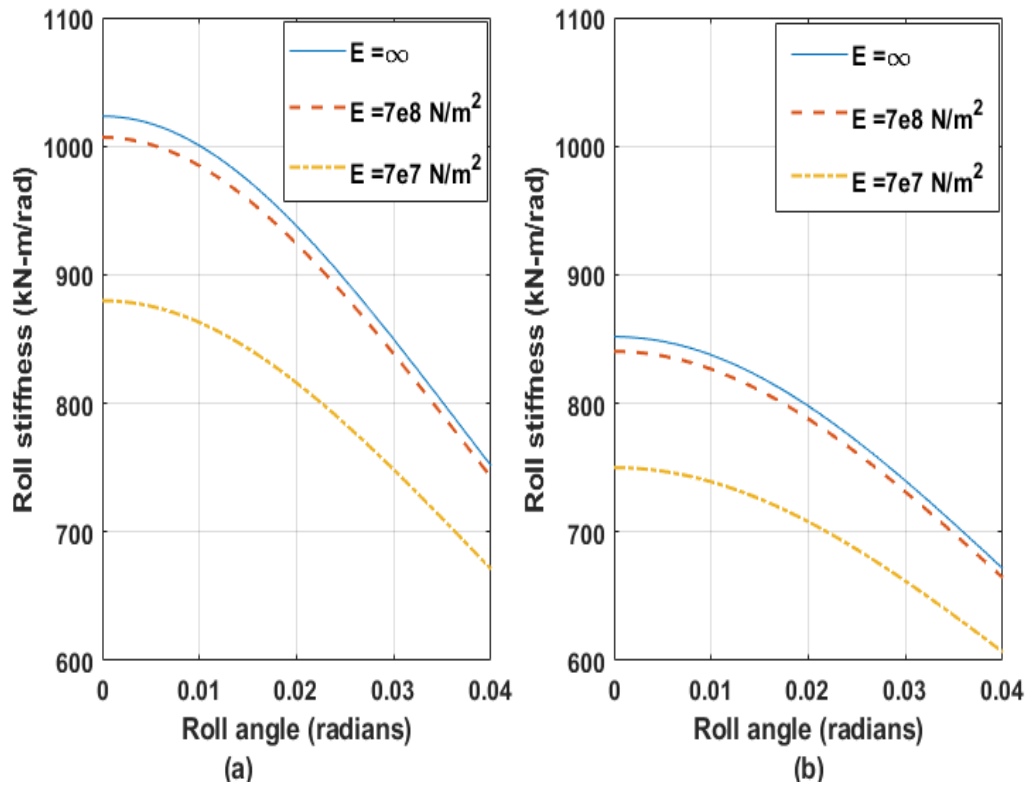


Figure 3.4: Roll stiffness of interconnected suspension configurations and the effect of fluid bulk modulus: (a) IC- I configuration; and (b) IC-II and IC-IIa configurations.

The results show large roll stiffness corresponding to the static equilibrium position. The effective roll stiffness, however, decreases rapidly with increasing roll deflection. Owing to its smaller static equilibrium gas volume, the IC-I configuration yields considerably higher roll stiffness compared to the IC-II and IC-IIa configurations, in the entire range of roll deflection. The larger ratio of main piston area to the floating piston area of type-I struts also contributes to a higher reduction rate in the roll stiffness as the roll deflection increases. The static roll stiffness of the IC-II and IC-IIa configurations are nearly 17% lower than that of the IC-I configuration, when the fluid compressibility is neglected. The difference in roll spring rates of type-II and type-I struts tend to be slightly smaller, when fluid compressibility is considered (14.7 – 16.5%). This suggests that type-II struts with relatively larger gas volume are less sensitive to the fluid compressibility effect. Furthermore, the relatively larger floating piston area of the type-II struts yields lower rate of change in the roll stiffness with increasing roll deflection. It should be noted that effective roll stiffness of the IC configurations can be varied by varying the geometric parameters of the struts. As explained in Equations (2.93), (2.94) and (2.104), increase in the main piston (A_1) and annular (A_3) areas can lead to greater roll stiffness.

Unlike the IC configurations, there is no fluid flow across the struts in the UC configurations, which results in considerably lower effective roll stiffness, as shown in Figure 3.5. The lower roll stiffness of the UC configuration can be attributed to two main factors. Firstly, the change in gas volume is smaller compared to the corresponding IC configurations due to relatively smaller floating piston deflection. Secondly, the hydraulic flow to the annular chamber in the UC struts yields lower change in the gas volume and thus the spring rate compared to the IC struts. The above factors are also evidenced from Equations (2.97) and (2.98). The unconnected suspensions, invariably, employ an anti-roll bar to supplement the suspension roll stiffness. Figure 3.5 illustrates the effective roll stiffness of the UC suspension with an anti-roll bar. The anti-roll bar in this case is selected to achieve total roll stiffness equal to that of the IC-IIa configuration, as presented in Table 3.3. The Figure 3.5 also illustrates the effect of fluid bulk modulus on the effective roll stiffness. A reduction in the fluid bulk modulus yields lower vertical stiffness and thereby the effective roll stiffness.

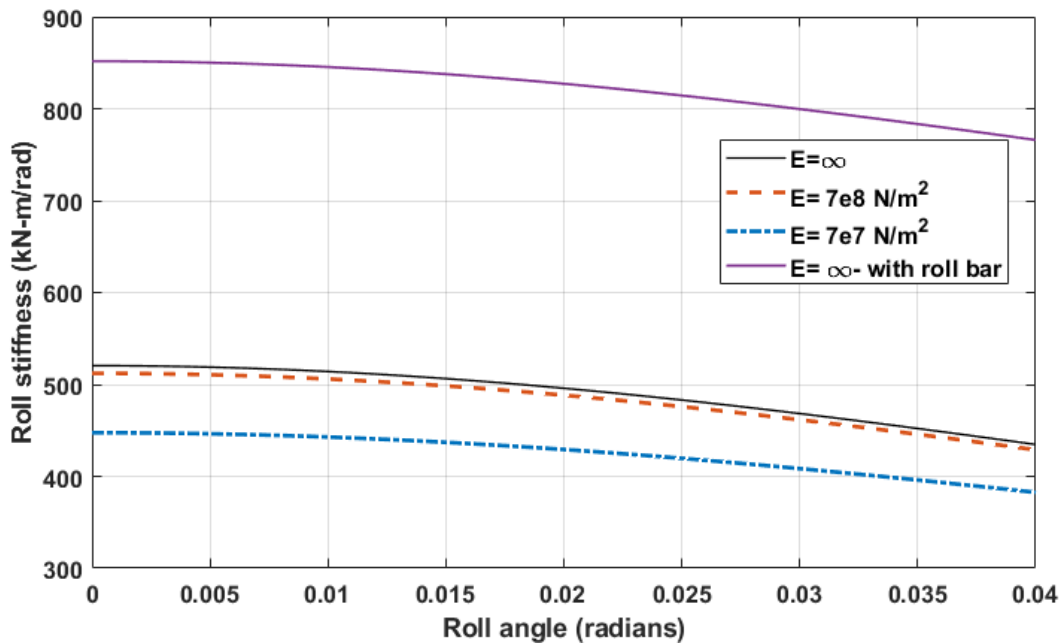


Figure 3.5: Roll stiffness of the unconnected suspension configurations with and without antiroll bar, and the effect of fluid compressibility.

The roll stiffness of the UC and IC suspension configurations is also related to the strut geometry, namely, A_1 and A_3 , as seen in Equations (2.93) and (2.94). Figures 3.6(a) and 3.6(b) illustrate the effect of variations in (A_1) on the roll stiffness of the IC-I and IC-II (IC-IIa) configurations, respectively. The results are obtained for $\pm 5\%$ variations in A_1 , while the static equilibrium pressure and effective area of the strut are held to the nominal values. An increase in

A_1 thus yields an increase in A_3 . The results show that an increase in the cross-sectional area of the main piston (A_1) yields higher roll stiffness of all the interconnected configurations. Though IC-II and IC-IIa strut configurations yield relatively lower roll stiffness compared to IC-I configuration in the entire range of roll deflection considered, the IC-I struts exhibit greater rate of reduction with increasing roll deflection. This is due to relatively larger displacement of the floating piston in IC-I struts.

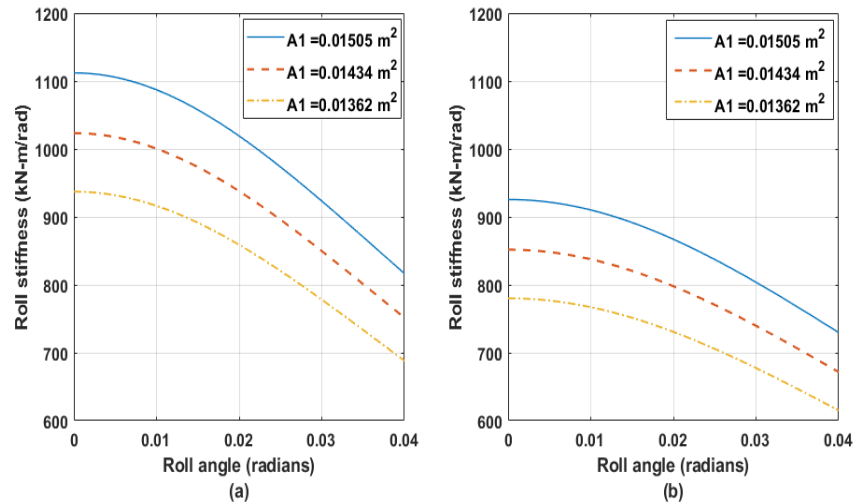


Figure 3.6: Effect of variation in main piston area on the roll stiffness of the interconnected suspension configurations: (a) IC- I configuration; and (b) IC-II and IC-IIa configurations.

It should be noted the vertical spring rate of an IC-I struts depends on the floating piston area alone, which directly relates to the change in gas volume. The vertical suspension rate of an IC-I strut thus does not directly depend on the main piston area, A_1 . The vertical suspension rates of the IC-II and IC-IIa struts, however, are dependent on the cross-sectional area of the main piston, as shown in Figure 3.7. This is due to identical floating and main piston areas, and the results are obtained considering incompressible hydraulic fluid. The results show that the equivalent static stiffness of the IC-II and IC-IIa struts increases with increase in the main piston or floating piston area, although effect of area is very small during extension.

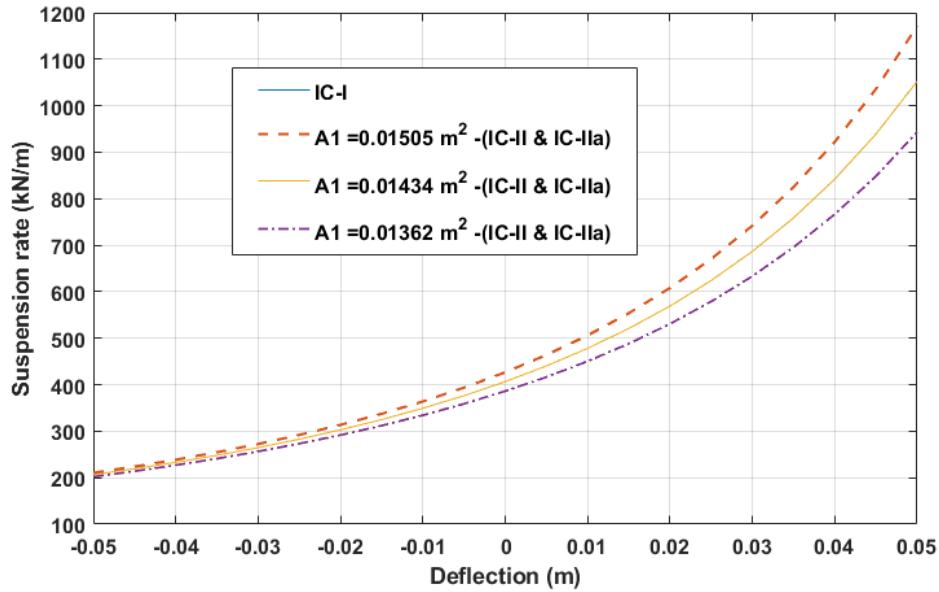


Figure 3.7: Effect of main piston area (A_1) on the vertical suspension rates of the struts.

3.3 VERTICAL DAMPING PROPERTIES

The damping characteristics of the unconnected and interconnected configurations are evaluated while the hydraulic fluid is considered as incompressible. It should be noted that the number and sizes of orifices in both types of struts are selected so as to achieve identical flow rates through orifices and thereby identical force-velocity characteristics. The flows through constant area orifices yield nearly quadratic relationship between the damping force and the velocity, as seen in Equation (2.84). The damping force thus increases rapidly with increasing velocity. Such damping characteristics of the strut are known to be detrimental in view of control of ride vibration of the vehicle. The dampers are invariably designed to provide high damping coefficient at a lower velocity but substantially lower damping coefficient at higher velocities to achieve improved ride performance [6]. Damping valves are thus introduced so as to control the increase in hydraulic pressure and resistance to flows at higher velocities. In this study, shim-stack valves are considered in the main piston, which permit higher flow areas across the piston when the velocity exceeds 0.15 m/s. The damping force-velocity characteristics of a suspension strut can be conveniently tuned through valve design, namely, the flow area ratio, the transition velocity and rate of change of the valve opening area. The area ratio for an unconnected strut is defined as the ratio of the total flow area due to orifices and valve to that of the orifices alone. Transition velocity refers to the strut velocity at which the valve begins to open. As an example, Figure 3.8(a) illustrates the variations in the flow area and the resulting force-velocity characteristics of the unconnected strut

considering three different area ratios (G), ranging from 2 to 3. It can be seen that total flow area increases gradually from the effective orifice area ($A= 0.75 \times 10^{-4} \text{ m}^2$) to the maximum flow area, as described by the following relationship:

Total flow area =

$$\left\{ \begin{array}{ll} \frac{u_2 a_{12i}}{(2N+1) u_2 a_{12i}} & 0 \leq \Delta P < P_{cl} \\ -(Nu_2 a_{12i}) \cos\left(\frac{\pi}{(P_{ch}-P_{cl})}(\Delta P - P_{cl})\right) + (N+1) u_2 a_{12i} & P_{cl} \leq \Delta P < P_{ch} \\ (2N+1) u_2 a_{12i} & P_{ch} \leq \Delta P \end{array} \right. \quad (3.6)$$

where N is the smoothing parameter selected to achieve smoother variation in the opening area, P_{cl} is lower limit of the pressure difference across chambers 1 and 2 at which the valve opening begins and P_{ch} is the pressure difference when valve approaches its fully open position. The results, presented in Figure 3.8(b), are obtained considering identical valve characteristics in the compression and extension modes for three different area ratios, $G= 2, 2.5$ and 3. The transition velocity is taken as 0.15 m/s, which corresponds to pressure differential P_{cl} across the valve. The pressure differential, however, increases with further increase in strut velocity, while the rate of increase in pressure differential depends on the instantaneous strut velocity and thereby the valve flow area. The valve opening saturates near the maximum flow area, as the pressure differential reaches P_{ch} . The valves are configured to provide gradual increase in the flow area until the strut velocity approaches 0.6 m/s. A larger valve opening constitutes a relatively lower flow resistance and thus greater reduction in the resulting damping force. Meanwhile, such damping valves could also be configured with relatively lower transition velocities, due to smaller effective orifice area, and utilized in interconnected configurations to reduce the high speed damping force.

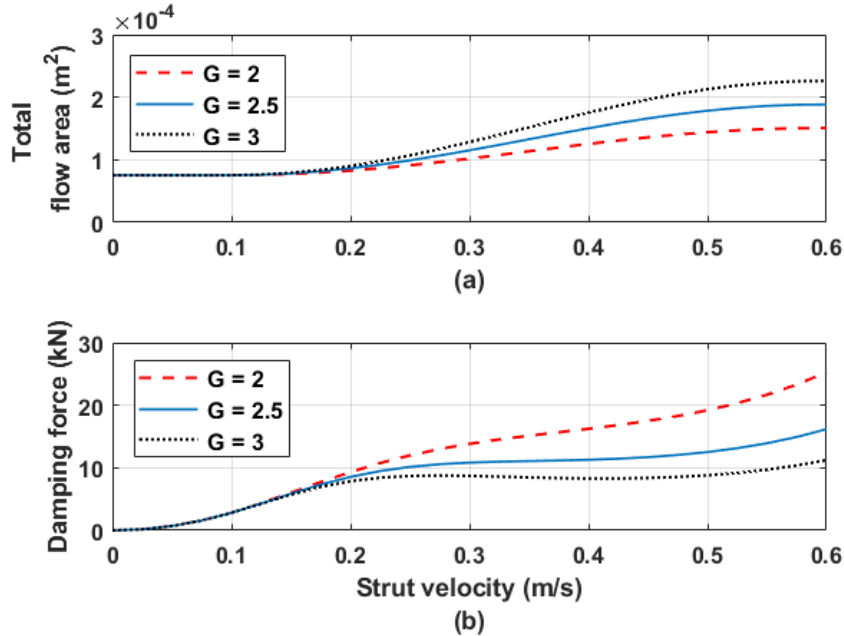


Figure 3.8: Variations in (a) total flow area and (b) force-velocity characteristics of the strut for different area ratios.

Figure 3.9 compares the force-velocity characteristics of each strut employed in the IC-I, IC-II and IC-IIa interconnection arrangements when subjected to an in-phase vertical excitation. The results are obtained considering flows only through the orifices and interconnecting pipes. Identical effective orifice area ($A = 58 \times 10^{-06} \text{ m}^2$) is chosen for both IC-I and IC-II suspension struts. The IC-I and IC-II suspensions thus yield identical fluid flow rates through orifices and connecting pipelines. The IC-IIa configuration, however yields substantially higher total damping force (FDT) due to absence of negative coupling component (FDC) associated with orifice flows in the connected strut. Consequently, a relatively larger orifice opening area ($A = 70 \times 10^{-06} \text{ m}^2$) was selected for the IC-IIa struts to achieve comparable damping force at low speeds.

The total vertical damping force (FDT) developed by a strut in the IC-I and IC-II suspension configurations comprises three damping force components, namely, damping force attributed to flows through orifices within the same strut (FDS), damping force obtained due to flows through orifices in the connected strut (FDC) and damping force due to flow across the two struts via the interconnecting pipes (FDL). The force developed by the IC-IIa configuration, however, consists of only two components, FDL and FDS, as evident in Equations (2.83). The individual damping force components of three different suspension configurations are analyzed so as to gain knowledge on the negative feedback damping effect, which are subsequently explored to seek tuning of the damping force without the flow modulations by a valve within the strut. However,

damping valves in interconnected configurations are configured with a transition velocity of 0.045 m/s to reduce the high speed damping force, which could control the ride vibration of the vehicle at higher velocities.

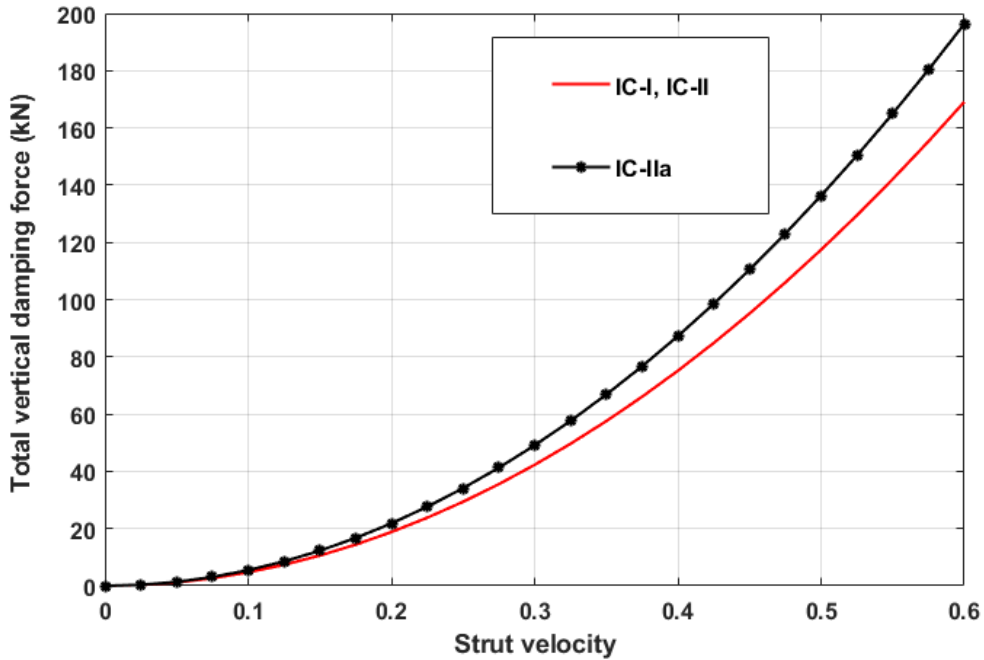


Figure 3.9: Total vertical mode force-velocity characteristics of each strut in different interconnected configurations.

To summarize, the flows through the damping valves help reduce the total damping force developed at high velocities to enhance ride comfort. The damping properties of a hydraulic damper are thus tuned by tuning the valve flow characteristics. However, limited accessibility of the valve deters the tuning of valves in a strut. Unlike the unconnected struts, the negative feedback effects, inherent in the IC configurations, offer an attractive potential for tuning of the overall damping force. The factors affecting the negative damping force are thus further explored in order to utilize these for tuning of the total damping force. These include the diameter and length of the interconnecting pipes, and effective flow areas.

3.4 ENHANCEMENT OF NEGATIVE DAMPING AND DAMPING FORCE TUNING

The negative damping effect of the interconnected suspensions can be enhanced by increasing the magnitudes of FDC and FDL components. The coupling component, FDC, is directly influenced by the effective orifice area of the strut and discharge coefficient, as seen in Equation (2.82), which could be tuned by employing damping valves in the IC-I and IC-II struts. Variations

in these factors also affect the magnitude of FDS, which is the dominant component of the total damping force developed by a strut. Variations in the orifice area and discharge coefficient thus resulted in relative small changes in the proportion of FDC in the total damping force (FDC/FDT). However, the enhancement of negative damping force via these design factors is determined as like unconnected struts and the responses of the vehicle model, with IC suspensions, employing damping valves are presented in the next chapter.

Alternatively, the negative feedback effect of an interconnection may be emphasized by increasing the damping force component attributed to flows across the connected struts (FDL). This can be realized through variations in the flow resistance of the interconnecting pipes, which do not affect the FDS component. The enhancement of the FDL component can thus permit variations in the total force in an IC suspension configuration, in a manner similar to the damping valves. From Equations (2.82) and (2.83), it is evident that FDL component could be varied to a greater extent by varying the diameter of the interconnecting pipe rather than its length. The pipe diameter could be altered in multiple ways to vary the flow resistance across the struts. Two different methods for enhancing the FDL component are explored, which include:

- (i) Introduction of capillary tubes across the struts.
- (ii) Introduction of a normally-open valve in the connecting pipelines.

The effects of these methods on the resulting FDL component and the overall damping force are presented in the following subsections.

3.4.1 Effect of Capillary Interconnecting Tubes

Although all three IC configurations possess identical fluid flow rates across the struts, as observed in section 2.5.3, comparable resultant damping forces are achieved, which are obtained from summation of the individual force components. Preliminary simulations suggested that a reduction of 60% in the diameter of the interconnecting pipes from the nominal diameter ($D = 0.03$ m) could yield appreciable FDL components in the IC-I and IC-II configurations. The diameter of the interconnecting pipes has thus been varied by $\pm 60\%$ ($D = 12, 30$ and 48 mm) to identify the effect on the FDL components of the IC-I and IC-II configurations. On the other hand, owing to absence of the coupling component, FDC, in case of the IC-IIa configuration, the interconnecting pipe diameter is varied by $\pm 70\%$ ($D = 9, 30$ and 51 mm). Table 3.5 summarizes the effects of interconnecting pipe diameter on the FDL force component, which is expressed as a proportion of the total damping force (FDT).

The fluid flow across the struts via interconnection lines is considered laminar, assuming negligible contributions due to entry and exit losses. The viscous damping force of the hydraulic fluid flow dominates at very low velocities, while the ratio FDL/FDT decreases considerably at higher velocities. This is due to the fact that the total damping force increases substantially at higher velocities due to flows through constant area orifices, as seen in Figure 3.8. The results are thus limited to low velocities of 0.01 and 0.05 m/s. As seen in Table 3.5, decreasing the pipe diameter to 12 and 9 mm yields substantially higher FDL/FDT ratio in all the IC configurations at the very low strut velocity of 0.01 m/s. This ratio decreases considerably for the strut velocity of 0.05 m/s. The results also show that increasing the pipe diameter to 48 or 51 mm results in negligible magnitude of the FDL component compared to the total damping force.

Table 3.5 also presents the effect of the pipe diameter on the damping force components attributed to orifice flows within the same strut (FDS) and flows in the coupled strut (FDC). It can be seen that the damping force is mostly dominated by the flows within the same strut, which increases substantially with decrease in the pipe diameter, especially at low velocities. The FDC component for the IC-I and IC-II configurations also increases, although only slightly, with decrease in the pipe diameter. It should be noted that the FDC component does not exist for the IC-IIa configuration. The results thus suggest that decreasing the interconnecting pipe diameter enhances the ratios of the FDL and FDS components to FDT at low velocities. Decreasing the pipe diameter to 9 mm yields 42% and 170% increase in the negative FDL and FDS components at the low velocity of 0.01 m/s, respectively, for the IC-I and IC-II configurations. The corresponding changes at 0.05 m/s are 6% and 127%. The IC-IIa configuration yields largest increases in FDL and FDS components, 416% and 516%, respectively, at the low velocity of 0.01 m/s. These reduce substantially to 19% and 119% at the velocity of 0.05 m/s.

Table 3.5: Vertical mode damping force component ratios for different pipe diameters with low strut velocities.

Damping force component ratio	Diameter of the interconnecting pipe (m)											
	0.012 m		0.009		0.03				0.048		0.051	
Strut velocity (m/s)	IC-I/IC-II		IC-IIa		IC-I/IC-II		IC=IIa		IC-I/IC-II		IC=IIa	
	0.01	0.05	0.01	0.05	0.01	0.05	0.01	0.05	0.01	0.05	0.01	0.05
FDS/FDT	1.70	1.27	5.16	1.19	1.2	1.2	1.0	1.0	1.2	1.2	1	1
FDC/FDT	-0.28	-0.21	0	0	-0.2	-0.2	0	0	-0.2	-0.2	0	0
FDL/FDT	-0.42	-0.06	-4.16	-0.19	0	0	0	0	0	0	0	0

3.4.2 Effect of Normally Open Valves in the Interconnecting Pipes

Alternatively, the variations in the negative damping force components are explored using a normally open valve in the interconnecting pipes, which tends to close with increasing pressure difference. Figure 3.10(a) presents a schematic of the normally open valve, which is introduced in the interconnection, as shown in Figure 3.10(b). As described in Equation (2.114), the valve yields higher pressure differentials across the struts as the valve opening decreases with increasing strut velocity. The fluid flow across the interconnecting pipes is considered to be laminar except for the flow through the valve, where it is considered to be turbulent. Referring to Figure 3.10(b), the total pressure drop (ΔP_{Total}) across the interconnecting pipe is the sum of drops in the pipe segments and the valve, such that:

$$\Delta P_{Total} = (P_1 - P_1') + (P_1' - P_2') + (P_2' - P_2) \quad (3.7)$$

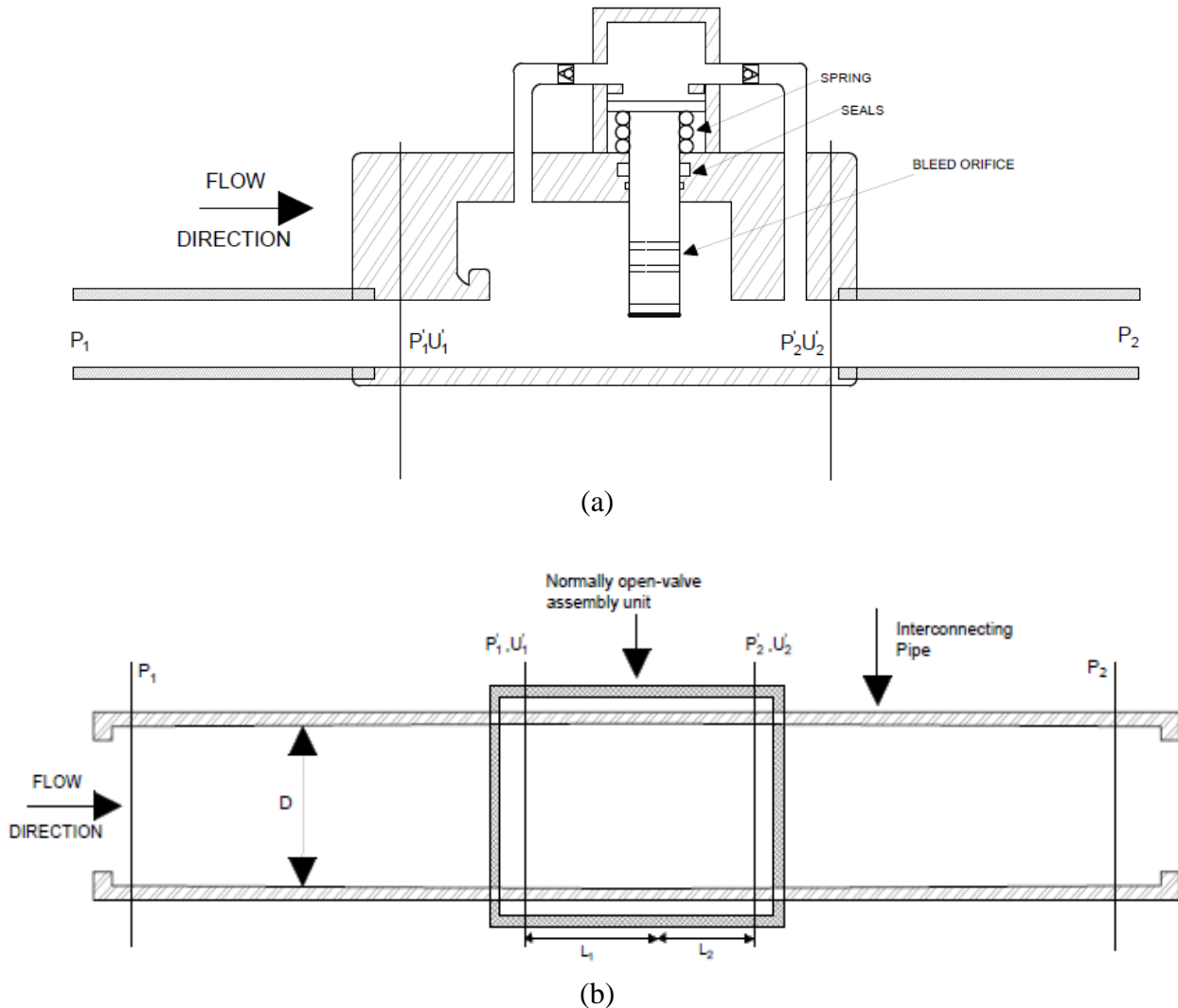


Figure 3.10: (a) Schematic of the normally open valve; and (b) pressure drop in the interconnecting pipe with the valve.

In above Equation, P_1' and P_2' refer to the fluid pressures in the upstream and downstream directions of flow across the valve, as shown in Figure 3.10(a). u_1' and u_2' are the upstream and downstream flow velocities, respectively. P_1 and P_2 denote the fluid pressures at the inlet and outlet of the interconnecting pipe, respectively. The pressure drops are computing assuming incompressible fluid and negligible contributions due to entry and exit losses. The pressure difference across the valve, $P_1' - P_2'$ is related to difference in squares of the flow velocities. For incompressible flow, the mass flow rate of the fluid across the valve can be estimated from [66]:

$$Q_m^* = \frac{C_d}{\sqrt{1-\beta^4}} A_v \sqrt{2\rho\Delta P} \quad (3.8)$$

Where C_d is discharge coefficient of the valve, β is ratio of instantaneous valve opening diameter (D_v) to the pipe diameter (D). A_v is the valve opening area. The discharge coefficient, C_d , of the

valve is related to the Reynold's number and the diameter ration, and is estimated from the *Stoltz* Equation, as [67]:

$$C_d = 0.5959 + 0.0312\beta^{2.1} - 0.184\beta^8 + 0.0029\beta^{2.5} \left(\frac{10^6}{Re_D}\right)^{0.75} + \frac{0.09L_1\beta^4}{(1-\beta^4)} - 0.0337L_2\beta^3 \quad (3.9)$$

Where Re_D is the Reynold number of the flow, L_1 and L_2 are the constant distances of the valve inlets and outlets, as shown in Figure 3.10(b). The ΔP across the valve is further estimated from [67]:

$$\Delta P = P_1' - P_2' = \frac{(1-\beta^4)Q_m^*{}^2}{2C_d^2\rho(A_{outlet})^2} \quad (3.10)$$

The total pressure differential across the interconnecting pipes with the valve is obtained by summing the pressure drops in the valve and the pipe sections, where the flow is assumed to be laminar, as:

$$\Delta P_{Total} = \frac{8\rho Q^2}{C_d^2\pi^2 D_v^4} \left(1 - \frac{D_v^4}{D^4}\right) + 2 \left(\frac{128\mu L Q}{\pi D^4}\right) \quad (3.11)$$

The first term in the above Equation, refers to the differential pressures related to fluid flow across the valve, which results in nearly quadratic relationship between the pressure difference and the velocity. The second term is dominated by the viscous damping force associated with laminar flows through the two pipe sections of identical length L .

Figure 3.11 presents the change in opening area of the valve as a function of the pressure drop, $P_1' - P_2'$. The opening area of the normally open valve is identical to that of the cross-sectional area of the pipe at very low velocities. The valve begins to close at a preset pressure differential corresponding to transition flow velocity of 0.08 m/s. Subsequently, the valve opening area decreases with increase in the pressure difference and approaches to its minimum opening corresponding to flow velocity of 0.6 m/s.

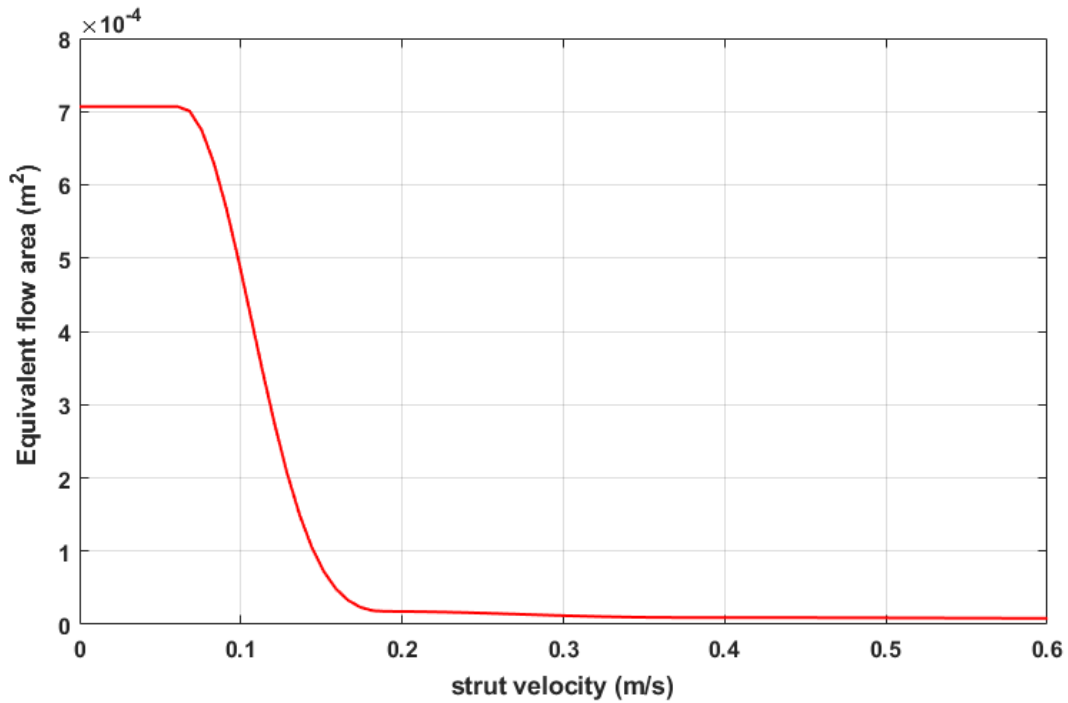


Figure 3.11: Variation in opening area of the normally open valve with respect to strut velocities.

Figure 3.12 illustrates variations in the resulting total damping force and its component due to each interconnected strut in the IC-I and IC-II configurations. The results are presented for the two configurations with and without the valve. It is evident that the interconnection without the valve yields negligible FDL component compared to the FDS component. The addition of the valve yields substantially higher FDL component with negligible effect on the FDS and FDC components, as seen in Figure 3.12(b). For the chosen valve opening, the magnitude of the FDL component exceeds that of the FDC component as the strut velocity exceeds 0.23 m/s. The increase in magnitude of the FDL component is mainly due to turbulent flows across the valve, as evidenced in Equation (3.11). The addition of the valve thus yields substantial reduction the total damping force (FDT) as velocity exceeds 0.23 m/s. The total damping force at 0.6 m/s is only about 28% of that achieved in the absence of the valve. The valve opening approaches its minimum at this velocity. It should be noted that a further reduction in the valve opening can lead to higher magnitude of FDL component compared to the FDS component, which can lead to negative overall damping.

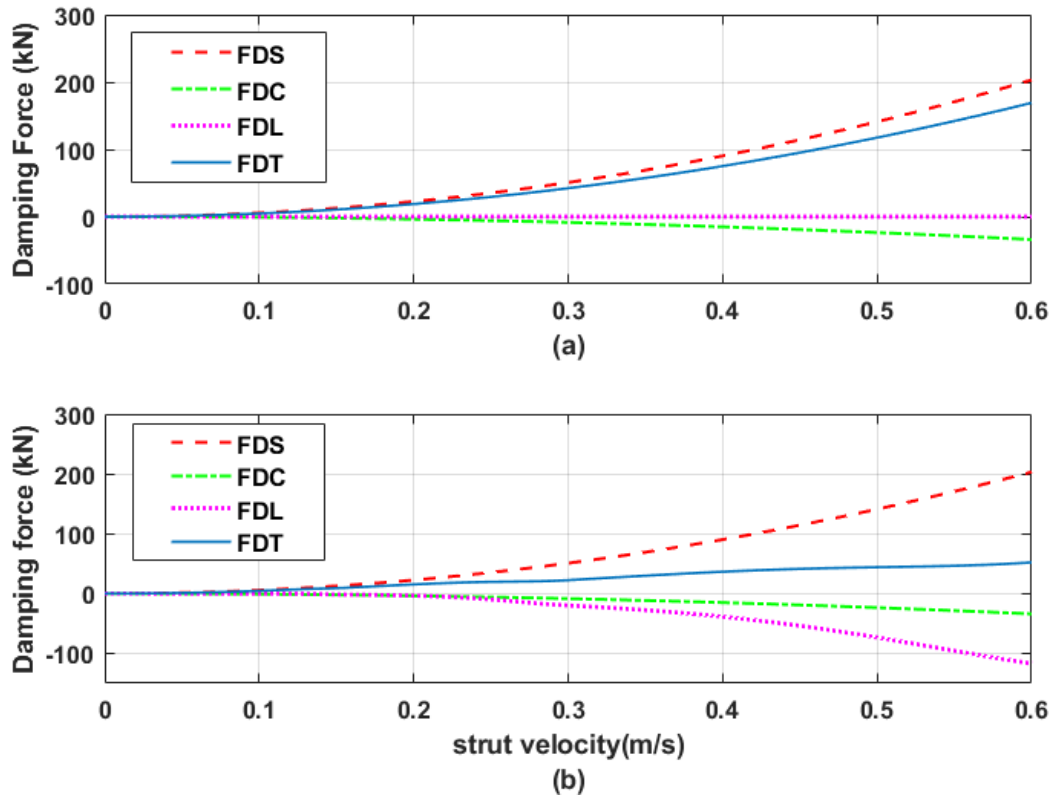


Figure 3.12: Variations in total damping force and force components developed by a strut in the IC-I and IC-II configurations with the strut velocity: (a) without valve; and (b) with normally open-valve.

The variations in the total damping force and force components of the strut used in IC-IIa configuration are illustrated in Figure 3.13. The results are presented for the interconnection without and with the normally open valve (Interconnection valve). Owing to the absence of the FDC component in this configuration, the valve final effective valve opening is further reduced to 3 mm in order to realize similar variations in the total damping force. This resulted in relatively higher magnitude of the FDL component, as seen in Figure 3.13(b). The results presented in Figures 3.12(b) and 3.13(b) suggest that addition of normally open valves in the interconnecting pipes emphasizes the negative damping force component FDL and thereby helps limit the total damping force at higher velocities. Table 3.6 summarizes the proportions of different damping force components of all the three IC suspension configurations in the 0.1 to 0.6 m/s velocity range.

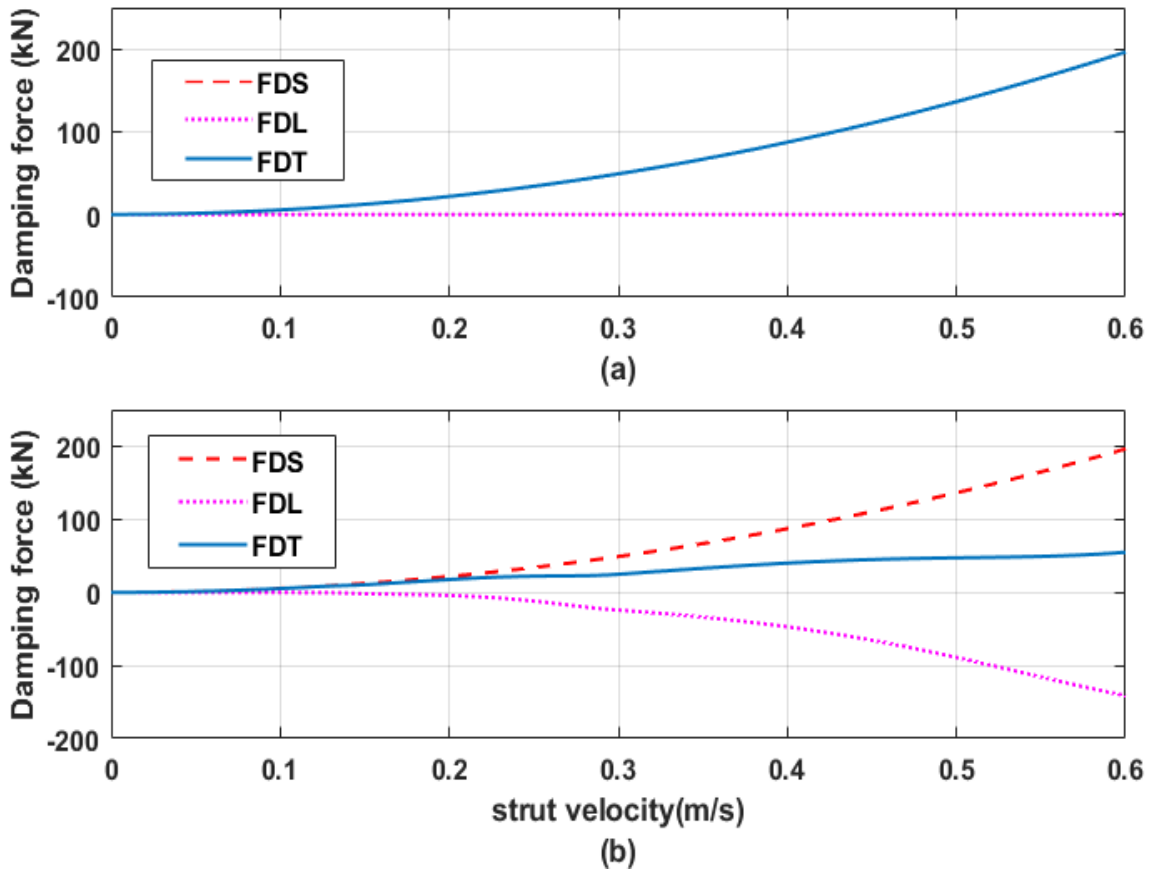


Figure 3.13: Variations in total damping force and force components developed by a strut in the IC-IIa configurations with the strut velocity: (a) without valve; and (b) with normally open valve.

Table 3.6: Vertical mode damping force component ratios for the struts in different IC suspension configurations employing normally open valves in the interconnecting pipes.

Strut velocity (m/s)	IC-I/IC-II			IC-IIa	
	FDS/FDT	FDC/FDT	FDL/FDT	FDS/FDT	FDL/FDT
0.1	1.25	-0.20	-0.04	1.03	-0.03
0.2	1.49	-0.25	-0.24	1.25	-0.25
0.3	2.27	-0.38	-0.89	1.98	-0.98
0.4	2.48	-0.41	-1.07	2.18	-1.18
0.5	3.21	-0.53	-1.67	2.89	-1.89
0.6	3.9	-0.65	-2.24	3.57	-2.57

3.5 ROLL DAMPING PROPERTIES

The roll damping moment due to interconnected struts are obtained by imposing out-of-phase velocity excitations to the left- and right-struts ($\dot{x}_l = -\dot{x}_r$), as described in section 2.5.5. The roll damping moment of an IC configuration is not only dependent on the relative velocity of the same strut but also the velocity of the connecting strut. Due to fluid flow across the struts, roll damping moments of all the IC configurations are considerable larger than those of the corresponding unconnected configurations, which is also evident from Equations (2.107), (2.109) and (2.111). Figure 3.14 illustrates roll damping moment-roll velocity characteristics of the three IC suspension configurations together with those of the unconnected struts without the damping valves. The results are also presented for the unconnected struts with damping valves integrated within each strut in order to illustrate the effects of the damping valves. Unlike the vertical mode damping, the negative damping force components (FDC and FDL) yield positive damping roll moment, as seen in Equations (2.109) and (2.111) for all the IC suspension configurations. The IC suspensions thus yield substantially higher roll damping moment when compared to the UC suspension.

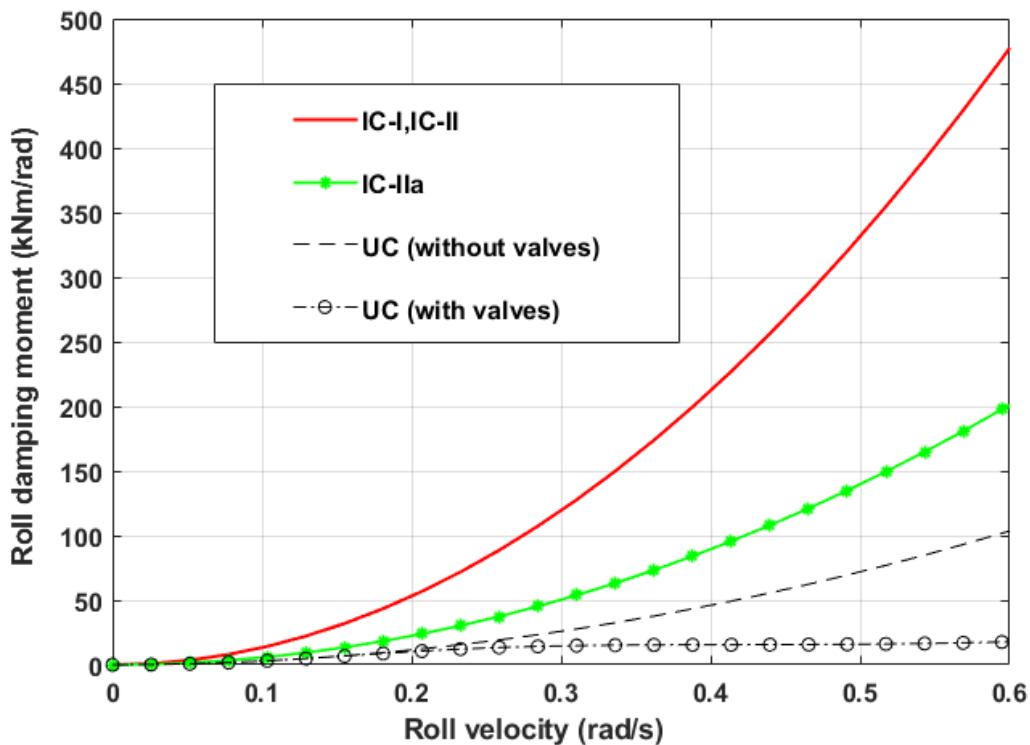


Figure 3.14: Comparisons of roll damping moment developed by of different interconnected and unconnected suspension configurations.

It should be noted that an anti-roll bar does not contribute to the roll mode damping property of the unconnected suspension. An unconnected suspension will thus yield substantially lower roll damping compared to an IC suspension. Moreover, addition of the shim-stack valves in the UC struts yields further reduction in the damping moment, as observed in Figure 3.14. The results also show considerably lower roll damping moment of the IC-IIa configuration compared to the IC-I and IC-II suspensions. This is due to absence of coupling component FDC associated with the orifice flows in the connected struts, as observed in Figures 3.12 and 3.13. The results show that the roll damping moment of the IC-IIa configuration is nearly 43% of that of the IC-I and IC-II configurations at the roll velocity of 0.6 rad/s.

Figure 3.15(a) illustrates variations in the roll damping moment developed by the IC-I and IC-II suspension configurations, as a function of the roll velocity. The roll damping moment for the IC-IIa suspension configuration is presented in Figure 3.15(b). The roll velocity is computed considering the out-of-phase velocity excitation and the suspension track width. The results are presented for the configurations without and with valves in the interconnecting pipes. It is evident that the roll damping moment increases with the roll velocity in a quadratic manner for all the configurations. The addition of valves in the interconnecting pipes yield higher roll moment as the roll velocity exceeds 0.28 rad/s. The magnitude of roll moment due to IC-IIa suspension is relatively smaller than that of the IC-I/IC-II suspensions in the entire roll velocity range. This is due to absence of the FDC component in the IC-IIa suspension.

From the results presented in Figure 3.15, it is evident that enhancement of negative damping effect would contribute to even greater roll damping moment, while it limits the effective vertical mode damping, as seen in Figures 3.12 and 3.13. The IC suspensions with appropriately tuned interconnecting flow valves can thus lead to high roll damping for improving handling performance of the vehicle and lower vertical mode damping at higher velocities for realizing improved ride performance.

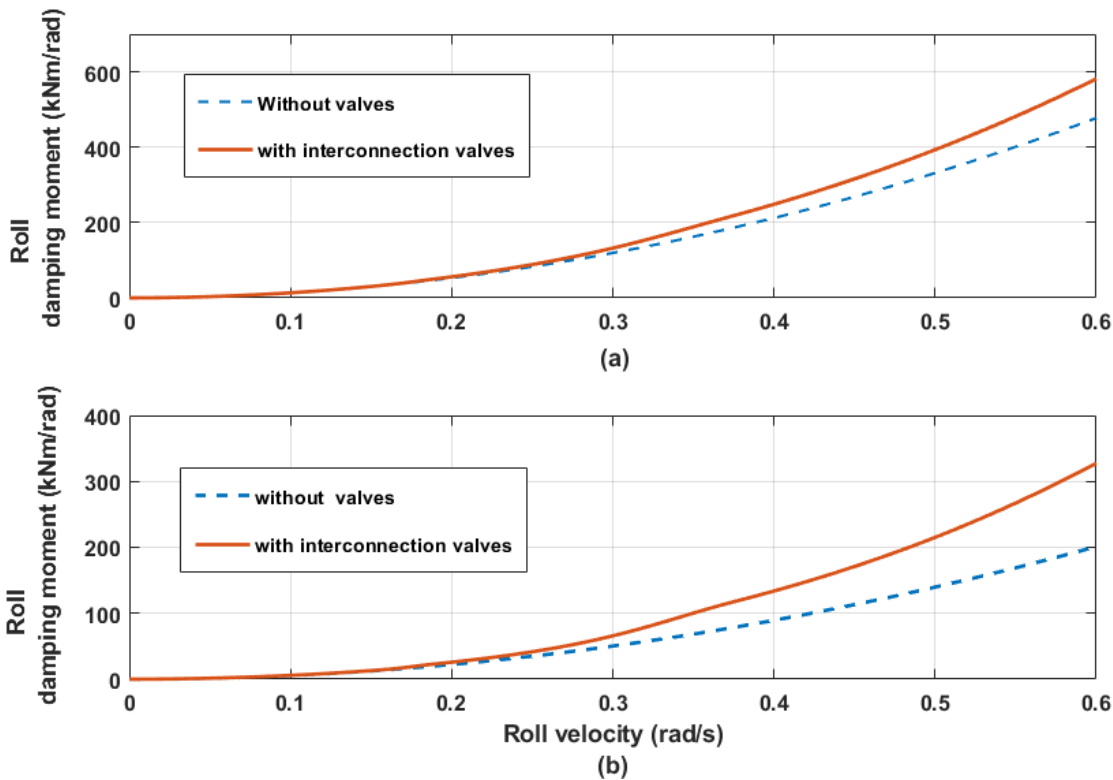


Figure 3.15: Roll damping moment –roll velocity characteristics of IC suspensions without and with valves in the interconnecting pipes: (a) IC-I/IC-II suspension; and (b) IC-IIa suspension.

3.5 SUMMARY

The strut parameters of the unconnected and interconnected configurations are selected to obtain identical load carrying capacity, static deflection, and static vertical suspension rate. Ride height valves are installed in the vehicle to maintain the identical static ride height for various static load conditions. The restoring and dissipative forces of the different configurations are analyzed in the vertical and roll modes. Stiffness properties of the struts are investigated in view of the fluid compressibility effect. It is shown that the struts interconnected in the roll plane yield substantially higher roll stiffness compared to that of the unconnected struts. The roll plane interconnection of the struts can thus serve as an effective hydraulic antiroll bar. The properties of damping force developed by the interconnected struts are thoroughly investigated to emphasize the negative feedback effects while considering the hydraulic fluid as incompressible. A methodology is proposed to enhance the negative damping effect attributed to flows across the connected struts. The addition of pressure-sensitive valves in the interconnected pipes showed enhanced negative damping force component with negligible effect of the force component attributed flows within the struts. It is shown that enhancement of negative damping effect would

contribute to even greater roll damping moment, while it limits the effective vertical mode damping. The IC suspensions with appropriately tuned interconnecting flow valves can thus lead to high roll mode damping for improving handling performance of the vehicle and lower vertical mode damping at higher velocities for realizing improved ride performance. The performance characteristics of the IC suspensions with and without the valves is explored are further investigated in the following chapter using a roll-plane vehicle model subject to excitations arising from the road and a steering input.

CHAPTER 4

DYNAMIC RESPONSE CHARACTERISTICS OF DIFFERENT SUSPENSION CONFIGURATIONS

4.1 INTRODUCTION

The ride and handling performance of a vehicle strongly relies on properties of the suspension system, road roughness and tire-road interactions. It has been shown that the proposed interconnected hydro-pneumatic suspensions can provide high roll stiffness while preserving low natural frequency in the vertical mode. The interconnected suspensions are thus expected to provide vertical ride performance similar to those of the unconnected suspensions. The ride performance of the vehicle, however, is also affected by damping characteristics of the suspension system. The conventional suspensions are designed to provide higher damping coefficient at low suspension velocities so as limit low frequency roll oscillations and thereby improved handling performance [15, 19]. Such suspensions provide considerably lower damping coefficient at higher velocities to achieve effective attenuation of terrain-induced ride vibration [18]. Such variable damping characteristics of the conventional suspensions are realized through modulations of hydraulic flows through damping valves such as blow-off and shim-disc valves, as described in section 3.3.

In the previous chapters, it is shown that interconnected hydro-pneumatic suspensions exhibit negative damping force components due to cross flows and interconnections between the individual wheel suspensions. The negative damping features of the interconnected suspensions could be explored to achieve variable suspension damping in lieu of the damping valves. The modulations of flows through the pipes coupling the right- and left-suspension struts, in-particular, could help enhance the negative damping feature of the coupled suspension, as it is demonstrated in section 3.4. In this chapter, the response characteristics of the coupled hydro-pneumatic suspension configurations with damping and interconnecting valves are investigated under idealized road- and maneuver-induced excitations. The vertical and roll vibration isolation properties of the suspension system are evaluated through simulation of the roll plane vehicle model under in-phase and out-of-phase harmonic excitations at the tire-road interfaces. The vertical and roll mode responses are also evaluated under a road bump input. The roll dynamic response is further evaluated under a rounded-step lateral acceleration excitation idealizing a steady-turn maneuver. Both the ride and handling performance potentials of the proposed suspensions with enhanced negative damping force components are discussed on the basis of the

responses in terms of vertical and roll displacements and accelerations of the sprung and unsprung masses, and sprung mass roll rate. The significance of the negative damping is illustrated by comparing the responses of the coupled suspensions with and without the interconnection valves.

4.2 DESCRIPTION OF EXCITATIONS

The handling and anti-roll performance potentials of suspensions can be assessed in terms of roll displacement and roll rate of the vehicle's sprung mass under both road- and steering maneuver-induced excitations [26, 32, 68]. In this study, the lateral acceleration excitation encountered during a steady-turning maneuver is considered for analyses of roll response characteristics of the vehicle model with different interconnected hydro-pneumatic suspension configurations. The lateral acceleration excitation is idealized by a rounded step function [28], as shown in Figure 4.1, and expressed as:

$$a_y(t) = X_{max}[1 - e^{-\sigma t}(1 + \sigma t)] \quad (4.1)$$

where a_y is the lateral acceleration excitation, X_{max} is magnitude of steady lateral acceleration, and σ is a smoothing parameter, which also determines the rise rate, and is given by:

$$\sigma = \frac{\pi}{f\tau_s} \quad (4.2)$$

where f denotes the oscillation frequency and τ_s is a constant. Reported studies have shown that the steady-turning rollover threshold acceleration of commercial high c.g. vehicles may range from 0.35 to 0.5 g [69]. The steady lateral acceleration magnitude of 3 m/s^2 is thus chosen to evaluate responses of the proposed suspension configurations.

The response characteristics of the suspension configuration are also evaluated under transient excitations arising from a road bump, while the vehicle is assumed to travel at a constant forward speed v . The vehicle model is analyzed under in-phase and out-of-phase pulse excitations at the right and left tire-road interfaces. The responses of the sprung and unsprung masses are obtained to assess shock attenuation characteristics of the suspension configurations. The instantaneous displacement excitation due to the road bump $x_{oi}(t)$, idealized by a pulse shown in Figure 4.2, can be expressed as:

$$x_{oi}(t) = \begin{cases} a \sin(2\pi\gamma) * (t - b_o); & b_o \leq t \leq b_e \\ 0; & \text{otherwise} \end{cases} ; (i=l, r) \quad (4.3)$$

In the above equation, subscript $i=l, r$ refers to left and right tire, a determines the height of the pulse input, γ is the pulse frequency, b_o is the lapse time, when the contact between the wheel and the pulse is initiated and b_e is the time when the wheel exits the pulse input. The pulse input is synthesized using the following parameters: $a = 0.05$, $\gamma = 1.333$, while the vehicle speed is held at 8 m/s , as shown in Figure 4.2.

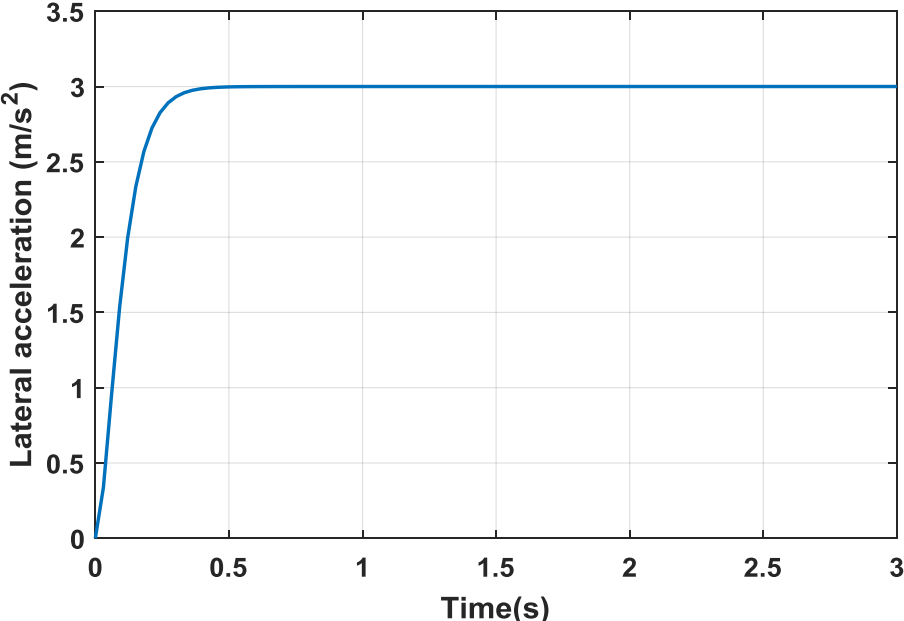


Figure 4.1: Rounded step lateral acceleration excitation.

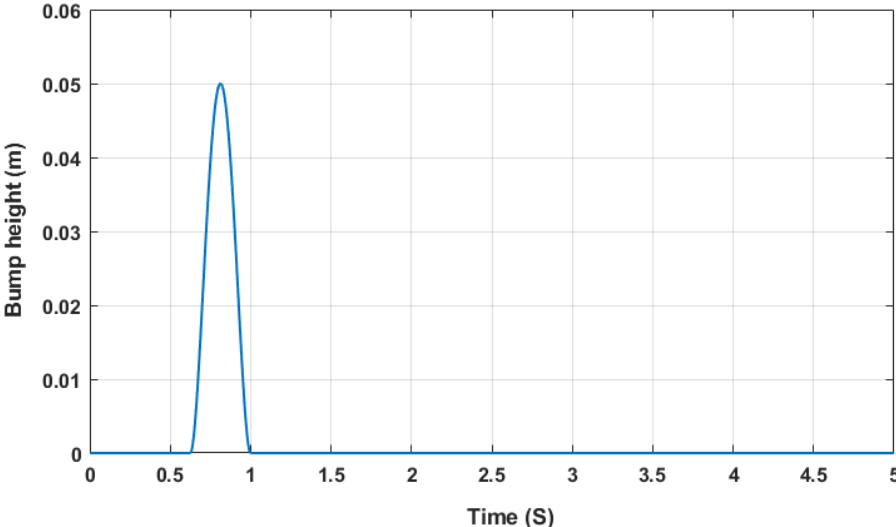


Figure 4.2: Vertical displacement due to the pulse input applied at the tire-road interface.

4.3 RESULTS AND DISCUSSIONS

The vertical and roll response characteristics of the proposed interconnected suspension configurations are analyzed using the roll plane vehicle model, presented in chapter 3 together with the simulation parameters. The response characteristics obtained for the IC-I, IC-II and IC-IIa suspension configurations are compared with those of the unconnected suspension system with and without an antiroll bar to illustrate the relative performance benefits of the connected suspensions. The unconnected suspension with the antiroll bar, hereafter, is denoted as 'UC-Rollbar'. The responses are also obtained, considering incompressible hydraulic fluid, for connected and unconnected struts suspensions employing damping valves and interconnection valves. The results are subsequently discussed in view of the damping tuning via negative damping force components of the interconnected struts.

4.3.1 Responses to Lateral Acceleration Excitation

Figure 4.3(a) compares the sprung mass roll angle responses of the vehicle models with unconnected and connected suspension struts. The UC suspension configuration with considerably lower roll stiffness exhibits highest peak roll angle response. The peak roll angle response of the UC suspension approaches nearly 0.06 radians, while the oscillation frequency is about 0.63 Hz. The addition of the anti-roll bar to the UC suspension yields a relatively lower peak roll angle of 0.05 radians, while the oscillation frequency increases to about 0.68 Hz due to additional roll stiffness of the anti-roll bar. All of the IC suspension configurations exhibit considerably lower peak sprung mass roll angle and higher roll mode frequency due to higher roll mode stiffness and damping of the suspension, as illustrated in sections 3.2 and 3.5, respectively. Though IC-IIa and UC-Rollbar configurations possess identical static roll stiffness, the magnitude of the peak response for the IC-IIa configuration is smaller due to its larger roll damping moment. The IC-I suspension exhibits higher roll mode frequency of 0.92 Hz due to its higher roll mode stiffness compared to the IC-II and IC-IIa suspensions, which show roll mode frequencies of 0.83 and 0.85 Hz, respectively. Furthermore, the IC-I suspension exhibits lowest peak roll angle response, in the order of 0.027 radians, while the peak roll angle responses of IC-II and IC-IIa suspensions are 0.031 and 0.035 radians, respectively.

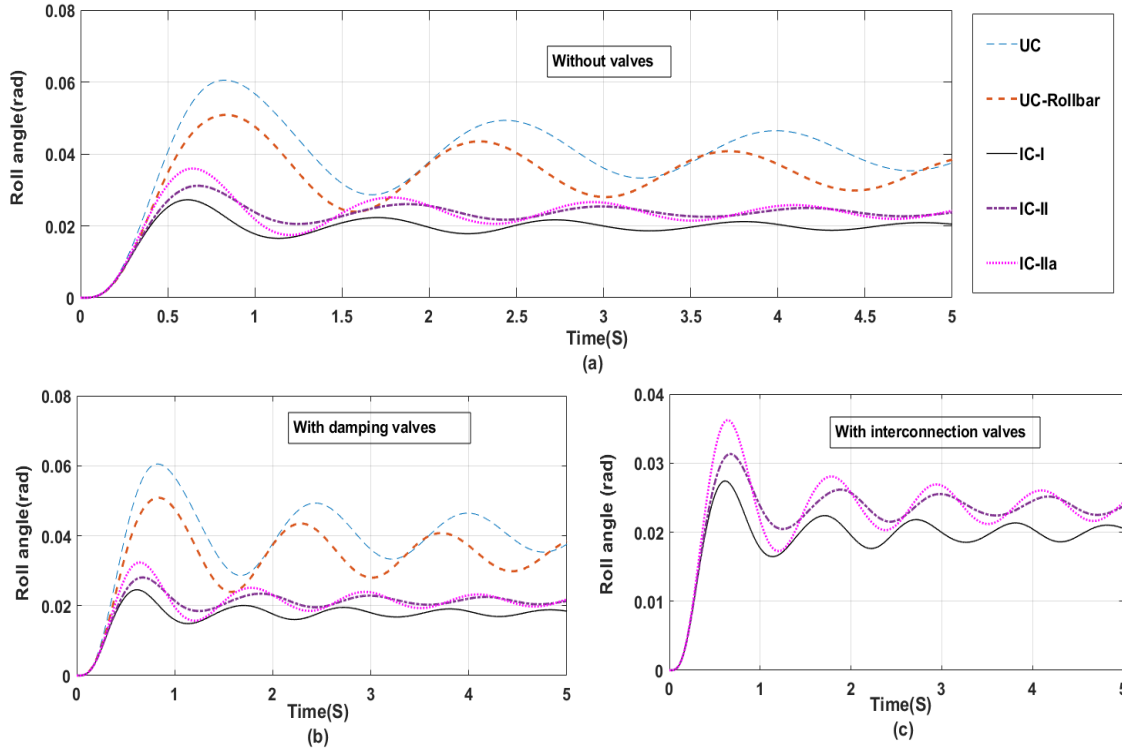


Figure 4.3: Comparisons of sprung mass roll angle responses of the vehicle model employing different suspension configurations under a rounded-step lateral acceleration excitation: (a) unconnected (UC and UC-Rollbar) and connected (IC-I, IC-II and IC-IIa) suspensions; (b) unconnected and connected suspensions with damping valves; and (c) connected suspensions with interconnection valves.

The considerably lower peak roll response of the IC suspensions is mostly due to their higher roll mode damping. In section 3.5, it was shown that the negative damping force components (FDC and FDL) of the IC suspensions yield positive roll moment and thereby substantially higher roll mode damping, when compared to that of the UC suspensions. The higher effective damping of the IC suspensions is also evident from the relative rapid decays in the sprung mass roll responses. The addition of damping flow valves across chambers 1 and 2, as described in section 3.3, yield relatively lower sprung mass roll angle responses of all the IC suspension configurations, as illustrated in Figure 4.3(b). This is due to the fact that damping valves in the IC suspensions are tuned at relatively lower transition velocities to reduce the roll angle and roll rate responses of the sprung mass. It should be noted that the damping valves for the IC and UC suspensions were configured to yield transition velocities of 0.045 m/s and 0.15 m/s , respectively. A higher transition velocity for the UC struts was selected to its relatively larger orifices. A reported study has also shown that the damper valve with low transition velocity is beneficial for better vibration control performance, especially when the vehicle is travelling on rough roads [30]. Since the

interconnection valves do not affect the low velocity damping characteristics, the sprung mass roll responses of IC suspension with such valves are comparable with those with damping valves, as seen in Figure 4.3(c). The flow valves, installed in pipelines, emphasize the negative damping force components only at higher velocities, as illustrated in section 3.4. Such valves thus do not affect the vertical and roll mode damping properties of the struts at very low velocities.

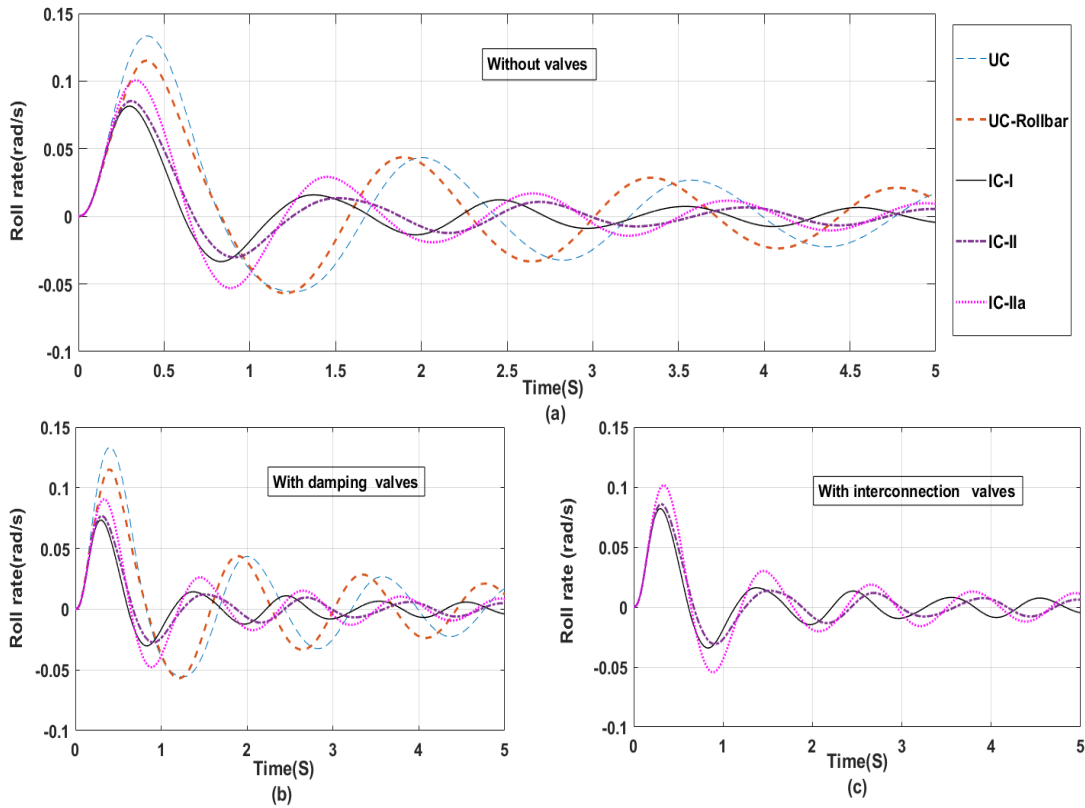


Figure 4.4: Comparisons of sprung mass roll rate responses of the vehicle model employing different suspension configurations under a rounded-step lateral acceleration excitation: (a) unconnected (UC and UC-Rollbar) and connected (IC-I, IC-II and IC-IIa) suspensions; (b) unconnected and connected suspensions with damping valves; and (c) IC suspensions with interconnection valves.

Figure 4.4(a) illustrates the sprung mass roll velocity responses of the vehicle model with unconnected and connected suspensions. The roll rate responses of the suspensions with damping valves and IC suspensions with interconnecting valves are shown in Figures 4.4(b) and 4.4(c), respectively. The roll rate responses of the unconnected and connected suspensions exhibit trends similar to those observed in roll angle responses, shown in Figures 4.3(a) and 4.3(b). The unconnected suspensions exhibit higher roll rate and lower oscillation frequencies compared to the IC suspensions. The addition of interconnecting valves show only negligible effect on the roll rate

responses, shown in Figure 4.4(c). The comparisons of the roll rate responses of the IC suspensions with interconnecting valves suggest relatively higher sprung mass roll rate of the IC-IIa suspension compared to the IC-I and IC-II suspensions. This is attributed to the absence of FDC component in the IC-IIa configuration, which leads to relatively smaller roll damping moment. Although the IC-I and IC-II configurations possess identical roll mode damping properties, the relatively larger gas volume of the IC-II struts contributes to slightly lower low roll stiffness, and thereby higher peak roll angle and roll rate responses.

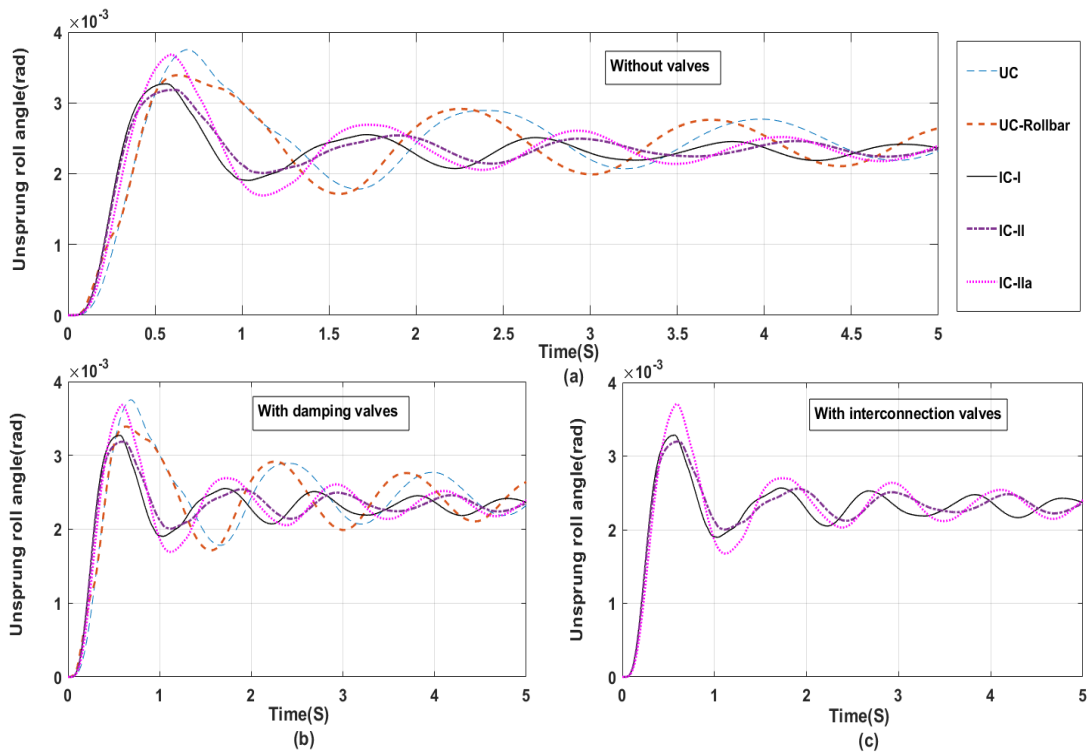


Figure 4.5: Comparisons of unsprung mass roll angle responses of the vehicle model employing different suspension configurations under a rounded-step lateral acceleration excitation: (a) unconnected (UC and UC-Rollbar) and connected (IC-I, IC-II and IC-IIa) suspensions; (b) unconnected and connected suspensions with damping valves; and (c) IC suspensions with interconnection valves.

Figures 4.5 illustrate the unsprung mass roll angle responses of the vehicle model with different UC and IC suspension configurations with and without the damping and interconnection valves. The unsprung mass roll angle during a steering maneuver directly relates to the dynamic load transfer from the inboard to the outboard track of the vehicle, which is considered as an effective indicator of the dynamic roll stability of the vehicle [70]. The results show that IC suspensions yield relatively lower unsprung mass roll compared to the UC suspensions, with the exception of

the IC-IIa suspension, as seen in Figure 4.5(a). The peak roll angle response of the vehicle model with IC-IIa suspension configuration is higher than that of the model with UC-Rollbar suspension. This is due to the larger gas volume and thus the lower roll stiffness of the IC-IIa suspension. This suspension also provides relatively lower roll mode damping compared to the IC-I and IC-II suspensions, as discussed above. The damping and interconnecting valves in the suspensions yield only negligible effects on the unsprung mass roll angle as observed in Figures 4.5(b) and 4.5(c), respectively.

4.3.2 Responses to Transient Pulse Excitations

Figures 4.6 and 4.7 illustrate sprung mass vertical displacement and acceleration responses, respectively, of the vehicle model with different UC and IC suspensions subject to in-phase pulse excitation (Figure 4.2). Owing to their nearly identical vertical mode properties, the UC and IC suspensions yield comparable vertical displacement responses of the sprung mass, as shown in Figure 4.6(a). The IC suspensions exhibit slightly faster decay in the displacement response compared to the UC suspensions. This is due to relatively higher vertical mode damping of the IC suspension struts, which employ slightly smaller size orifices compared to the UC suspension struts. The IC-IIa suspension with damping valves shows slightly faster decay in the vertical displacement response compared to the IC-I and IC-II suspensions, as seen in Figure 4.6(b). This is due to slightly different vertical mode damping properties of the IC-IIa suspension struts, as described in section 2.5. Comparisons of the responses in Figures 4.6(b) and 4.6(c) suggest that the damping tuning via interconnecting flow valves yields slightly lower negative peak displacement response compared to that obtained with the damping valves. The results exhibit similar trends and further suggest that interconnecting valves provide damping tuning similar to the damping valves.

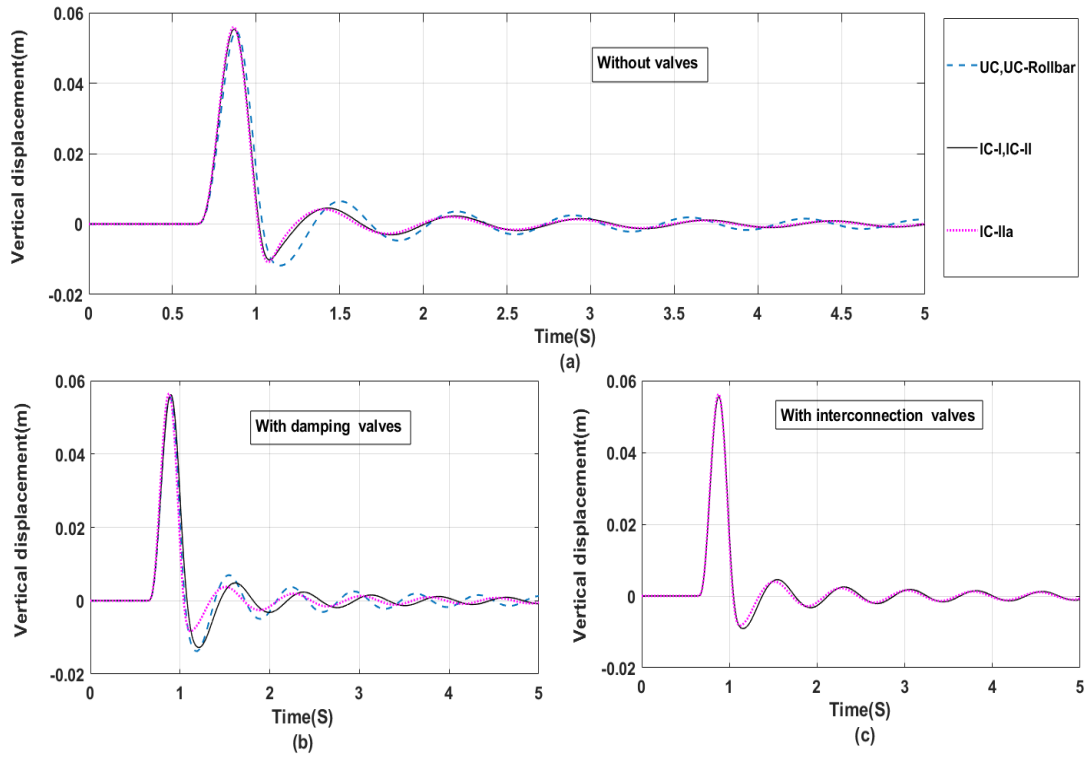


Figure 4.6: Comparisons of sprung mass vertical displacement responses of the vehicle model to an in-phase pulse excitation: (a) unconnected (UC and UC-Rollbar) and connected (IC-I, IC-II and IC-IIa) suspensions; (b) connected suspensions with damping valves; and (c) IC suspensions with interconnection valves.

The vertical acceleration response of the sprung mass constitutes an important performance measure related to vehicle ride, and shock and vibration control performance of the suspension system [53]. The IC suspensions yield slightly higher acceleration peaks compared to the UC suspensions, as seen in Figure 4.7(a). The magnitude of the negative peak occurring near $0.87s$ is particularly slightly higher for the IC suspensions. This is due to differences in damping properties, especially at higher velocities, corresponding to the IC and UC suspensions. The magnitude of the second peak of the UC and UC-Roll bar configurations is about $7.34 m/s^2$, and it reduces to $6.54 m/s^2$ when damping valves are employed, as shown in Figure 4.7(b). The damping tuning via damping valves does not affect the magnitude of the first peak, but the magnitudes of the second and third peaks are reduced considerably for both the UC and IC suspension configurations. Additionally, while employing damping valves, there is considerable reduction in the magnitude of the negative peak (Figure 4.7(b)) for the IC-I and IC-II suspensions (from about $7.84 m/s^2$ to nearly $5.82 m/s^2$). Comparisons of the results shown in Figures 4.7(b) and 4.7(c) suggest that interconnection flow valves yield considerably lower acceleration responses comparable to those

obtained with the damping valves, especially in reducing the negative peak magnitude of the IC-IIa suspension configuration. This is due to relatively larger FDL/FDT ratio of the IC-IIa configuration, as compared with other two configurations. This suggests that the interconnecting flow valves can provide equally effective damper tuning through enhancement of the negative damping force components of the IC suspensions.

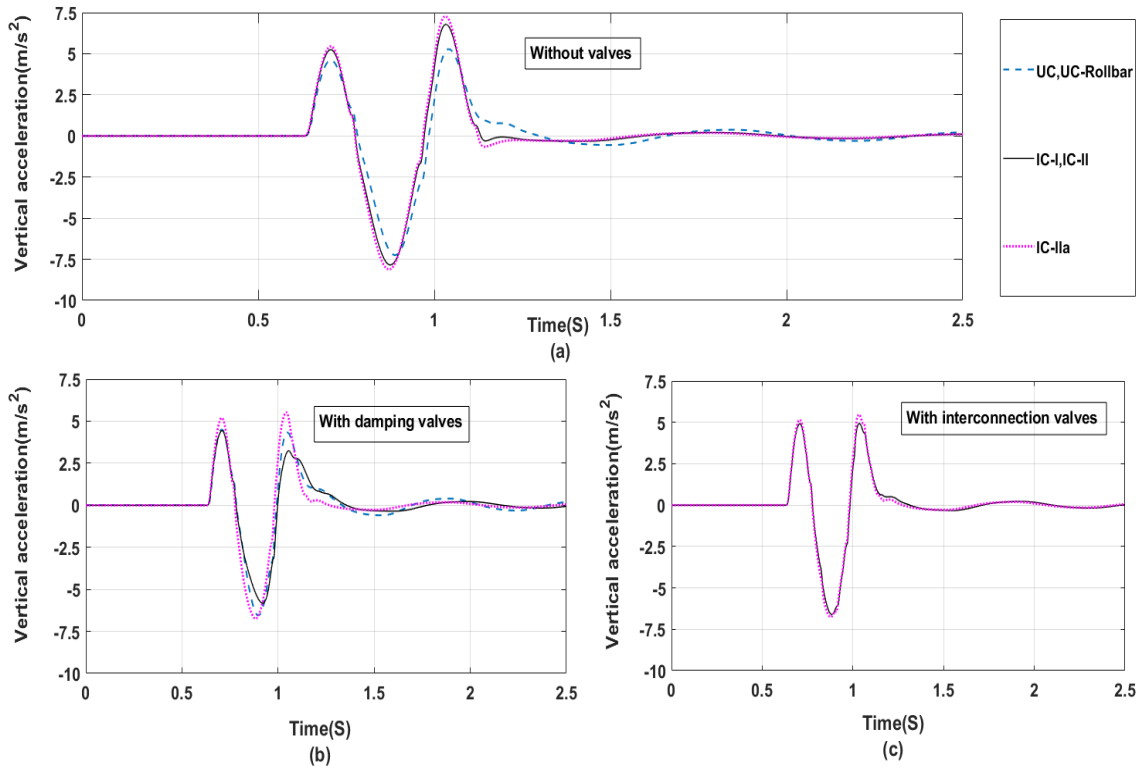


Figure 4.7: Comparisons of sprung mass vertical acceleration responses of the vehicle model to an in-phase pulse excitation: (a) unconnected (UC and UC-Rollbar) and connected (IC-I, IC-II and IC-IIa) suspensions; (b) connected suspensions with damping valves; and (c) IC suspensions with interconnection valves.

The vehicle model responses to out-of-phase pulse excitation are presented in Figures 4.8 and 4.9 in terms of roll angle and roll acceleration of the sprung mass, respectively. The results are presented for the UC, UC-Rollbar, IC-I, IC-II and IC-IIa suspensions in Figures 4.8(a) and 4.9(a). The responses are also presented for the suspension struts with damping valves in Figures 4.8(b) and 4.9(b), and the interconnection valves in Figures 4.8(c) and 4.9(c). The UC and UC-Rollbar suspensions yield considerably higher peak roll angle of the sprung mass (0.09 and 0.075 radians, respectively) compared to the IC suspensions, as seen in Figure 4.8(a). The UC suspensions also exhibit substantially lower rate of decay of roll oscillations and require considerably longer settling

time compared to the IC suspensions. This is due to lower roll mode damping of the UC suspensions. The peak sprung mass roll angle responses of the IC-I and IC-II suspensions are considerably reduced when damping valves are employed, as compared with the identical configurations equipped with interconnecting valves. It shows that tuning of damping valves improve both the vertical and anti-roll performance of the corresponding IC configurations. Whereas, the roll angle responses of the IC-IIa configuration (Figure 4.8(b)) is slightly larger than those of the IC-I and IC-II configurations, as seen in Figure 4.8(a). This is not only due to absence of the FDC component in IC-IIa, but also the presence of damper valves that reduce the total roll damping moment. Furthermore, the relatively longer settling period is also evident for the IC-IIa suspension compared to the IC-I and IC-II suspensions. The roll responses of the sprung mass are negligibly affected by the interconnection valves, as seen in Figure 4.8(c), and this is due to the relatively higher transition velocity of the interconnection valves. Moreover, similar trend is also observed in terms of the roll acceleration responses, as shown in Figures 4.9(a) and 4.9(c).

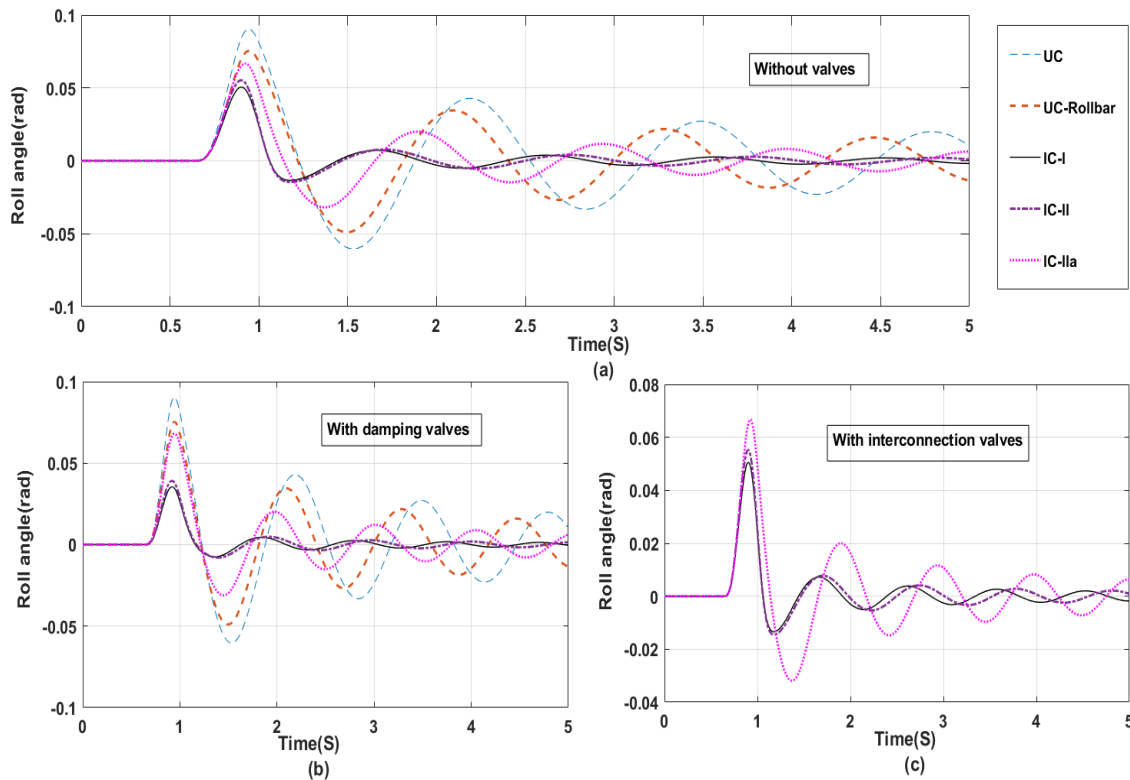


Figure 4.8: Comparisons of sprung mass roll angle responses of the vehicle model to out-of-phase pulse excitation: (a) unconnected (UC and UC-Rollbar) and connected (IC-I, IC-II and IC-IIa) suspensions; (b) unconnected and connected suspensions with damping valves; and (c) IC suspensions with interconnection valves.

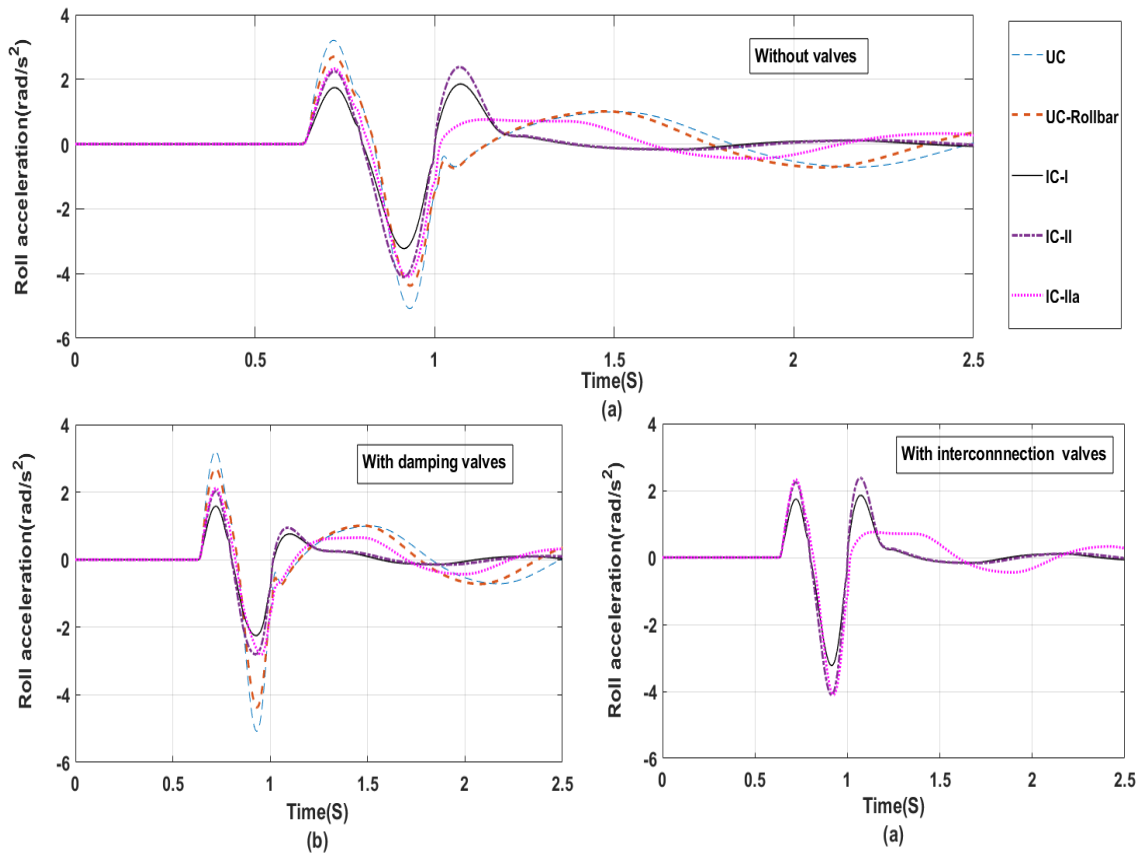


Figure 4.9: Comparisons of sprung mass roll acceleration responses of the vehicle model to out-of-phase pulse excitation: (a) unconnected (UC and UC-Rollbar) and connected (IC-I, IC-II and IC-IIa) suspensions; (b) unconnected and connected suspensions with damping valves; and (c) IC suspensions with interconnection valves.

Owing to relatively higher transition velocity of the damper valves employed in the UC suspensions, the responses obtained with and without the damping valves are quite comparable, as seen in Figures 4.9(a) and 4.9(b). The addition of the damping valves to the IC-I configuration, however, shows a reduction in the peak roll acceleration from 3.22 rad/s^2 to 2.44 rad/s^2 . The IC-II and IC-IIa configurations also exhibit reductions in the peak acceleration responses from nearly 4.10 rad/s^2 to 2.80 rad/s^2 , when damping valves are introduced. The results thus suggest that damping tuning via valves could improve both anti-roll and ride performance of the IC suspensions. The IC suspensions with flow valves in the interconnecting pipelines also yield improved ride performance, while preserving the low speed roll mode damping property.

4.5 VIBRATION TRANSMISSIBILITY CHARACTERISTICS

Frequency response characteristics of the 4-DOF roll plane vehicle model employing different suspension configurations are evaluated in terms of vertical and roll displacement transmissibility characteristics of the sprung and unsprung masses. The relative vertical and roll displacement transmissibilities of the sprung and unsprung masses are evaluated under in-phase and out-of-phase harmonic excitations at the left –and-right tires, respectively, such that $x_e(t)=X_e\sin(\omega t)$. A constant amplitude of excitation (0.01m) is considered and the steady-state transmissibility magnitudes are evaluated in the 1 to 15 Hz frequency range, as:

Vertical displacement transmissibility of sprung mass, $Z_{xs} = \frac{X_s}{X_e}$

Vertical displacement transmissibility of unsprung mass, $Z_{xu} = \frac{X_u}{X_e}$

Roll displacement transmissibility of sprung mass, $Z_{\theta_s} = \frac{T\theta_s}{X_e}$

Roll displacement transmissibility of unsprung mass, $Z_{\theta_u} = \frac{T\theta_u}{X_e}$

Where T refers to the suspension track, X_s and X_u are magnitudes of vertical displacements of the sprung and unsprung masses, respectively; X_e is the amplitude of harmonic excitation; θ_s and θ_u are magnitudes of roll angles of the sprung and unsprung masses, respectively.

Figures 4.10(a) and 4.10(b) present comparisons of displacement transmissibility of the sprung and unsprung masses of the model with UC and IC suspensions without the damping/flow valves. The results show vertical mode resonance frequencies of the sprung mass near 1 and 1.2 Hz, respectively, for the IC and UC suspensions. The peak transmissibility magnitudes of the UC suspensions (2.15) are substantially higher than those of the IC suspensions (near 1.8). Although the UC and IC suspensions struts were configured to yield identical spring rates, the UC struts employed relatively larger size orifices, which contributed to lower damping compared to the IC struts. Relatively higher peak magnitudes and resonance frequencies of the UC suspensions are due to their lower damping compared to the IC suspensions. The lower damping of the UC suspensions, however, yields considerably lower transmissibility magnitudes at frequencies above 2.5 Hz, as seen in Fig. 4.10(a).

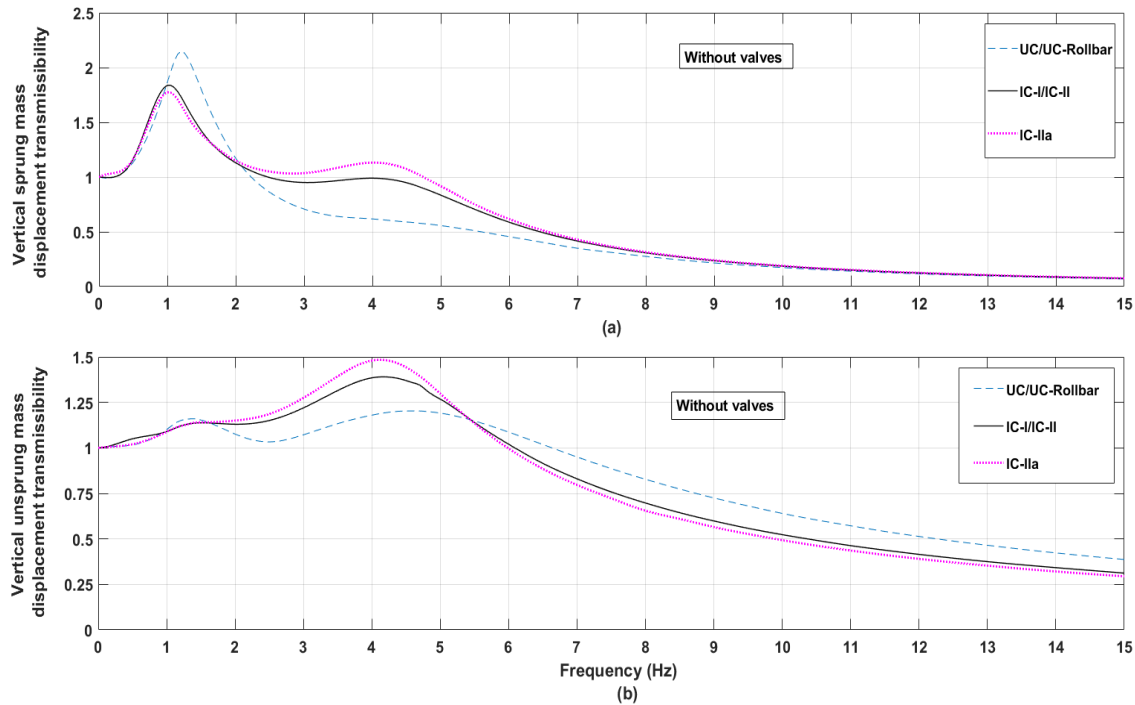


Figure 4.10: Comparisons of vertical mode transmissibility responses of the vehicle model equipped with unconnected and connected suspension configurations: (a) sprung mass; and (b) unsprung mass.

The relatively higher damping of the IC suspension struts yields unsprung mass peak responses at considerably lower frequencies compared to the typical unsprung mass resonance frequencies, as seen in Figure 10(b). The unsprung mass displacement transmissibility peaks are observed near 4.2 Hz for the IC-I and IC-II suspension, and about 4.05 Hz for the IC-IIa configuration. The UC suspensions exhibit peak responses at a relatively higher frequency of 4.5 Hz. Both the sprung and unsprung mass transmissibility magnitudes of the IC suspensions are substantially higher than those of the UC suspensions at frequencies above 2.5 Hz. From the results, it is evident that high damping attributed to smaller size orifice flows in IC struts is beneficial for sprung mass resonance control but detrimental for the ride performance. The reduction in the high-speed damping property of the struts via damping or interconnecting valves is thus essential to achieve better ride performance.

The presence of damping valves in the IC struts could alter the FDS and FDC components, which contribute to lower total damping force at higher velocities. Figures 4.11 illustrate sprung and unsprung mass vertical displacement transmissibility responses of the suspension configurations with damping valves. The struts with the damping valves thus yield considerable reductions in the sprung mass transmissibility magnitudes at frequencies above 2 Hz, when

compared to the responses of the suspensions without the valves, shown in Figure 4.10(a). The peak sprung mass transmissibility magnitudes of the suspensions with damping valves, however, are comparable with those of the suspensions without the valves. Lower suspension damping at higher velocities causes the unsprung mass response peaks to shift to a substantial higher frequency, in the order of 10 Hz, as seen in Figure 4.11(b). Comparisons of the responses in 4.10(b) and 4.11(b) show that the damping valves results in higher peak unsprung mass transmissibility of the UC suspensions, while the effect on the peak response of the IC suspensions is very small.

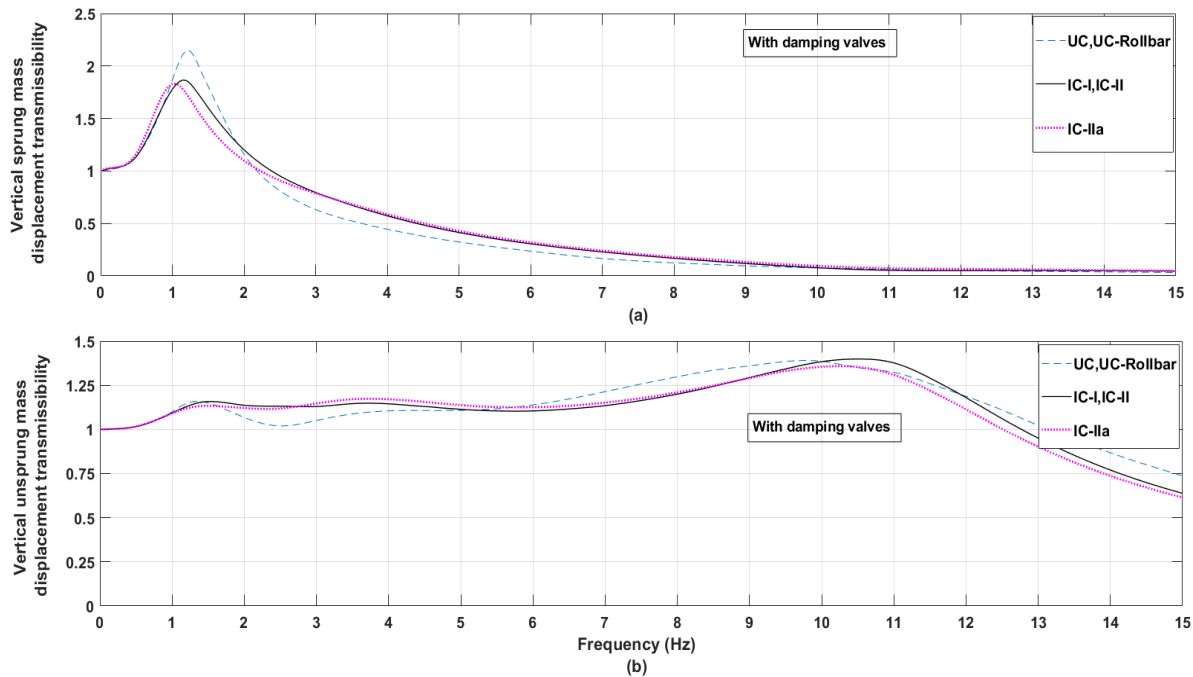


Figure 4.11: Comparison of vertical mode transmissibility responses of the vehicle model with different suspension configurations with damping valves: (a) sprung mass responses; and (b) unsprung mass responses.

Figures 4.12 present the vertical displacement transmissibility responses of the sprung and unsprung masses of the IC suspensions employing interconnecting valves in lieu of the damping valves. The results show that the peak responses in the vicinity of the sprung mass resonance frequency are comparable with those obtained with the damping valves. The tuning of the negative damping component, FDL, via the interconnection valves also yields reductions in the higher frequency transmissibility magnitudes comparable to the damping valves. Although the magnitudes of the unsprung mass transmissibility are considerably lower compared to those obtained for the struts without the valves, the IC suspensions with interconnection valves exhibit peak response in the 3.5 to 4 Hz range, as seen in Fig. 12(b). The results, however, show relatively

lower displacement transmissibility of the unsprung mass in the 7 to 15 Hz frequency range, as compared to those of the configurations employed with damping valves, shown in Figure 4.11(b). The results suggest that damping tuning can be effectively achieved through external interconnection valves, although further efforts would be desirable to seek optimal settings of the valves for realizing improved ride comfort performance.

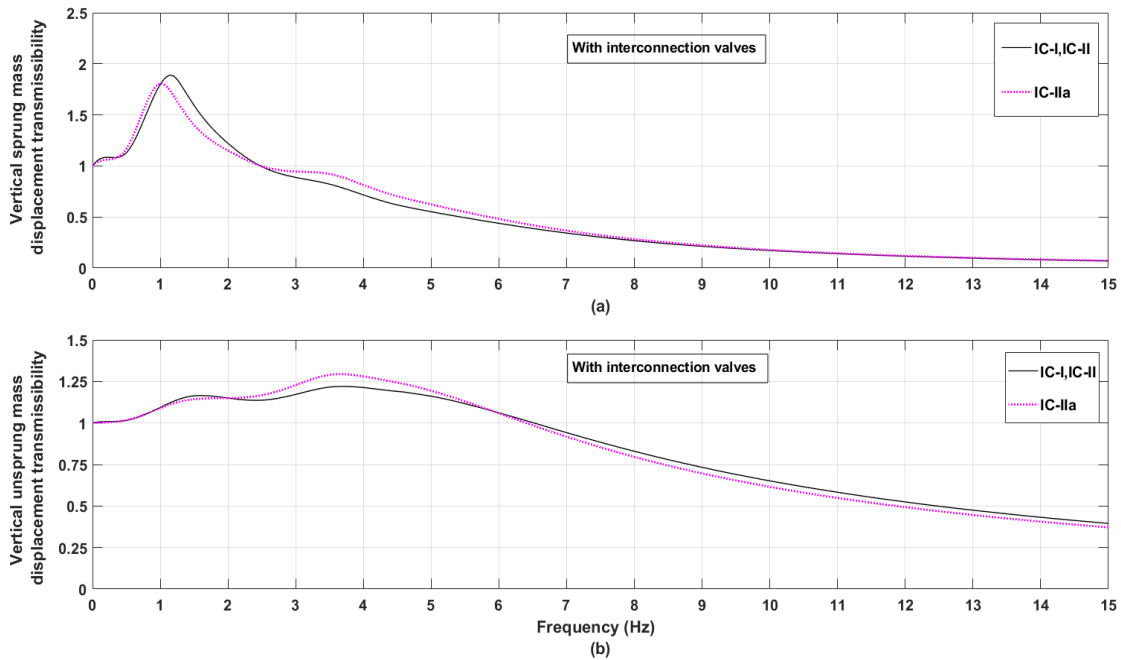


Figure 4.12: Comparison of vertical mode transmissibility responses of the vehicle model with IC suspensions employing interconnection valves: (a) sprung mass responses; and (b) unsprung mass responses.

Tables 4.1 and 4.2 summarize frequencies corresponding to the peak vertical mode sprung and unsprung mass responses, respectively, of the model with different suspension configurations under 0.01 m in-phase harmonic excitations. These may be considered as resonance frequencies of the model, which in case of the IC suspensions differ considerably from the target natural frequencies of the model due to higher damping. The results suggest comparable sprung mass frequencies of the UC and IC suspensions with damping valves, although the frequency of the IC-IIa suspension is lower due to its relatively larger gas volume. The reduction in the high-speed damping via interconnection valves (FDL component) also yields lower sprung mass resonance frequency compared to the suspension with damping valves. The UC and IC suspensions without the damping valves yield peak unsprung mass responses in the 4 to 4.5 Hz range. This frequency, however, increases to 9.8 Hz for the UC suspensions, and above 10 Hz for the IC-I suspensions, when high-speed damping is reduced via the damping valves. The frequencies corresponding to

the unsprung mass peak responses, however, tend to be lower when interconnection valves are used. The results suggest that damping tuning can be effectively achieved through external interconnection valves, although further efforts would be desirable to seek optimal settings of the valves for realizing improved ride comfort performance. The interconnection valves in IC suspensions offer superior design/tuning flexibility compared to the damping valves placed inside the IC struts.

Table 4.1: Frequencies corresponding to peak sprung mass displacement transmissibility of the vehicle model with different suspension configurations.

Suspension configurations	UC/UC-Rollbar	IC-I/IC-II	IC-IIa
Without valves	1.2 Hz	1 Hz	1 Hz
With damping valves	1.2 Hz	1.15 Hz	1 Hz
With interconnection valves	-	1.15 Hz	1 Hz

Table 4.2: Frequencies corresponding to peak unsprung mass displacement transmissibility of the vehicle model with different suspension configurations.

Suspension configurations	UC/UC-Rollbar	IC-I/IC-II	IC-IIa
Without valves	4.5 Hz	4.2 Hz	4.05 Hz
With damping valves	9.8 Hz	10.8 Hz	10.4 Hz
With interconnection valves	-	3.7 Hz	3.6 Hz

Roll displacement transmissibility characteristics of the sprung and unsprung masses of the vehicle model with UC and IC suspension configurations are compared in Figure 4.13. The UC and UC-Roll bar suspensions, owing to their relatively lower roll stiffness, yield peak roll angle responses near the respective resonance frequencies of 0.63 and 0.68 Hz, as seen in Figure 4.13(a). The IC suspensions exhibit higher resonance frequencies and lower peak responses, which are attributable to their higher roll stiffness and damping compared to the UC suspensions. The IC-I and IC-II suspensions are configured to yield identical roll mode damping properties, the slightly higher gas volume of the IC-II struts contributes to lower roll stiffness compared to the IC-I suspension. The peak roll response magnitude of the IC-II suspension is thus slightly higher than

the IC-I suspension. As described in section 3.3, the effective roll damping of the IC-IIa suspension is considerable smaller than the IC-I/IC-II configurations due to absence of the damping force component FDC, associated with orifice flows in the connected strut. This suspension thus yields substantially higher peak roll response compared to the other IC configurations. The UC suspensions with their low roll mode damping provide substantially lower sprung mass roll response in the 1 to 8 Hz frequency range compared to the IC suspensions at frequencies. Similarly, the IC-IIa suspension also yields relatively lower roll response in the 1.3 to 8 Hz frequency range compared to IC-I/IC-II suspensions. The lighter damping of the UC and IC-IIa suspensions, however, cause higher roll response of the unsprung mass at frequencies above 4 Hz, as seen in Fig. 4.13(b).

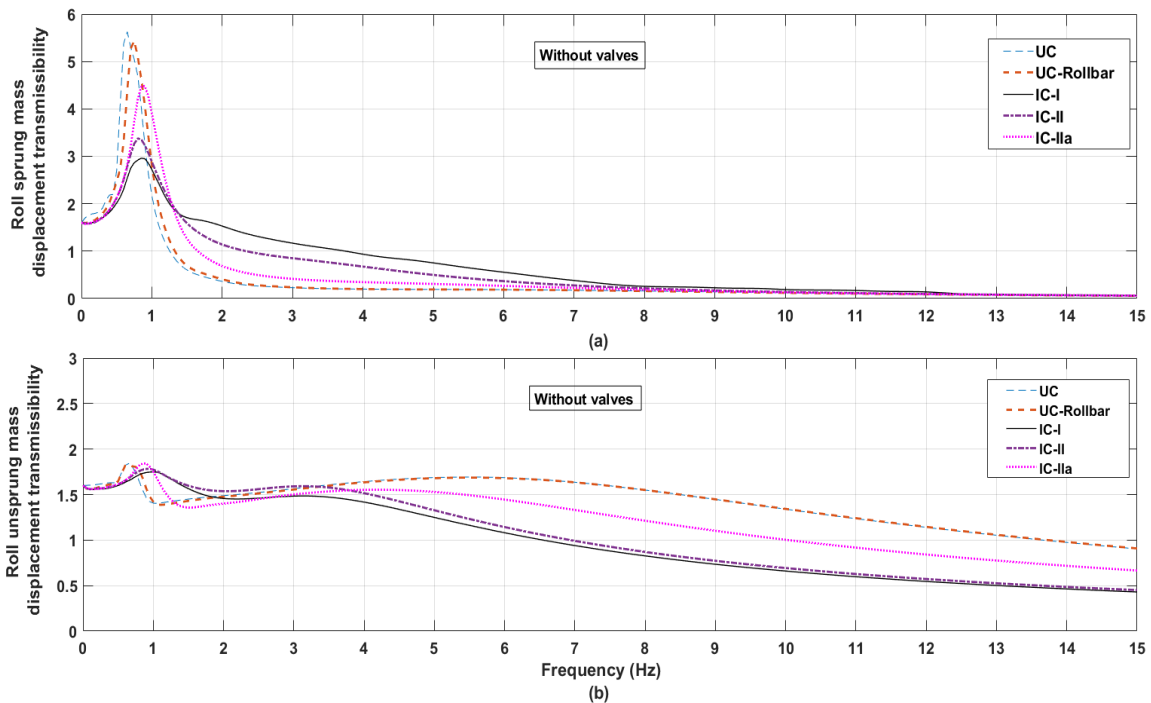


Figure 4.13: Comparison of roll transmissibility responses of the vehicle model with UC and IC suspensions: (a) sprung mass responses; and (b) unsprung mass responses.

Figure 4.14 illustrates the sprung and unsprung mass roll transmissibility responses of the vehicle model with UC and IC suspensions with damping valves. The valves limit the damping force of the struts at higher speeds, especially the FDS and FDC components of the IC suspensions. This contributes to lower roll mode damping and thereby relatively lower roll transmissibility at frequencies above 1 Hz. The lower roll mode damping also causes the peak unsprung mass roll response to shift to higher frequencies, which is clearly evident for the UC. UC-Rollbar and IC-IIa configurations, as seen in Figure 4.14(b). The magnitudes of the unsprung mass roll response,

however, are considerably higher compared to the IC-I/IC-II suspensions. This can be attributed to greater contributions of the negative FDC component to the overall roll mode damping of the IC-I/IC-II configurations. Figures 4.15(a) and 4.15(b) also show similar effects of the interconnecting valves on the roll responses of the vehicle model confirming that the interconnecting valves can provide equally effective damping tuning of the suspension system.

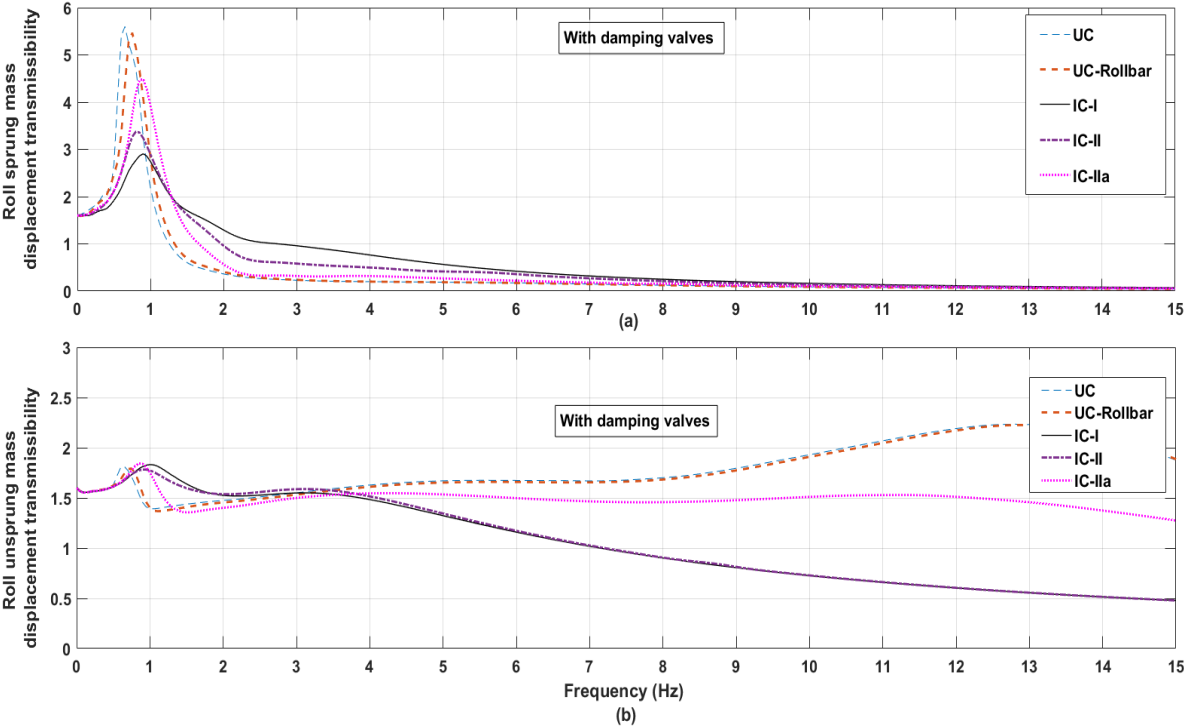


Figure 4.14: Comparison of roll transmissibility responses of the vehicle model with UC and IC suspensions with damping valves: (a) sprung mass responses; and (b) unsprung mass responses.

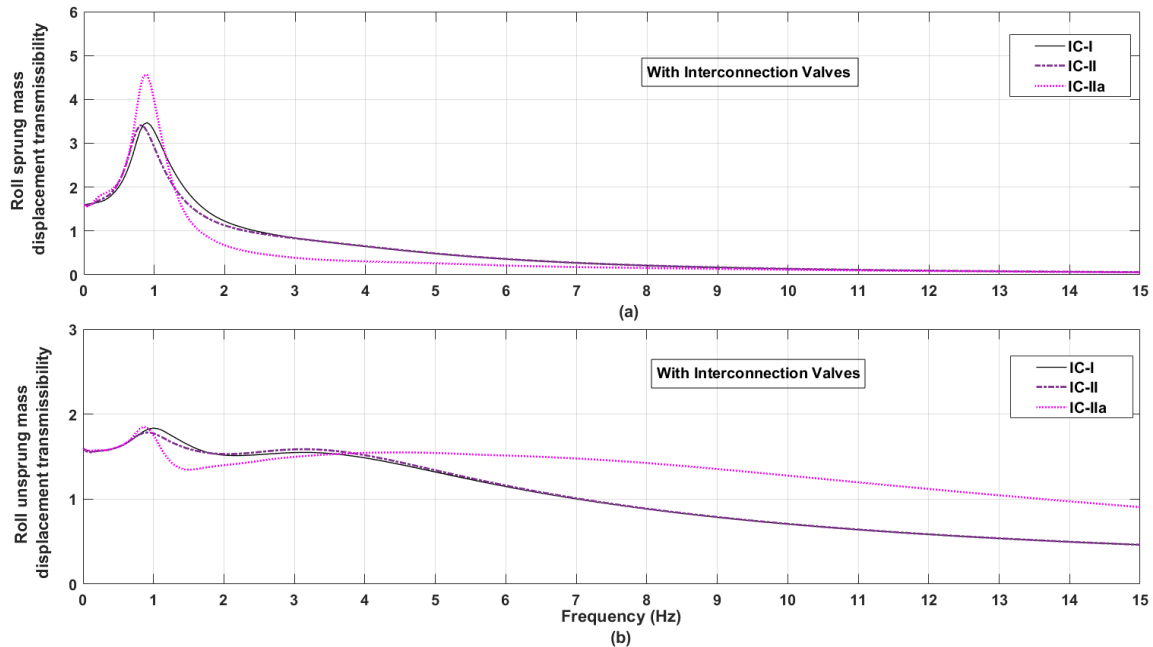


Figure 4.15: Comparison of roll transmissibility responses of the vehicle model with UC and IC suspensions with interconnection valves: (a) sprung mass responses; and (b) unsprung mass responses.

Tables 4.3 and 4.4 summarize frequencies corresponding to the peak roll mode sprung and unsprung mass responses, respectively, of the model with different suspension configurations under 0.01 m out-of-phase harmonic excitations. The results suggest comparable sprung mass roll mode resonance frequencies of the UC and IC suspensions, while the IC-I suspension exhibits highest resonance frequency (0.92 Hz) followed by the IC-IIa and IC-II suspensions. The sprung mass roll resonance frequency is not affected by the damping valves for all the suspension configurations. This is due to relatively low suspension velocity (below the transition velocity) in the vicinity of the resonance frequencies. The interconnection valves also exhibit identical roll mode frequencies. The UC suspensions without the damping valves yield peak unsprung mass roll responses in the 5.5 to 5.6 Hz range. This frequency, however, shifts to 12.8 Hz, when high-speed damping is reduced via the damping valves. The IC suspensions with their high roll mode damping, however, suggest relatively small effects of the damping or interconnection valves on the unsprung mass resonance frequencies. This is due to the fact that the damping valves help limit the contributions of the FDS and FDC damping force components, with only small effect on the overall roll mode damping. The interconnected valves, on the other hand, emphasize the FDL damping force component and thereby the roll damping moment.

Table 4.3: Frequencies corresponding to peak sprung mass roll displacement transmissibility of the vehicle model with different suspension configurations.

Suspension configurations	UC	UC-Rollbar	IC-I	IC-II	IC-IIa
Without valves	0.63	0.68	0.92	0.83	0.85
With damping valves	0.63	0.68	0.92	0.83	0.85
With interconnection valves	-	-	0.92	0.83	0.85

Table 4.4: Frequencies corresponding to peak unsprung mass displacement transmissibility of the vehicle model with different suspension configurations.

Suspension configurations	UC	UC-Rollbar	IC-I	IC-II	IC-IIa
Without valves	5.55	5.6	3.1	3.2	4.1
With damping valves	12.8	12.8	3.3	3.24	4.4
With interconnection valves	-	-	3.2	3.26	4.8

4.6 SUMMARY

The ride and handling performance of different hydro-pneumatic suspension configurations are investigated in terms of vertical and roll responses to steady lateral acceleration, and in-phase and out-of-phase road bump excitations. It is shown that the high damping of the IC suspensions can provide improved handling but relatively poor ride performance compared to the UC suspensions. The tuning of the suspension damping via valves is thus considered vital to achieve adequate vibration isolation. It is further shown that the interconnection valves can provide tuning of the suspension damping similar to the conventional damping valves by making use of the negative damping features of the hydraulic interconnections. The externally mounted interconnection valves, however, offer superior design/tuning flexibility.

CHAPTER 5 CONCLUSIONS AND RECOMMENDATIONS

5.1 MAJOR CONTRIBUTIONS

In this dissertation research, the negative damping features of hydraulically interconnected suspensions are explored and a methodology is proposed to achieve tuning of the damping property through control of flows across the coupled suspension struts. The major contributions of this thesis research are summarized below:

- a. Three different configurations of the roll coupled hydro-pneumatic suspension struts are analytically modeled to describe the negative damping mechanisms.
- b. Interconnection flow valves are proposed to emphasize the negative damping component attributed to the hydraulic flows across the coupled struts.
- c. The negative damping force component is exploited to achieve tuning of the damping property of the suspension for improved ride and handling performance potentials of the suspension system. It is shown that the proposed interconnection valves can provide damping tuning similar to the conventional damping valves, while providing high roll mode damping for enhanced control of the roll motion.
- d. A strut design with greater floating piston area (type-II) is proposed in order to reduce the gas charge pressure of the strut for a given load carrying capacity.
- e. Ride height valves are introduced to achieve nearly constant vertical and roll mode natural frequencies of the vehicle, irrespective of the load.
- f. The ride and handling performance potentials of the coupled suspensions with damping as well as interconnecting valves are investigated to demonstrate significance of the negative damping and relative merits of the interconnection valves.

5.2 MAJOR CONCLUSIONS

Major conclusions drawn from the study are summarized below:

- The damping force components of the coupled hydro-pneumatic suspensions are strongly related to the interconnection layout, while the load carrying capacity and the stiffness property is affected by the strut design.
- Hydraulic interconnections yield substantially higher suspension roll stiffness, which can effectively substitute for the antiroll bar. The roll stiffness, however, tends to decrease with increase in the roll angle. The rate of reduction in the roll stiffness can

be reduced by decreasing the ratio of the main piston area to that of the floating piston. It is thus suggested to design struts with identical areas of the floating and main pistons (type-II).

- The ride height control via height valves ensures not only the constant ride height of the sprung mass but also provides nearly constant roll and vertical mode natural frequencies of the vehicle, irrespective of variations in the payload.
- The roll coupled hydro-pneumatic suspensions yield negative damping force components attributed to hydraulic flows across the struts and pressure drop across the orifices in the connected strut. The primary vertical mode damping of each strut is directly related to orifice flows within the same strut.
- The negative damping force components help to reduce the overall vertical mode damping of each strut but significantly emphasize the effective roll damping moment of the coupled struts.
- Owing to relatively smaller annular area, the pressure drops across the interconnecting pipes exhibit dominant effect on the overall negative damping force. Higher flow resistance of the interconnecting lines can lead to overall negative damping of the suspension, which may affect the system stability.
- The negative damping force component attributed to hydraulic flows across the struts can be enhanced by increasing the flow resistance of the interconnecting pipes. This negative force component can be applied to achieve lower effective damping at higher velocities for improving ride performance potential of the suspension.
- Reducing the effective damping at higher velocities via flow valves integrated within the suspension dampers is vital for limiting the peak acceleration response of the sprung mass under a transient road excitation and for achieve improved vibration isolation in the ride frequency range.
- The interconnection valves permit tuning of the damping property similar to the conventional damping valves. The externally mounting interconnection valves, however, provide greater design/tuning flexibility.

5.3 RECOMMENDATIONS FOR THE FUTURE WORK

This dissertation research is carried out to evaluate the anti-roll and ride performance potentials of three different interconnected hydro-pneumatic suspension configurations. The results of the

study show important negative damping features of the coupled suspension struts, which can be applied for tuning of the suspension damping similar to the conventional damping valves. Since the external interconnection valves offer superior design/tuning flexibility of the suspension systems, it is suggested that further systematic investigations be carried out to explore the design factor affecting the magnitudes of the negative force components. Some of the potential further studies are listed below:

- ❖ The externally tunable negative damping force together with a conventional damping valve can provide variable damping forces due to flows within the same strut and flows across the coupled struts. A more comprehensive model of the struts is thus desirable to explore the effects of both the flow valves.
- ❖ Since the negative damping features of the coupled suspension have not yet been explored, it is strongly recommended to undertake laboratory experiments to establish thorough understanding of such features. For this purpose, a comprehensive experiment design should be undertaken for characterizing each damping force component through measurements of pressure drops across: (i) interconnecting lines; and (ii) piston orifices. The component attributed to orifice flows of the connected strut can perhaps be quantified by imposing motion of one of the struts, while holding one of the struts stationary.
- ❖ Further efforts are also needed to develop reliable models of the flow coefficients. In this regard, it would be worthy to develop fluid-structure interaction (FSI) models of the hydro-pneumatic struts with computational fluid dynamics (CFD) tools.

REFERENCES

1. Newton, K. Steeds, W. Garrett, T.K. (1983) *The motor vehicle*, Butterworth, London (UK).
2. Hawley Jr John, B. (1927) Shock absorber and the like for vehicles. U.S. Patent No. 1,647,518. Washington, DC: U.S. Patent and Trademark Office.
3. Felez, J., Vera, C. (1987) Bond graph assisted models for hydro-pneumatic suspensions in crane vehicles. *Vehicle system dynamics*, 16(5-6), pp. 313-332.
4. Rakheja, S., Liu, P., Ahmed, A. K. W., & Su, H. (1993) Analysis of an interlinked hydro-pneumatic suspension. *In Proc. of ASME Winter Annual Meeting, DSC- Vol. 52*, pp. 279-289.
5. Liu, P., Rakheja, S., Ahmed, A. (1995) Properties of an interconnected hydro-pneumatic suspension system. *Trans of Canadian Society Mech Eng*, 19(4):383-96.
6. Chaudhary, S. (1998) Ride and roll performance analysis of a vehicle with spring loaded interconnected hydro-pneumatic suspension. MASC Thesis, Concordia University.
7. Wu, L. (2003) Analysis of hydro-pneumatic interconnected suspension struts in the roll plane vehicle model. MASC Thesis, Concordia University
8. Cao, D., Rakheja, S., Su, C. Y. (2005) Roll plane analysis of interconnected hydro-pneumatic suspension struts. *International Mechanical Engineering Congress and Exposition*, pp. 133-142.
9. Jeyakumaran, J., Smith, W., Zhang, N. (2007) Transient Characteristics of a Hydraulically Interconnected Suspension System. SAE paper no 2007-01-0582.
10. Smith W, Zhang N. (2009) Experimental and theoretical investigation into the dynamics of a half-car with an interconnected passive suspension. SAE Paper no 2009-01-0579, 11p.
11. Zapletal, E. (2000) Balanced suspension. SAE Paper no 2000-01-3572, 11p.
12. Buj, J. F. I. (2002) Integral suspension system for motor vehicles based on passive components. SAE Paper no 2002-01-3105. 14p
13. Sharp, R. S., Hassan, S. A. (1986) An evaluation of passive automotive suspension systems with variable stiffness and damping parameters. *Vehicle System Dynamics*, 15(6), pp. 335-350.
14. Crosby, M. J., Karnoop, D. C. (1973) The active damper-a new concept for shock and vibration control. *Shock and Vibration Bulletin*, 43(4), pp. 119-133.
15. Krasnicki, E. J. (1981) The experimental performance of an on-off active damper. *Shock and Vibration Bulletin*, Pt. 1, pp. 125-131

16. Rakheja, S., Sankar, S. (1985) Vibration and shock isolation performance of a semi-active “on-off” damper. *Journal of Vibration, Acoustics, Stress, and Reliability in Design*, 107(4), pp. 398-403.
17. Alanoly, J., Sankar, S. (1987) A new concept in semi-active vibration isolation. *Journal of mechanisms, transmissions, and automation in design*, 109(2), pp. 242-247.
18. Rakheja, S., Su, H., Sankar, T. S. (1990) Analysis of a passive sequential hydraulic damper for vehicle suspension. *Vehicle System Dynamics*, 19(5), 289-312.
19. Woodrooffe, J. (1995) Heavy truck suspension damper performance for evaluating road friendliness and ride quality. SAE Paper no 952636, pp. 49-54.
20. Rakheja, S., Woodrooffe, J. (1996). Role of suspension damping in enhancement of road friendliness of heavy vehicles. *Int. J. Heavy Vehicle Systems*, 3(1-4), pp. 363-381.
21. Rakheja, S., Ahmed, A. K. W., Yang, X., Guenette, C. (1999) Optimal suspension damping for improved driver-and road-friendliness of urban buses. SAE Paper no 1999-01-3728, pp. 9-20.
22. Joarder, M. N. (2003) Influence of nonlinear asymmetric suspension properties on the ride characteristics of road vehicle. MSc Thesis, Concordia University.
23. Winkler, C. B., Karamihas, S. M., Bogard, S. E. (1992) Roll-stability performance of heavy-vehicle suspensions. SAE Paper no 922426, pp. 1-13.
24. Cole, D. J. (2000) Evaluation of design alternatives for roll-control of road vehicles. *In Proc of Int Symposium on Advanced Vehicle Control (AVEC 2000)*, pp. 561-568.
25. Joo, F. R. (1991) Dynamic analysis of a hydro pneumatic suspension system. MSc Thesis, Concordia University.
26. Cao, D., Rakheja, S., Su, C. Y. (2008). Dynamic analyses of roll plane interconnected hydro-pneumatic suspension systems. *Int. J of vehicle design*, 47(1-4), pp. 51-80.
27. Cao, D., Rakheja, S., Su, C. Y. (2005) Comparison of roll properties of hydraulically and pneumatically interconnected suspensions for heavy vehicles. SAE Paper no 2005-01-3593, pp. 1-11.
28. Liu, P. (1994) An analytical study of ride and handling performance of an interconnected vehicle suspension. MSc Thesis, Concordia University.
29. Dixon, J. (2008) The shock absorber handbook. John Wiley & Sons, London (UK).
30. Cao, D., Rakheja, S., Su, C. Y. (2007) Optimal damping design of heavy vehicle with interconnected hydro-pneumatic suspension. SAE Paper no 2007-01-0584, 7p.

31. Ramrath, J. M. (1967). A brief simple method for designing shock absorbers. *Journal of Machine Design*, 39(4), 217.
32. Cao, D., Rakheja, S., Su, C. Y. (2005) Roll plane analysis of interconnected hydro-pneumatic suspension struts. *Intl Mech Engineering Congress and Exposition*, pp. 133-142.
33. Smith, W., Zhang, N., Jeyakumaran, J. (2007) Hydraulically Interconnected Suspension Parameter Sensitivity in Half-Car Ride Performance. SAE Paper no 2007-01-0583, 7p.
34. Smith, W., Zhang, N., Jeyakumaran, J. (2007) High frequency parameter sensitivity in hydraulically interconnected suspensions. *Applied Mechanics (ACAM 2007)*, Vol- 1, pp. 608-613.
35. Zhang, N., Smith, W. A., Jeyakumaran, J. (2010) Hydraulically interconnected vehicle suspension: background and modelling. *Vehicle System Dynamics*, 48(1), pp. 17-40.
36. Smith, W. A., Zhang, N., Hu, W. (2011) Hydraulically interconnected vehicle suspension: handling performance. *Vehicle System Dynamics*, 49(1-2), pp. 87-106.
37. Cao, D., Rakheja, S., Su, C. Y., Ahmed, A. K. W. (2007) Analysis of a twin-gas-chamber hydro-pneumatic vehicle suspension. *In Advances in Dynamics, Instrumentation and Control*, Vol II, pp. 267-276.
38. Cao, D., Rakheja, S., Su, C. Y. (2007) Roll plane analysis of a hydro-pneumatic suspension with twin-gas-chamber struts. *Intl J of heavy vehicle systems*, 14(4), pp. 355-375.
39. Cao, D., Rakheja, S., Su, C. Y. (2008) Property analysis of an X-coupled suspension for sport utility vehicles. *Intl J of Passenger Cars-Mechanical Systems*, SAE paper no 2008-01-1149, 853-862.
40. Darling, J., Dorey, R. E., Ross-Martin, T. J. (1992) A low cost active anti-roll suspension for passenger cars. *J of dynamic systems, measurement, and control*, 114(4), pp. 599-605.
41. Sharp, R. S., Pan, D. (1993) On the design of an active roll control system for a luxury car. *Proc of the Institution of Mech Eng: J of Automobile Engineering*, 207(4), pp. 275-284.
42. Darling, J., Hickson, L. R. (1998) An experimental study of a prototype active anti-roll suspension system. *Vehicle System Dynamics*, 29(5), pp. 309-329.
43. Rosam, N., Darling, J. (1997) Development and simulation of a novel roll control system for the Interconnected Hydragas Suspension. *Vehicle System Dynamics*, 27(1), pp. 1-18.
44. Cronje, P. H., Els, P. S. (2010) Improving off-road vehicle handling using an active anti-roll bar. *Journal of Terra mechanics*, 47(3), pp. 179-189.

45. Wang, L., Zhang, N., Du, H. (2009) Design and experimental investigation of demand dependent active suspension for vehicle rollover control. *Proceedings of the 48th IEEE Conference on Decision and Control; Shanghai*. pp. 5158–5163.
46. Olley, M. (1934) Independent wheel suspension- Its whys and wherefores. SAE paper no 340080.
47. Sharp, R.S., Pilbeam, C. (1993) Achievability and value of passive suspension designs for minimum pitch response. *IMechE Conference: Vehicle Ride and Handling*, pp 243-259.
48. Best A. (1984) Vehicle ride-stages in comprehension. *Physics in Technology*, 15 (4), pp. 205-210.
49. Crolla, D. A., King, R. P. (1999) Olley's" flat ride" revisited. *Vehicle system dynamics supplement, Proceedings of the 16th IAVSD*, vol- 33, pp. 762-774.
50. Odhams, A.M.C., Cebon, D. (2006) An analysis of ride coupling in automobile suspensions. *Proceedings of the institution of mechanical engineers, Part D: Journal of Automobile Engineering*, pp 1041-1061.
51. Sharp, R. S. (2002) Wheelbase filtering and automobile suspension tuning for minimizing motions in pitch. *Proc of the Institution of Mech Eng, J of Automobile Engg*, 216(12), pp. 933-946.
52. Moulton, A. E., Best, A. (1979). Hydragas suspension SAE paper no 790374.
53. Moulton, A. E., Best, A. (1970). Rubber springs and inter-connected suspension systems. *In Engineering Design Show Conference*, Paper no. 15a, 31p.
54. Cao, D., Rakheja, S., Su, C. Y. (2006). A generalized model of a class of interconnected hydro-pneumatic suspensions and analysis of pitch properties. *Int Mech Engg Congress and Exposition, (IMECE-2006)*, pp. 137-146.
55. Cao, D., Rakheja, S., Su, C. Y. (2007) Pitch attitude control and braking performance analysis of heavy vehicle with interconnected suspensions. SAE Paper no 2007-01-1347, pp. 1-9.
56. Cao, D., Rakheja, S., Su, C. Y. (2008) Pitch plane analysis of a twin-gas-chamber strut suspension. *Proc of the Institution of Mech Eng, J of Automobile Engg*, 222(8), pp. 1313-1335.
57. Cao, D., Rakheja, S., Su, C. Y. (2008) Dynamic analyses of heavy vehicle with pitch-interconnected suspensions. *Int J of Heavy Vehicle Systems*, 15(2-4), pp. 272-308.
58. Rosam, N., Darling, J. (1994). Modelling and Testing of the Interconnected Hydragas Suspension. *In Proc. 6th Intl. Congress on Hydraulic Engineering*. 7p.

59. Rideout, G., Anderson, R. J. (2003) Experimental testing and mathematical modeling of the interconnected hydro gas suspension system. SAE Paper no 2003-01-0312, 9p.
60. Zhang, J. W., Chen, S. Z., Yang, L. (2012) Research on Nonlinear Stiffness Characteristics of Hydro-Pneumatic Spring. *In Applied Mechanics and Materials*, Vol. 128, pp. 421-425.
61. Wilde, J. R., Heydinger, G. J., Guenther, D. A., Mallin, T., Devenish, A. M. (2005) Experimental evaluation of fishhook maneuver performance of a kinetic suspension system. SAE Paper no 2005-01-0392, 10p.
62. Wang, L., Zhang, N., Du, H. (2012) Experimental investigation of a hydraulically interconnected suspension in vehicle dynamics and stability control. *Int J of Passenger Cars-Mechanical Systems*, SAE Paper no 2012-01-0240, pp. 759-768.
63. Zhou, M., Wang, L., Zhang, J., Zhang, N. (2015) Experimental Investigation of Interconnected Hydraulic Suspensions with Different Configurations to Soften Warp Mode for Improving Off-Road Vehicle Trafficability. SAE Paper no 2015-01-0658, 9p.
64. Hua, H., Wang, L., Qi, H., Zhang, J., Zhang, N. (2015). Implementation and Experimental Study of a Novel Air Spring Combined with Hydraulically Interconnected Suspension to Enhance Roll Stiffness on Buses. SAE Paper no. 2015-01-0652, 9p.
65. Rakheja, S., Ahmed, A. K. W., and Stiharu, I. Urban bus optimal passive suspension study. Concave Research Centre, Concordia University, Canada, 2001.
66. ISO, E., 2003. 5167-1: 2003. Measurement of fluid flow by means of pressure differential devices inserted in circular cross-section conduits running full—Part-1, pp.5167-1.
67. Reader-Harris, M. (2015) Orifice plates and venturi tubes. Cham: Springer International Publishing.
68. Gillespie TD. (1992) Fundamentals of vehicle dynamics. Warrendale, PA: SAE, Inc.
69. Hetrick, S. (1997) Examination of driver lane change behavior and the potential effectiveness of warning onset rules for lane change or "Side" Crash Avoidance Systems. MAsc Thesis, Virginia Polytechnic Institute and State University, USA.
70. Aleksander, H (2002) Rollover stability index including effects of suspension design. SAE Paper no 2002-01-0965, 13p.